CHEMICAL AND OPTICAL PROPERTIES OF ORGANIC AEROSOLS IN THE ATMOSPHERE OVER CONTINENTAL US: FORMATION, PARTITIONING, AND LIGHT ABSORPTION

A Dissertation
Presented to
The Academic Faculty

by

Jiumeng Liu

In Partial Fulfillment
of the Requirements for the Degree
Doctor of Philosophy in the
School of Earth and Atmospheric Sciences

Georgia Institute of Technology
December 2013

CHEMICAL AND OPTICAL PROPERTIES OF ORGANIC AEROSOLS IN THE ATMOSPHERE OVER CONTINENTAL US: FORMATION, PARTITIONING, AND LIGHT ABSORPTION

Approved by:

Dr. Rodney J. Weber, Advisor
School of Earth and Atmospheric Sciences
Georgia Institute of Technology

Dr. Armistead G. Russell
School of Civil and Environmental Engineering
Georgia Institute of Technology

Dr. Michael H. Bergin
School of Civil and Environmental Engineering
Georgia Institute of Technology

Dr. Greg Huey
School of Earth and Atmospheric Sciences
Georgia Institute of Technology

Dr. Nga Lee (Sally) Ng
School of Chemical and Biomolecular Engineering
Georgia Institute of Technology

Date Approved: October 31, 2013

To my parents

ACKNOWLEDGEMENTS

I would like to start by thanking my advisor, Dr. Rodney Weber, for helping to guide and shape my graduate experience. I am truly grateful for the opportunity that he trusted me and admitted me into his group in the first place, when I was a new college graduate with barely any knowledge about the atmospheric sciences. I thank him for his hands-on guidance throughout the process from pre-experiments to writing this thesis, for his tolerance when I made mistakes, and for his encouragement when I was down. I am also thankful for his willingness to conduct research that was not funded and for his belief and continuous support in this work, which led to a large portion of my dissertation. His high expectation on me is the most important motivation that keeps me moving forward. My passion to become an atmospheric scientist is due largely to his influence.

I would like to acknowledge my committee, Drs. Michael Bergin, Sally Ng, Greg Huey, and Armistead Russell, for their scientific insights. They have shown me the fascinating part of atmospheric science from different perspectives. A special thank you to Dr. Michael Bergin, for his advice throughout the brown carbon study, and for the support from his “yes” for all the time.

I have been fortunate to work with many excellent colleagues during CalNex, my first field campaign. I would like to thank Professor Jennifer Murphy and Reluca Ellis from the University of Toronto for their contribution to the E-AIM model analysis, Dr. Patrick Veres from NOAA for providing the CIMS formic acid data, Dr. Jose Jimenez and Patrick Hayes from the University of Colorado Boulder for providing the AMS data and invaluable manuscript comments. I greatly appreciate Dr. Joost de Gouw from NOAA Chemical Sciences Division for the insightful discussions at various conferences,

and for his support and referral during my job search. I am also very grateful to my research collaborators during the brown carbon study and NASA projects (DC3 and SEAC^{4}RS), especially Drs. Jack Dibb and Eric Scheuer from University of New Hampshire, for their patient, considerate, continuous logistic support to make the NASA project work, and their invaluable manuscript comments.

I would like to thank my current and former group members, Dr. Arsineh Hecobian, Dr. Michelle Oakes-Jones, Dr. Vishal Verma, Dr. Neeraj Rastogi, Eric Parker, Ting Fang, Zhenyu Du, and Gabby Agostini, for their help with my research from different aspects. I appreciate Dr. Xiaolu Zhang, Laura King and Hongyu Guo, whom I spent most time with during my PhD study at Georgia Tech, for all the joyful moments we spent together. I would like to thank my friends, especially Wenxian Zhang, Tianyu Jiang, Guofeng Shen, Peng Liu and Liwen Zhang, for being with me. I enjoyed the time spent with them very much.

Finally, I thank my fiancé Yuan, for his love that could not be obstructed by the long distance. I am also grateful to my parents, for their unconditional love and unending support that made all these possible.

TABLE OF CONTENTS

LIST OF TABLES

LIST OF FIGURES

LIST OF SYMBOLS AND ABBREVIATIONS

SYMBOLS

AAE: Absorption Ångström Exponent, unitless

AAE_{BC}: Absorption Ångström Exponent for black carbon

AAE_{BrC}: Absorption Ångström Exponent for brown carbon

AAE_{PSAP}: Absorption Ångström Exponent based on the PSAP data

A_{λ}: light absorbance measured by the spectrophotometer, unitless

$Abs(\lambda)$: light absorption measured in a solution at wavelength λ (M/m)

b_{ap}: Light absorption coefficient (M/m)

b_{ap_Aeth}: Aethalometer (7-λ) fine particle ($PM_{2.5}$) light absorption with scattering correction (M/m), wavelength is specified in text.

b_{ap_EC}: Mie predicted fine particle BC light absorption based on MOUDI EC (M/m), wavelength is specified in text.

b_{ap_MAAP}: Multi-Angle Absorption Photometer (MAAP) fine particle measurement of light absorption (M/m), operates at 670 nm.

$b_{ap,\ H2O\_BrC}(\lambda)$ or $b_{ap,\ H2O}(\lambda)$: Mie predicted fine particle brown carbon absorption from water extracts (M/m), wavelength is specified in text.

$b_{ap,\ MeOH}(\lambda)$: Mie predicted fine particle brown carbon absorption from MOUDI methanol extracts (M/m), wavelength is specified in text.

$b_{ap,\ Total\_BrC}(\lambda)$: Mie predicted fine particle brown carbon absorption from the sum of water and methanol extracts (M/m), wavelength is specified in text.

$b_{ap,BC1}(\lambda)$: Light absorption coefficient of BC at wavelength λ (M/m), estimated from PSAP absorption at 660 nm, assuming non-BC light absorbers are minimal at 660 nm and an AAE_{BC} of 1

$b_{ap,BC2}(\lambda)$: Light absorption coefficient of BC at wavelength λ (M/m), estimated using a mass absorption cross section of 7.5 m2/g at 550 nm and an AAE_{BC} of 1

$b_{ap,PSAP}(\lambda)$: Light absorption coefficient of fine particles at wavelength λ (M/m) determined from the PSAP data.

$b_{ap2(\lambda)}$:	Light absorption coefficient of fine particles at wavelength λ (M/m) determined from $b_{ap,BC2}(660)$ and AAE_{PSAP}
α/ρ:	Solution mass absorption efficiency, (m^2g^{-1})
λ:	Wavelength, nm
ρ:	Particle density, g/cm^3
$H_2O\_Abs(\lambda)$:	light absorption measured in water-extract at wavelength λ (M/m)
$MeOH\_Abs(\lambda)$:	light absorption measured in methanol-extract at wavelength λ (M/m)

ABBREVIATIONS

AMS:	Aerosol Mass Spectrometer
ATL:	Atlanta
BC:	Black Carbon
BrC:	Brown Carbon
CALNEX:	California Nexus; Research at the Nexus of Air Quality and Climate Change
CIMS:	Chemical Ionization Mass Spectrometer
CO:	Carbon monoxide
DC3:	Deep Convective Clouds and Chemistry
EC:	Elemental Carbon
EDT:	Eastern Daylight Time
EPA:	Environmental Protection Agency
GC-MS:	Gas Chromatography Mass Spectrometry
GIT:	Georgia Institute of Technology
$HCOO^-$:	Formate anion
HCOOH:	Formic acid
HOA:	Hydrocarbon-like Organic Aerosol
HULIS:	HUmic-Like Substances
IC:	Ion Chromatography
JST:	Jefferson Street site
LA:	Los Angeles
LOD:	Limit Of Detection

LV-OOA:	Low-Volatility Oxygenated Organic Aerosol
LWC:	Liquid Water Content
LWCC:	Liquid Waveguide Capillary Cell
MAAP:	Multi-angle Absorption Photometer
MAC:	Mass Absorption Cross-section
MeOH:	methanol
MOUDI:	Micro-Orifice Uniform Deposit Impactor
NH_4^+:	Ammonium ion
NI-PT-CIMS:	Negative ion-proton transfer-chemical ionization mass spectrometry
NO_3^-:	Nitrate ion
NO_3:	Nitrate radical
NOAA:	National Oceanic and Atmospheric Association
NOx:	Nitrogen Oxides (NO + NO2)
O_3:	Ozone
OA:	Organic Aerosol
OC:	Organic Carbon
ODR:	Orthogonall Distance Regression
OH:	Hydroxy radical
OM:	Organic matter (µg/m3)
OOA:	Oxygenated Organic Aerosol
p/g:	Particle/Gas
PAH:	Polycyclic Aromatic Hydrocarbon
PDT:	Pacific Daylight Time
PILS:	Particle-Into-Liquid Sampler
PM:	Particulate Matter
PM_1:	Particulate Matter with aerodynamic diameter less than 1µm
$PM_{2.5}$:	Particulate Matter with aerodynamic diameter less than 2.5 µm
POA:	Primary Organic Aerosol
PSAP:	Particle Soot Absorption Photometer
Q:	Single Particle Absorption Efficiency
RF:	Radiative Forcing

RH:	Relative Humidity
RS:	Roadside site
SCAPE:	Southeastern Center for Air Pollution & Epidemiology
SEARCH:	Southeastern Aerosol Research and Characterization SOA: Secondary Organic Aerosol
SO_4^{2-}:	Sulfate ion
SOA:	Secondary Organic Aerosol
SP2:	Humidified Dual Single Particle Soot Photometer
SVOC:	Semi-Volatile Organic Compound
SV-OOA:	Semi-Volatile Oxygenated Organic Aerosol
TOC:	Total Organic Carbon
Total_Abs(λ):	Sum of H2O_Abs(λ) and MeOH_Abs(λ) for a filter extracted sequentially using the two solvents (water then methanol).
UV:	Ultraviolet
VOC:	Volatile Organic Compound
WSOC:	Water-Soluble Organic Carbon
WSOCg:	Gas-phase Water-Soluble Organic Carbon
WSOCp:	Particle-phase Water-Soluble Organic Carbon
YRK:	Yorkville site

SUMMARY

Organic aerosol (OA) is an important component of tropospheric fine aerosols and can have a large influence on climate, visibility and human health. To gain a better understanding of the role played by OA, chemical and physical properties that determine the formation processes of organic aerosols and their interaction with solar radiation are investigated in this thesis.

As part of the thesis work, gas-particle partitioning behavior of formic acid was tracked to investigate the formation mechanisms of secondary organic aerosols. Gas and fine particle ($PM_{2.5}$) phase formic acid concentrations were measured with online instrumentation during separate one-month studies in the summer of 2010 in Los Angeles (LA), CA, and Atlanta, GA. In both urban environments, median gas phase concentrations were on the order of a few ppbv (LA 1.6 ppbv, Atlanta 2.3 ppbv) and median particle phase concentrations were approximately tens of ng/m^3 (LA 49 ng/m^3, Atlanta 39 ng/m^3). LA formic acid gas and particle concentrations had consistent temporal patterns; both peaked in the early afternoon and generally followed the trends in photochemical secondary gases. Atlanta diurnal trends were more irregular, but the mean diurnal profile had similar afternoon peaks in both gas and particle concentrations, suggesting a photochemical source in both cities. LA formic acid particle/gas (p/g) ratios ranged between 0.01%-12%, with a median of 1.3%. No clear evidence that LA formic acid preferentially partitioned to particle water was observed, except on three overcast periods of suppressed photochemical activity. Application of Henry's Law to predict partitioning during these periods greatly under-predicted particle phase formate

concentrations based on bulk aerosol liquid water content (LWC) and pH determined from thermodynamic models. In contrast to LA, formic acid partitioning in Atlanta appeared to be more consistently associated with elevated relative humidity (i.e., aerosol LWC), although p/g ratios were somewhat lower, ranging from 0.20%-5.8%, with a median of 0.8%. Differences in formic acid gas absorbing phase preferences between these two cities are consistent with that of bulk water-soluble organic carbon, which is potentially attributed to the contrasting volatile organic compounds (VOC) mixture between the two cities, i.e. the predominance of anthropogenic precursors in LA and the uniquely abundant biogenic emissions in Atlanta.

In addition to SOA formation behavior, light-absorbing properties of the soluble organic aerosols also revealed contrasting features in the comparative study between Atlanta and LA [*Zhang et al.*, 2013]. Light absorbing organic carbon, often termed brown carbon (BrC), has the potential to significantly contribute to the visible light absorption budget, particularly at shorter wavelengths. Currently, the relative contributions of particulate brown carbon to light absorption, as well as the sources of brown carbon are poorly understood. With this in mind field measurements were made at three ground sites in Georgia: a typical urban central site (JST), a roadside site adjacent to a major highway near the city center (RS), and a rural site (Yorkville). Size-resolved atmospheric aerosol samples were collected using a cascade impactor and analyzed for water-soluble organic carbon (WSOC), organic and elemental carbon (OC and EC), and solution light absorption spectra of water and methanol extracts. Absorption refractive indices of the organic extracts were then calculated from solution measurements for a range of wavelengths and used with Mie theory to predict the light absorption by fine particles comprised of these components, under the assumption that brown carbon and other aerosol components were externally mixed. For all three sites, chromophores were predominately in the accumulation mode with an aerodynamic mean diameter of 0.5 µm, an optically effective size range resulting in predicted particle light absorption being a factor of 2 higher than bulk solution absorption. Predicted brown carbon absorption at 350 nm contributed a significant fraction (20 to 40%) relative to total light absorption, with highest contributions at the rural site where organic to elemental carbon ratios were highest. Brown carbon absorption, however, was highest by the roadside site due to vehicle emissions. Overall, this study established a connection on how to estimate light absorption of ambient brown carbon aerosols from solution extracts. The direct measurement of brown carbon in solution definitively shows that it is present and this Mie analysis suggests it is optically important in the near UV range in both rural and urban environments during summer when biomass burning emissions are low.

The prevalence of brown carbon in the free tropospheric column was then investigated through filter samples collected from the DC-8 research aircraft operating over central USA, during DC3 campaign in summer 2012. In this study, spectrophotometric absorption measurements of methanol and water-extracts of bulk filter samples were analyzed to directly quantify the extent of BrC, and the conversion factor between solution extracted BrC level and that of ambient BrC aerosols from the MOUDI study were applied to estimate the optical importance of BrC. Data were segregated into biomass burning events and all else referred to as background conditions. BrC was found to be prevalent throughout the 1 to 13 km altitude measurement range, but highest in biomass burning plumes. In both background and biomass burning plumes

much of the BrC was not soluble in water and there is evidence that water-soluble BrC from biomass burning evolves to a more water-insoluble form with age. Estimates of aerosol optical absorption coefficients at 365 nm for black carbon (BC), and that of BrC were compared to estimates of ambient aerosol light absorption from a 3-wavelength Particle Soot Absorption Photometer (PSAP) extrapolating to 365 nm based on inferred absorption Ångström exponent (AAE). The relative contribution of directly observed BrC significantly increased with altitude, as did the deviation of PSAP AAEs from one. A closure analysis comparing the sum of BC and BrC to observed PSAP absorption was within 16% for background conditions and 19% for biomass burning. This data set indicates that PSAP AAEs larger than nominally 1 were due to the presence of BrC and that BrC is ubiquitous and optically important throughout the continental free troposphere.

CHAPTER 1

INTRODUCTION

1.1 Impacts of Atmospheric Aerosols

Aerosols, also known as particulate matter (PM), are solid and liquid particles suspended in a gaseous medium. Ambient aerosols are an important and ubiquitous component of earth's atmosphere, and have been extensively studied because of their significant influence on global climate, atmospheric chemistry and human health.

The effect of aerosol on global climate occurs through several different mechanisms, which can be divided into direct and indirect effects. The direct effects refer to the scattering, reflection and absorption of radiation by particles. For example, particles composed of elemental carbon (EC) absorb light and have a warming effect on the climate [*Hansen et al.*, 2000], while particles composed of sulfate (SO_4^{2-}) do not absorb light, but instead scatter it and thus have a cooling effect on climate [*Charlson et al.*, 1992]. Ambient aerosol populations are frequently chemically complex and often have both absorptive and scattering properties. In addition to the direct impact aerosols have on the radiation balance, atmospheric aerosols also have a substantial but highly uncertain indirect effect, by affecting cloud albedo and lifetime. The sum of each of these components, which separately can have a positive (warming) or negative (cooling) effect, determines the energy balance on Earth. This can be quantified as radiative forcing, a measure of the influence a given factor has in altering the balance of incoming and outgoing energy in the Earth-atmosphere system (IPCC, 2007). The radiative effect of aerosols contributes the largest degree of uncertainty in the prediction of global climate change due to anthropogenic activities (Figure 1.1).

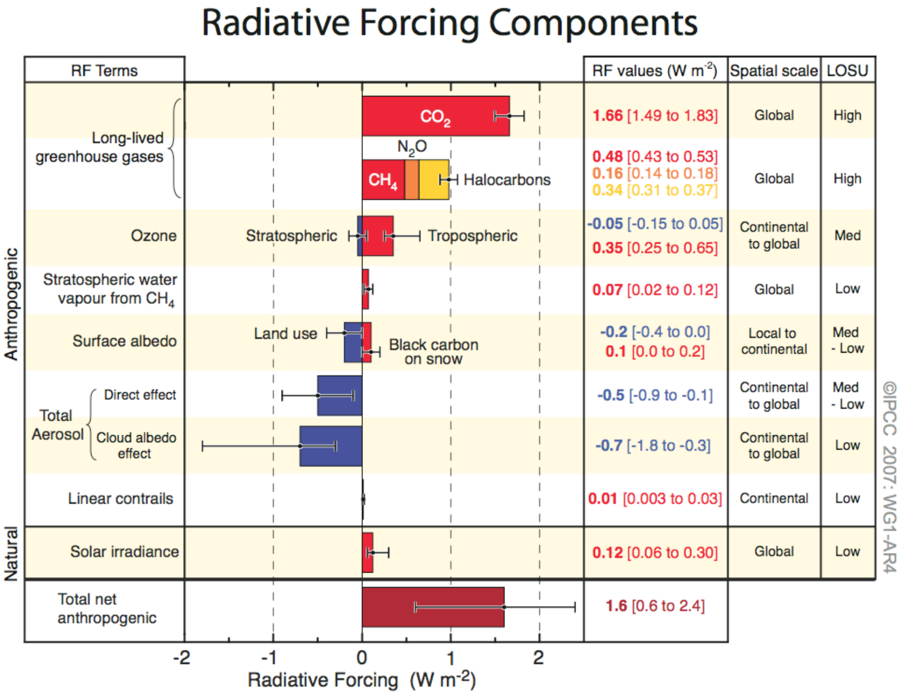

Figure 1.1 Global-average radiative forcing (RF) estimates and ranges in 2005 for anthropogenic emissions and other agents and mechanisms (IPCC, 2007).

Atmospheric aerosols also participate in heterogeneous chemical reactions, and affect the abundance and distribution of trace gases in the atmosphere [*Andreae and Crutzen*, 1997; *Haywood and Boucher*, 2000]. For example, stratospheric particles play a key role in ozone depletion. Aerosols can also act as sites for chemical reactions to take place.

Fine particles, the particulate matters with an aerodynamic diameter of less than or equal to 2.5μm (which is also known as $PM_{2.5}$), are of great health concern. Originating from a variety of both anthropogenic and natural sources, fine particles can contain hazardous inorganic and organic substances, such as heavy metals, benzene, polychlorinated biphenyls, and polycyclic aromatic hydrocarbons (PAHs). Numerous studies show that fine air particulate matter and traffic-related air pollution are correlated with severe health effects, including enhanced mortality, cardiovascular, respiratory, and allergic diseases [*Dockery et al.*, 1993; *Pope et al.*, 2002].

1.2 Organic Aerosols

Atmospheric aerosols are composed of inorganic compounds and organic compounds. Organic aerosols (OA) constitute a substantial fraction of atmospheric fine particulate matter, approximately 20-50% of aerosol mass at continental mid-latitudes [*Kanakidou et al.*, 2005] and even up to 90% in tropical forested areas [*Andreae and Crutzen*, 1997; *Roberts et al.*, 2001]. The presence of organic compounds in the particulate matter affects some important properties of aerosols such as hygroscopicity [*Novakov and Corrigan*, 1996] and thus cloud condensation nuclei activity [*Asa-Awuku et al.*, 2008].

Organic aerosols that are directly emitted by a variety of sources into the atmosphere are referred to as Primary Organic Aerosol (POA). The sources of POA include biomass burning, fossil fuel combustion, cigarette smoking, food cooking and primary biogenic aerosols [*Kanakidou et al.*, 2005 and references therein]. Organic aerosols that are transferred to particle phase from gas phase as products of homogeneous/heterogeneous oxidation of volatile and semi-volatile organic precursors are referred to as secondary organic aerosols (SOA). Studies suggest that SOA can be a significant fraction of $PM_{2.5}$ mass and thus a major contributor to the poor air quality under various conditions [*Zappoli et al.*, 1999; *Decesari et al.*, 2001], especially during summer when more intensive photochemical processes lead to highly oxidizing conditions. *Lim and Turpin* [2002] reported that SOA comprised approximately half of the total OA in metro Atlanta during summer. In rural areas, due to the lower concentration of primary OC, secondary OC fraction could be even larger [*Weber et al.*, 2007].

Estimates of global SOA production have been made by two major approaches. The traditional approach is a bottom-up estimate that combine biogenic and/or anthropogenic VOC precursor fluxes with laboratory data from oxidation experiments that lead to SOA formation, to obtain a global organic aerosol yield [*Chung and Seinfeld*, 2002; *Kanakidou et al.*, 2005; *Henze et al.*, 2008]. An alternative approach is a top-down inverse estimate based on constraining the eventual fate of known precursor emissions to infer the total SOA production rate [*Goldstein and Galbally*, 2007]. It has been shown that top-down estimates lead to higher estimates for SOA, which are approximately an order of magnitude larger than the bottom-up estimates. The difference clearly suggests that SOA production estimated by chamber oxidation experiments employing current SOA formation mechanisms has a substantial uncertainty, which also hinders an accurate estimate of global OA budget.

In addition to the global budget, the optical properties of organic aerosols are not well understood either, which leads to uncertainty in considering the role that organic aerosols play in global radiative balance. Organic aerosols have long been treated as only scattering in most radiative models, until recent studies found that light absorption by organics is ubiquitous, especially in UV ranges. Those light-absorbing organic aerosols are called “brown carbon”, due to the brownish color in visual appearance. Despite increasing interest in BrC aerosols and their effect on radiative forcing, there still exists a high degree of uncertainty about their properties, including origins, chemical compositions, emission inventories, optical properties as well as relative importance in global radiative forcing [*Alexander et al.*, 2008; *Andrea and Gelencser*, 2006].

On account of the important local, regional and global impacts of atmospheric organic aerosols, an in-depth understanding and a more accurate evaluation of the chemical and optical properties of SOA, including the production and evolution processes, will not only greatly reduce the uncertainty associated with climate change predictions, but are also informative for improving local air quality and human health.

1.3 Formation of Secondary Organic Aerosols

The mechanisms leading to the formation of secondary organic aerosol (SOA) are an important piece in the overall puzzle of the effect of aerosols on climate change. The traditional view is that SOA formation is dominated by gas-phase oxidation of volatile organic compounds (VOCs). The precursor volatile organic compounds (VOCs) of SOA are derived from a variety of natural and anthropogenic sources, including biogenic hydrocarbons, such as isoprene [*Kroll et al.*, 2006], monoterpenes [*Hoffmann et al.*, 1997; *Ng et al.*, 2007] and sesquiterpenes [*Cahill et al.*, 2006], as well as aromatic compounds [*Odum et al.*, 1997] and possibly a host of other unidentified semi-volatile organic species from anthropogenic emissions [*Robinson et al.*, 2007; *de Gouw et al.*, 2011]. The parent organic gases are then oxidized by atmospheric oxidants such as the hydroxyl radical (OH), ozone (O_3) and the nitrate radical (NO_3). Some of their oxidation products are believed to have low volatilities, then partition between gas and particle phases to form SOA. This formation pathway has been widely accepted and investigated by a series of smog chamber experiments as well as field measurements [*Seinfeld and Pankow*, 2003; *Kanakidou et al.*, 2005].

An increasing body of evidences suggested another formation pathway that involves heterogeneous reactions between semi-volatile condensed SOA products to yield compounds of much lower volatility (e.g., oligomer and polymer). This mechanism may account for the higher SOA yields based solely on traditional gas-phase chemistry [*Kanakidou et al.*, 2005]. The reactions that have been studied include the oligomerization of carbonyl + alcohol, carbonyl + gem-diol (or alcohol-ROH), and carboxylic acid + alcohol compounds [*Ervens and Kreidenweis*, 2007; *Mang et al.*, 2008].

Apart from the above-mentioned pathways, growing laboratory and field evidence support that a large amount of SOA is formed through aqueous phase chemistry in cloud and/or fog [*Ervens et al.*, 2008]. The SOA produced by cloud processing is mostly low volatility carboxylic acids such as oxalic acid [*Sorooshian et al.*, 2007]. This formation mechanism is currently missing from atmospheric models, leading to an underestimation of total SOA concentration.

Due to its complexity, SOA formation in the ambient atmosphere is still poorly understood. Current models employing these mechanisms tend to predict far less SOA concentrations systematically than observed [*de Gouw et al.*, 2005; *Volkamer et al.*, 2006]. The cause(s) of this divergence is still not clear: aside from uncertainties in the partitioning models, other factors, e.g., additional SOA precursors currently not considered and included, could be responsible [*Volkamer et al.*, 2009]. Furthermore, the relative importance of these competing reactions depends on the structure of the VOC and on the ambient conditions. Nevertheless, the semi-volatile nature of SOA has not been well studied, which leaves the gas/particle partitioning behavior of SVOCs unclear. Due to the variability of organic compounds involved in partitioning and the complexity of realistic atmospheric conditions, considerable uncertainty is present in the SOA formation processes. Further studies are needed to identify the important formation route of ambient SOA.

1.4 Light Absorption of Organic Aerosols

The climate impact of organic aerosols is highly uncertain. Organic aerosols have always been treated as only scattering in most radiative models, while black carbon (BC) is considered as the light absorber among aerosols. Recent studies found that light absorption by organics is ubiquitous, especially in the ultraviolet range, which is important since it may affect photochemistry and thus reduce tropospheric ozone concentration [*Jacobson*, 2001]. Those light absorbing organics are also termed as brown carbon (BrC).

BrC is a recently introduced name for a class of light-absorbing carbonaceous material, which, unlike BC, has an imaginary part k of its refractive index that increases towards shorter visible and UV wavelengths resulting in an absorption Ångström exponent (*AAE*) much larger than one and a brownish or yellowish color in visual appearance [*Alexander et al.*, 2008; *Luckas et al.*, 2007; *Andrea and Gelencser*, 2006]. In contrast the absorption Ångström exponent of pure BC is close to 1.

A variety of studies have investigated sources of brown carbon. Incomplete and smoldering combustion of hydrocarbons, especially those associated with biomass burning, is known to directly produce particulate brown carbon [*Hoffer et al.*, 2006; *Lukacs et al.*, 2007]. There is also evidence based on ambient studies for a secondary source [*Duarte et al.*, 2005] and laboratory studies show formation of chromophores (components of molecules that absorb light) through a variety of mechanisms, including ozonolysis of terpenes subsequently aged in the presence of ammonium ions and humidity [*Bones et al.*, 2010], and a variety of additional aqueous phase reactions, such as lignin [*Hoffer et al.*, 2006] and isoprene oxidation [*Limbeck et al.*, 2003], and reactions of carbonyls (e.g., glyoxal, methyglyoxal) in acidic solutions [*Sareen et al.*, 2010], with amino acids [*de Haan et al.*, 2009a], methyl amines [*de Haan et al.*, 2009b], or ammonium salts [*Sareen et al.*, 2010]. These aqueous reactions not only produce brown carbon but also other characteristics associated with HUmic-LIke Substances (HULIS), such as higher molecular weight and surface-active properties [*de Haan et al.*, 2009a, 2009b; *Sareen et al.*, 2010]. The chemical properties of brown carbon could help understand the formation/sink processes, lifetime of brown carbon and therefore influence the climate impacts.

Despite increasing interest in BrC aerosols and their effect on radiative forcing, the determination of BrC is currently controversial. Particle light absorption coefficients

(b_{ap}) are typically measured using optical instruments, which operate at a fixed number of wavelengths and quantify the "total" absorption by brown carbon together with black carbon, then subtract BC assuming an *AAE* to extrapolate from visible wavelengths [*Sandradewi et al.*, 2008]. However, quantifying brown carbon is extremely difficult, since potential range of *AAE* for BC in the atmosphere can reasonably lead to ~20% uncertainty in BC absorption in UV wavelengths [i.e., *Lack et al.*, 2013], not mentioning the possible amplifying of absorption by lensing effect [*Cappa et al.*, 2012]. Furthermore, most optical instruments suffered from limited numbers of operating wavelengths.

On the other hand, BrC could be determined by directly measuring light-absorbing chromophores in aerosol extracts since the method isolates BrC from other absorbers. The use of spectrometer and long path absorption cells provide wavelength-resolved, highly sensitive results, in contrast to the several fixed wavelengths by optical instruments [*Hecobian et al.*, 2010]. Brown carbon investigated by dissolution extracts could provide some insights on the chemical properties, formation process of brown carbon as well as its toxicity. *Zhang et al.* found a significantly difference in the mass absorption efficiencies of water-soluble brown carbon (6 to 7 times higher in Los Angeles compared to Atlanta) [*Zhang et al.*, 2011], potentially due to various SOA precursors. *Verma et al.* [2012] showed that BrC is correlated with dithiothreitol (DTT) activity, a measure of oxidative potential of aerosols. However, this method also loses some information of aerosols, including the mixing state, and morphology. Extracts-based measurements are inherently more prone to artifacts as they take particles out of their natural suspended state and dissolve them into solutions. Therefore, a more detailed investigation on the aerosol characteristics, including the size distribution, mixing state, and optical properties in the atmosphere, would be essential in understanding the role of brown carbon in a climate perspective.

1.5 Motivation and Scope of This Work

This dissertation investigates several important aspects of aerosols in the ambient environment, including both formation/partitioning characteristics of secondary organic aerosols, and optical properties of light-absorbing organic aerosols. Specific questions that will be addressed in this work include:

- Does formic acid behave similarly in gas/particle partitioning with WSOC in Atlanta and LA? Can the gas/partitioning behavior of a single compound be explained by thermodynamic theories?
- What are the controlling factors of SOA formation in LA? Is aqueous chemistry an important SOA formation route in LA? How about Atlanta?
- What is the size distribution of ambient brown carbon? And can the light absorption coefficients of ambient brown carbon be directly quantified based on aerosol solution extracts? Is the estimated brown carbon absorption consistent

with results from optical instruments?

- What is the distribution of brown carbon in the free troposphere? Is it important relative to BC? To what extent does brown carbon contribute to ambient aerosol light absorption?
- Can light-absorbing properties of organic compounds provide insights on the sources and formation of SOA?

Through conducting online and offline ambient measurements of gas-phase and particle-phase components, this study addresses the essential scientific questions listed above by providing detailed analyses and thorough discussions on the observational results. Specifically, this thesis evaluates and compares the gas/particle partitioning behavior of formic acid and that of WSOC (as a quantitative measure of SOA) in Atlanta and LA, and also applied thermodynamic principles to assess the formation preference of SOA in environments with different emission sources (Chapter 2). To bridge the gap between light absorption of brown carbon in solution extracts and ambient aerosols, a cascade impactor was used to gain knowledge about size distribution of ambient brown carbon, which was later applied into Mie theory to estimate brown carbon absorption of ambient particles. Predicted light absorption was roughly two times greater than the bulk solution light absorption, and this factor is consistent over a range of wavelengths (350 to 570 nm) at different sites including both urban and rural (Chapter 3). This conclusion was then applied to aircraft-collected filter samples throughout the free troposphere (up to 13 km) to investigate the vertical distribution of brown carbon (Chapter 4). Brown carbon was found to be prevalent and the relatively uniform profile with altitude (compared with the sharply decrease of BC) suggests secondary sources of organics in the atmosphere, possibly due to aqueous chemistry in liquid clouds. The samples were also segregated into different periods: biomass burning events and background tropospheric conditions. In both cases, estimated brown carbon absorption is in good agreement with BC and total aerosol absorption determined by optical instruments, indicating the conversion factor is reasonable to apply to ambient aerosols. The comparison of brown carbon to total aerosol absorption suggests that the contribution of brown carbon is not negligible, either secondary aerosols (Chapter 3) or aerosol largely impacted by primary emissions (Chapter 4), and the relative importance increases with altitude.

CHAPTER 2

GAS-PARTICLE PARTITIONING OF FORMIC ACID IN LOS ANGELAS AND ATLANTA

2.1 Background Information

Organic acids are a common component of ambient air [*Chebbi and Carlier*, 1996; *Sullivan and Weber*, 2006] and a range of acids has been detected and reported in remote, rural, polar, marine and urban environments in the gas phase as well as in clouds and in aerosols [*Khare et al.*, 1999; *Paulot et al.*, 2011; *Sorooshian et al.*, 2007]. Previous studies have shown that organic acids contribute significantly to the ionic composition in the atmosphere, represent a major fraction of the water-soluble organic carbon and take part in photochemical reactions and therefore their role in atmospheric transformations is potentially of great importance [*Chebbi and Carlier*, 1996; *Khare et al.*, 1999; *Sommariva et al.*, 2011]. Oxalate is often the most abundant aerosol organic acid identified [*Myriokefalitakis et al.*, 2011], whereas formic and acetic acids are amongst the most abundant gas phase organic acids and are ubiquitous in the aerosol phase but generally are minor mass fractions due to their high volatility [*Khare et al.*, 1999; *Loflund et al.*, 2001].

Formic acid has both primary and secondary sources [*Chebbi and Carlier*, 1996; *Khare et al.*, 1999; *Paulot et al.*, 2011]. The primary sources include fossil fuel combustion [*Khare et al.*, 1999; *Talbot et al.*, 1988], biogenic emissions [*Talbot*, 1990; *Kesselmeier et al.*, 1998; *Kesselmeier*, 2001] and biomass burning emissions [*Goode et al.*, 2000; *Christian et al.*, 2003; *Yokelson et al.*, 2009]. Secondary sources of formic acid involve photo-oxidation of volatile organic compounds (VOCs), such as the oxidation of alkenes and monoterpenes by ozone or OH radicals [*Madronich and Calvert*, 1990; *Neeb et al.*, 1997; *Lee et al.*, 2006], as well as aqueous phase degradation of larger organic components from photo-oxidation of semi-volatiles [*Ervens et al.*, 2008; *Paulot et al.*, 2011]. Recently the ageing of organic aerosols has also been proposed as a major global source of formic acid [*Paulot et al.*, 2011].

In highly polluted urban environments, typical concentrations of gaseous formic acid (HCOOH) can be up to several ppbv [*Khare et al.*, 1999; *Veres et al.*, 2011], while concentrations in the condensed phase, measured as the formate anion ($HCOO^-$), can reach tens of ng/m^3 [*Chebbi and Carlier*, 1996; *Khare et al.*, 1999]. Aerosol formate is typically about two orders of magnitude lower than formic acid gas phase concentrations [*Baboukas et al.*, 2000]. Most previous work on formic acid gas-particle partitioning was based on gas phase measurements using scrubbers (e.g., mist chambers) and particle phase measurements by integrated filter collection. These studies have found a higher fraction of formic acid in the condensed phase in winter than summer, apparently due to reduced saturation vapor pressures at lower temperatures [*Chebbi and Carlier*, 1996;

Khare et al., 1999]. Filter sampling, however, constrains partitioning studies by only providing highly time-integrated data (e.g., 12 to 24 hour averages) and limits investigating the response of formic acid to diurnally changing meteorological parameters. In this study formic acid ambient concentrations and particle/gas (p/g) ratios are investigated using online measurement techniques in two contrasting cities, Los Angeles (LA), CA and Atlanta, GA. Los Angeles is an urban environment dominated by anthropogenic emissions, whereas Atlanta air quality is influenced by a mix of anthropogenic and biogenic emissions.

2.2 Experimental Methods

2.2.1 Sampling sites

Ground-based measurements were made in Pasadena, CA on the California Institute of Technology campus as part of the 2010 CalNex (Research at the Nexus of Air Quality and Climate Change) experiment from 15 May to 15 June 2010. Located within the Los Angeles Basin (here-after referred to as LA) approximately 16 km downwind of central LA, the site (34.140582 N, 118.122455 W) was regularly impacted by emissions transported from the source-rich downtown LA area [*Hersey et al.*, 2011; *Veres et al.*, 2011]. Following CalNex, a subset of the instruments were moved to Atlanta for continuous sampling between 3 August and 10 September 2010. Identical measurements between the two studies included gas and particulate formic acid and water-soluble organic carbon (WSOC), $PM_{2.5}$ inorganic anions, and $PM_{2.5}$ organic and elemental carbon (OC and EC, respectively). The Atlanta measurements were conducted from the roof of the Environmental Science and Technology Building (33.778427 N, 84.396181 W) on the Georgia Institute of Technology (GIT) campus (~30-40 m above ground level). A summary of instruments/sampling setups for both the LA and Atlanta studies is given in Table 2.1.

Table 2.1 Summary of instrumentation and approximate sampling geometries for the various species reported.

Analytical Technique	Inlet height above ground level (m)	Inlet Length (m)	Species Measured
CalNex (LA)			
NOAA-CIMS	5	1.5	Gaseous organic acids and nitric acid
GIT-CIMS	1.5	2	Gaseous organic acids
Mist chamber-TOC	7	12	$WSOC_g$
Sunset OC/EC	7	12	OC and EC
PILS-TOC	7	12	$WSOC_p$
PILS-IC	7	12	$PM_{2.5}$ anions (including organic acids)
HR-ToF-AMS	5	7	PM_1 non-refractory compounds
Atlanta			
GIT-CIMS	~30m / 1 m *	4	Gaseous organic acids
Mist chamber-TOC	~30m / 4 m *	8	WSOCg
Sunset OC/EC	~30m / 4 m *	8	OC and EC
PILS-TOC	~30m / 4 m *	8	WSOCp
PILS-IC	~30m / 4 m *	8	$PM_{2.5}$ anions (including organic acids)

* Sampling was from a penthouse rooftop laboratory located roughly 30m above ground level with the inlet 1 to 4 m above the roof surface.

2.2.2 Instrumentation

2.2.2.1 Gases

A suite of organic and inorganic acids were measured by negative ion-proton transfer-chemical ionization mass spectrometry (NI-PT-CIMS) through proton transfer with acetate ions and detection of the conjugate anion with a quadrupole mass spectrometer [*Veres et al.*, 2008]. Two NI-PT-CIMS were deployed in LA while only the Georgia Institute of Technology (GIT) CIMS was deployed in Atlanta. In LA, Formic acid was measured by both GIT and the National Oceanic and Atmospheric Association (NOAA) CIMS, which were in reasonable agreement with a slope of 0.95 and r^2 of 0.80 (Figure 2.1). Nitric acid was only measured by the NOAA CIMS at LA and no nitric acid data is available for the Atlanta study. Details of the sampling configurations are given in Table 2.1. The limit of detection (LOD) and measurement uncertainty is estimated at 0.02 ppbv and 25% for formic acid, respectively, and 0.08 ppbv and 37% for nitric acid by NOAA CIMS during CalNex-LA campaign, while the LOD of GIT CIMS was 0.02 ppbv in LA and 0.12 ppbv in ATL with an uncertainty of 30%.

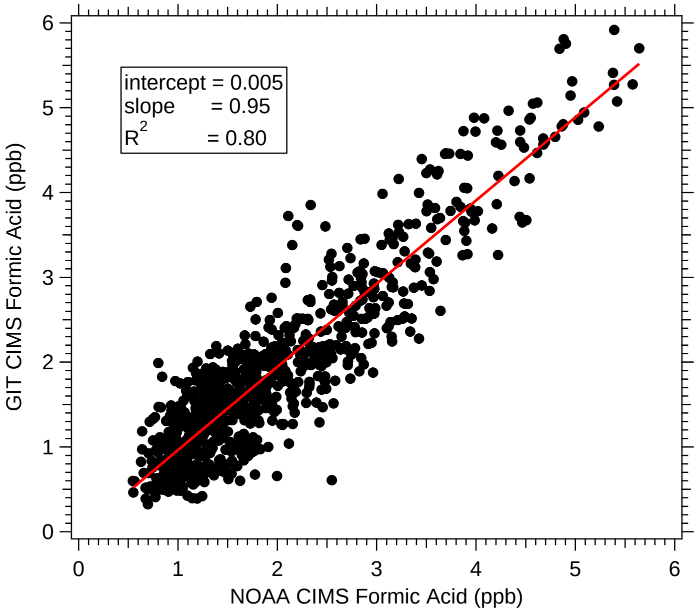

Figure 2.1 Calnex-LA study comparison between NOAA CIMS measurement and GIT CIMS measurement of gas phase formic acid.

Gas-phase water-soluble organic carbon (WSOC$_g$) was measured with a mist chamber [*Hennigan et al.*, 2008]. Air was sampled at roughly 21 ± 1 L/min and was first passed through a Teflon filter for particle removal and then scrubbed of soluble gases (gases with a Henry's Law constant greater than 10^3 M/atm) [*Spaulding et al.*, 2002] in a glass mist chamber [*Cofer and Edahl*, 1986] initially filled with 10 mL of ultra-pure deionized water (>18.0 MΩ-cm). WSOC$_g$ was then quantified with a Sievers Total Organic Carbon (TOC) analyzer (Model 800, GE Analytical Instruments; Boulder, CO) that was shared between the gas and particle WSOC instruments. Data were corrected by blank measurements performed prior to every mist chamber sampling cycle by loading the chamber with pure water, without sample airflow. The LOD and measurement uncertainty is estimated at 0.83 μgC/m^3 and 8%.

Along with the measurements of WSOC and formic acid, the mixing ratios for a variety of Volatile Organic Compounds (VOCs) were determined with a NOAA Gas Chromatography Mass Spectrometry (GC-MS) [*Gilman et al.*, 2009] during the CalNex-LA campaign. In both studies, meteorological data were provided by weather stations located on the respective campuses.

2.2.2.2 Aerosols

$PM_{2.5}$ soluble nitrate (NO_3^-) and formate ($HCOO^-$) concentrations, along with a range of other soluble anions, were determined using a Particle-Into-Liquid-Sampler coupled to an Ion Chromatograph (PILS-IC), similar to that described by *Orsini et al.* [2003]. Sample air was aspirated at 16.7 ± 0.7 L/min through a URG $PM_{2.5}$ cyclone, an parallel plate carbon denuder [*Eatough et al.*, 1993] and honeycomb acid (citric acid) and base (sodium carbonate) coated denuders, then mixed with water vapor near 100 ℃ generated from deionized water and the resulting droplets were collected by impaction. PILS liquid sample was analyzed online by a Dionex Ion Chromatograph (UTAC-ULP1 concentrator column, AG11guard column and AS11 anion column) using a gradient NaOH eluent procedure lasting 20 minutes. Systematic blank measurements were made throughout the study period by diverting sample flow through a HEPA filter downstream of the denuder and upstream of the PILS. A linear interpolation of blanks data was performed and subtracted from the ambient data. During the last several days of the study (12 June – 15 June, 2010), the inlet cyclone was alternated between cyclones of PM_1 and $PM_{2.5}$ cut sizes (URG) during daytime periods to investigate size-dependent concentration differences (this was done for anions, OC, EC, and particle WSOC). Sample heating due to the PILS particle condensation growth collection method may cause potential collection losses of semi-volatile components [*Sorooshian et al.*, 2006]. Of the measured compounds, the most susceptible is thought to be formate ($HCOO^-$) because it was the most volatile of the anions measured in this study. Sample heating may also promote some particulate organic constituents (e.g., glyoxylic acid) and oligomers to decompose and form small organic compounds prior to IC analysis, which might cause an over-estimation in formate [*Ervens et al.*, 2008]. Post study comparisons involving simultaneous ambient air sampling with a manually operated Mist Chamber, which does not heat the sample (in this case the Mist Chamber inlet filter was replaced with gas denuders) and PILS indicated that PILS formate concentrations can be systematically under-estimated by up to 30%. Data were not corrected for the potential systematic error. Random measurement uncertainty based on a quadrature sum of squares that included the precision of standards, variability in sample air flow rate, liquid flow rate, and blanks (all one standard deviation), was estimated at 13% for nitrate and 15% for formate. LODs are 0.03 $\mu g/m^3$ for nitrate and 0.02 $\mu g/m^3$ for formate, respectively.

A second PILS coupled to a TOC analyzer provided online measurements of $PM_{2.5}$ water-soluble organic carbon ($WSOC_p$) following methods implemented in previous studies [*Sullivan et al.*, 2004]. PILS-TOC included a URG $PM_{2.5}$ cyclone inlet and parallel plate carbon denuder upstream. An automated valve that directed sample flow through a Teflon filter located immediately upstream of the PILS and downstream of the denuders performed dynamic blanks twice daily. A linear interpolation between successive blanks was used to blank correct the online measurements. Instrument LOD and measurement uncertainty are estimated at 0.20 $\mu gC/m^3$ and 7%, respectively. More details on this measurement and discussion of WSOC partitioning results can be found in *Zhang et al.* [2012a].

A high-resolution time-of-flight aerosol mass spectrometer (HR-ToF-AMS, Aerodyne Research Inc., hereinafter "AMS" for short) was deployed in LA and provided measurements of non-refractory inorganic and organic aerosol components [*Hayes et al.*, 2012]. Ambient air was dried prior to sampling by the HR-ToF-AMS. The AMS measures submicron non-refractory species [*Canagaratna et al.*, 2007]. Differences in AMS and PILS upper size measurement limits and measurement of non-refractory versus soluble aerosol components likely account for the significant difference in nitrate concentrations measured by these two instruments while sampling at a site influenced by marine air masses; the linear regression (ODR fit) of AMS to PILS nitrate slope was 0.66 (r^2=0.86).

In the following analysis we interpret the AMS measurements to be dominated by volatile nitrate (i.e., ammonium nitrate) which is most important in the submicron mode, and the PILS both volatile and nonvolatile nitrate (e.g., ammonium nitrate plus sodium nitrate), the latter being more important in the 1-2.5 μm PM range [*Hayes et al.,* 2012]. AMS measurement uncertainty is estimated at 30% [*Middlebrook et al.*, 2012]. AMS/PILS sulfate were in good agreement, with regression slope of 1.01, and r^2 of 0.84.

$PM_{2.5}$ organic carbon and elemental carbon (OC and EC) were measured semi-continuously with a Sunset Labs OC/EC analyzer (Model 3F, Forest Grove, OR) following the NIOSH method [*NIOSH*, 1996]. Optical EC is used in this analysis since it was less noisy than thermal EC. A parallel plate carbon denuder [*Eatough et al.*, 1993] upstream of the instrument was installed to reduce positive sampling artifacts. Measurements were blank corrected based on systematic blank measurements made throughout the study period by installing a Teflon filter (47 mm dia., 2.0 μm pore size, Pall Life Sciences) on the cyclone inlet. A linear change in blank concentrations was assumed between consecutive blank measurements and was subtracted from the ambient data. OC blanks ranged from 1.3-2.6 μgC/m^3 and EC blanks varied from below LOD to 0.03 μgC/m^3. Uncertainty due to random measurement errors is estimated to be 28%; systematic errors due to particle volatility are possible [*Grover et al.*, 2009]. Significant discrepancies were observed between the AMS OA (organic aerosol mass, i.e., OM) and

Sunset Labs OC, with a study average OM/OC slope of 3.28 and r^2=0.76, where a slope closer to 2 is more realistic [*Turpin and Lim*, 2001; *Hayes et al.*, 2012]. Possible explanations include the loss of semi-volatile compounds from the collection filter media within the OC/EC analyzer or due to the presence of the denuder [*Grover et al.*, 2009], or other possible unidentified systematic errors associated with the measurements.

2.3 Results

2.3.1 Los Angeles Diurnal Variation in Air Pollutants Concentrations

As a coastal city with clean upwind sector (Pacific Ocean) and a basin-shaped topography, LA has been observed to have a regular and distinct diurnal pattern in air pollutants. Emissions from the western regions of the LA Basin were transported across the basin in a northeastward direction by land-sea breezes on a daily basis [*Veres et al.*, 2011]. The CalNex-LA sampling site at Pasadena, CA, located ~16 km NE of downtown LA, is a receptor of gaseous and particulate pollutants transported from downtown LA. The arrival of transported emissions is readily observed in the diurnal profiles of primary emissions (Figure 2.2). Acetylene and $PM_{2.5}$ EC reached daily maximum concentrations in Pasadena between 12:00 and 13:00 PDT after being transported from downtown LA over the course of a few hours. Only minor enhancements were observed between 6:00 and 9:00 PDT from local morning rush-hour traffic.

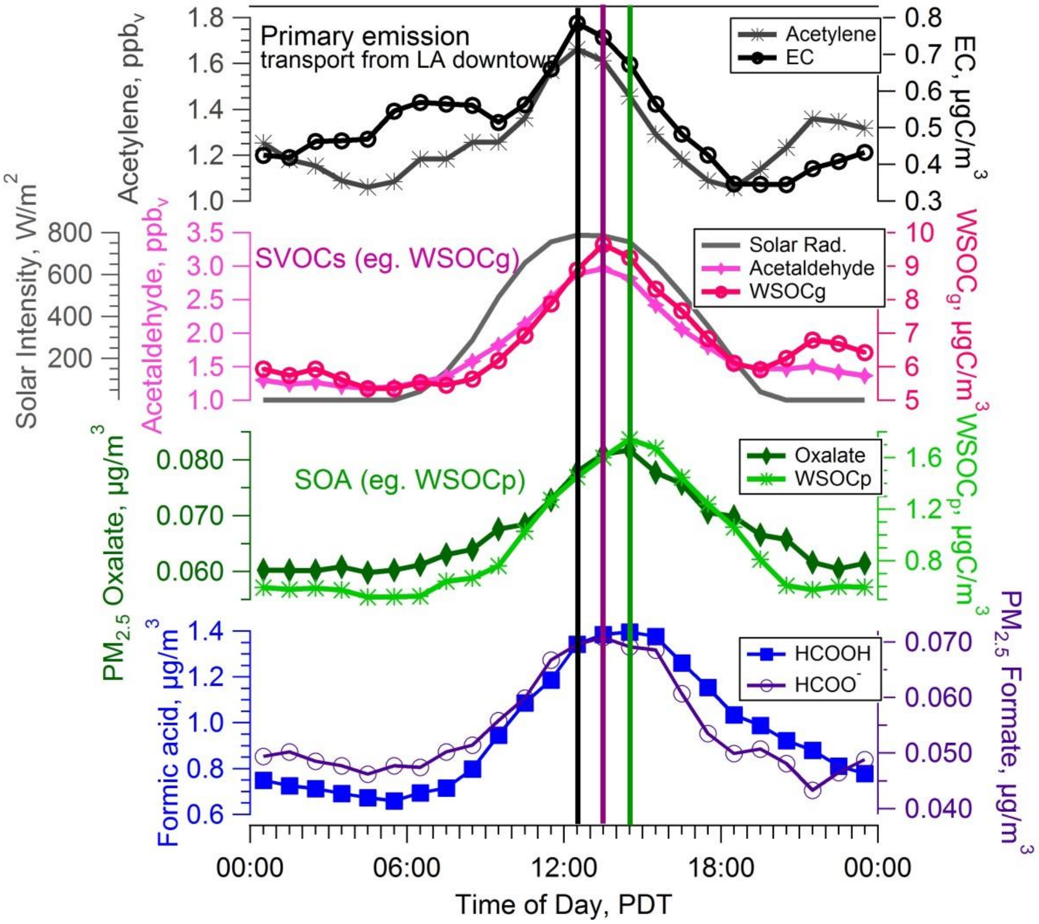

Figure 2.2 Los Angeles diurnal profiles of selected primary, secondary gases and particles, and gas and particle formic acid measured during CalNex. Means of hourly-binned data are plotted.

Secondary gas and aerosol components followed behind the arrival of primary species, coupled to both transport and photochemical processes. Diurnal maximum concentrations of gaseous photochemical products, such as acetaldehyde, formic acid, and WSOC$_g$, occurred at 13:30 PDT, which is near the peak for solar insolation and after primary emissions reached their peak (Figure 2.2). Secondary organic aerosol components, including oxalate and WSOC$_p$, then followed the secondary gases, with daily maximum concentrations approximately 1 hour later than the gases, indicating a gas-to-particle conversion process (Figure 2.2).

The complete study time series shows that gas and particle phase formic acid had consistent and clear diurnal trends (Figure 2.3). Both gas and particle phase formic acid followed other photochemical gas/particle products with peak concentrations in the early afternoon (Figure 2.2). However, the diurnal trends in both gas and particle phase formic acid were generally broader than other secondary gas and particle species (e.g., WSOC), and particle formic acid had a daily concentration peak that was closer in time to the peak of the gas phase components (13:30 PDT), compared to other SOA components ($WSOC_p$, oxalate) that were peaking at ~14:30 PDT (Figure 2.2).

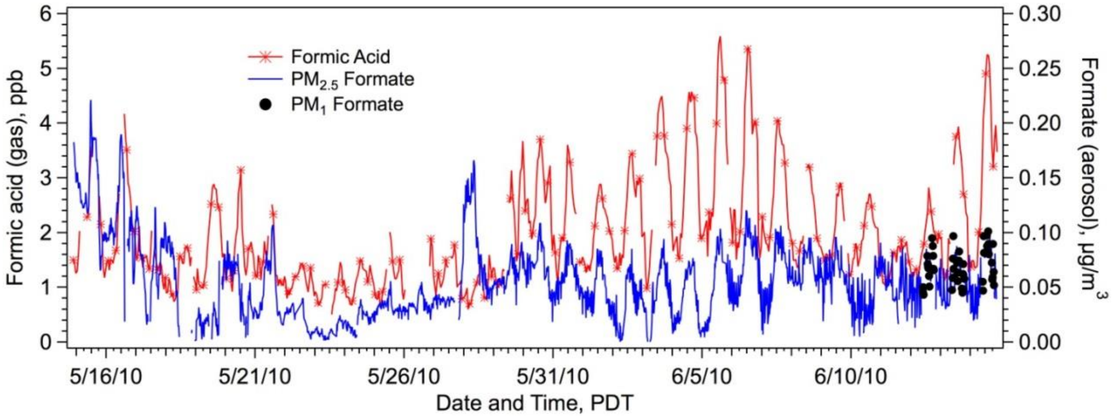

Figure 2.3 Los Angeles time series of gaseous (HCOOH) and particulate ($HCOO^-$) formic acid measured during CalNex (15 May 2010 to 15 June 2010) on the campus of the California Institiue of Technology. At the end of the study (12 June – 15 June 2010), the formate sample inlet was alternated between a PM_1 and $PM_{2.5}$ cyclone during daylight sampling periods.

For the entire CalNex-LA study, gaseous formic acid was in the range of 0.37 ppbv to 5.86 ppbv and had an average concentration of 1.89±0.59 ppbv (mean ±1σ, n=731) (see Table 2.2 for a summary). The data are consistent with previous studies in urban environments [*Kawamura et al.*, 1985; *Grosjean et al.*, 1988]. For the aerosol phase, the range of $PM_{2.5}$ formate concentrations observed during the entire campaign was from the LOD (0.02 $\mu g/m^3$) to 0.21 $\mu g/m^3$, and the mean formate concentration was 0.054 $\mu g/m^3$. Most formate was associated with particles below 1 μm since little difference was observed between PM_1 and $PM_{2.5}$ concentrations ($PM_1/PM_{2.5}$ mean ~ 104% ± 23%, n=48), when PM_1 and $PM_{2.5}$ cyclones were interchanged during daylight periods of the final week of sampling (Figure 2.3).

Table 2.2 Summary of gas and particulate phase formic acid concentrations and partitioning ratio (p/g, given in %), for Los Angles (LA) and Atlanta (ATL).

	mean	median	min	max	Stdev
Concentrations					
Formic acid (HCOOH), LA, ppbv	1.89	1.61	0.37	5.86	0.59
Formic acid (HCOOH), ATL, ppbv	2.79	2.29	0.12	7.93	1.01
Formate ($HCOO^-$), LA, ng/m^3	54	49	LOD*	210	34
Formate ($HCOO^-$), ATL, ng/m^3	43	39	LOD*	130	21
Formic acid p/g in percentage in LA					
p/g for whole campaign, %	1.64	1.31	0.01	11.9	1.35
p/g during night (8pm-8am next day**), %	1.84	1.43	0.01	11.9	1.61
p/g during day (8am-8pm), %	1.38	1.24	0.05	8.63	0.87
p/g during overcast periods, %	3.67	2.88	0.43	11.9	2.64
Formic acid p/g in percentage in ATL					
p/g for whole campaign, %	1.08	0.83	0.20	5.83	0.74
p/g during night (8pm-8am next day***), %	1.33	1.10	0.35	5.83	0.85
p/g during day (8am-8pm), %	0.82	0.69	0.20	3.53	0.49

*LOD =0.02 μg/m^3

**Sampling times are in PDT (Pacific Daylight Time).

***Sampling times are in EDT (Eastern Daylight Time).

Formic acid was predominately found in the gas phase with particle-to-gas (p/g) ratios typically between 1 to 2% throughout the study (Table 2.2), similar to what has been reported in previous studies [*Chebbi and Carlier*, 1996; *Loflund et al.*, 2001]. The high volatility and resulting minor partitioning to the particle phase may partially explain why the average diurnal trend of particle formic acid tended to track the gas phase species, instead of other SOA components that probably undergo further partitioning processes, such as oxalate and $WSOC_p$ (WSOC p/g ratios are closer to 10 to 20% [*Zhang et al.*, 2012a]).

The LA study mean ± standard deviation formic acid p/g ratio was 1.6% ± 1.3%, but at times it reached up to 10%. Highest partitioning to the particle phase observed in LA occurred during a few unique periods when partitioning to liquid water was most apparently observed. Factors that may contribute to this variability are investigated.

2.3.2 Los Angeles Formic Acid Partitioning

Gas-phase formic acid could partition to the particle phase through absorption to the preexisting organic phase, or undergo dissolution into aerosol water, or some combination of both. A schematic of possible partitioning routes for formic acid is shown in Figure 2.4. Due to its high solubility (Henry’s law constant at 20°C is ~5x10^3 M/atm [*Johnson et al.*, 1996; *Keene et al.*, 1995]), partitioning to the aqueous fraction of aerosols may be expected if particle water is present. *Chang et al.* [2010] performed a model simulation of overall SOA formation in the Los Angeles basin and found that SOA partitioning to both organic and aqueous phases are important and that the aqueous phase becomes more important during periods of low SOA concentrations. Similar behavior was observed for formic acid in this study.

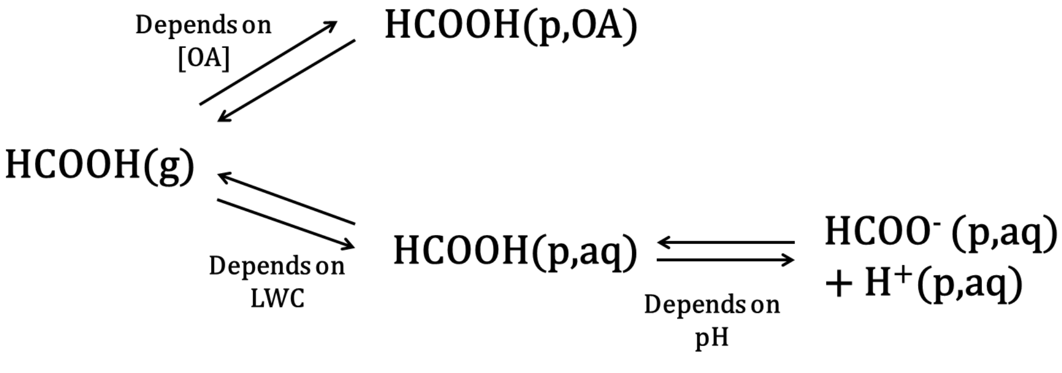

Figure 2.4 Schematic representation of possible partitioning routes for formic acid. OA stands for the total organic aerosol mass, of some sub-fraction that formic acid could partition to, while (p, aq) represents another route where formic acid undergoes dissolution into aerosol water and then resides in the condensed phase.

The regular LA diurnal temperature and relative humidity (RH) trends are shown in Figure 2.5. During CalNex RH often reached over 90% by midnight and remained at or near saturation levels until sunrise. RH rarely fell below 60% at its lowest point in mid-afternoon (Figure 2.5). Despite the expected higher nighttime particle water concentrations and formic acid's relatively high solubility, observed formic acid p/g ratios generally did not have a strong dependence on time of day (Figure 2.6a), or RH (Figure 2.7a), although p/g ratios were slightly more variable at night when RH was highest (Figure 2.6a). Part of this variability in the average diurnal profile occurred during unique isolated periods of overcast conditions when formic acid p/g ratios did follow RH trends. The median p/g value ranged from 1.33%-1.77% at night (20:00-08:00 PDT) and 1.15%-1.43% during day (08:00-20:00 PDT). However, during the three overcast periods shown in Figure 2.5 (14:30 May 17 to 9:30 May 18, 22:30 May 27 to 15:30 May 28, and 12:30 June 10 to 12:30 June 11, 2010, PDT), the p/g ratio was substantially higher than the study mean values (Figure 2.6b and 2.7b). Apart from these unique episodes, the formic acid p/g ratio seemed largely independent of RH (e.g., particle water) suggesting partitioning to some other phase, likely the organic aerosol phase.

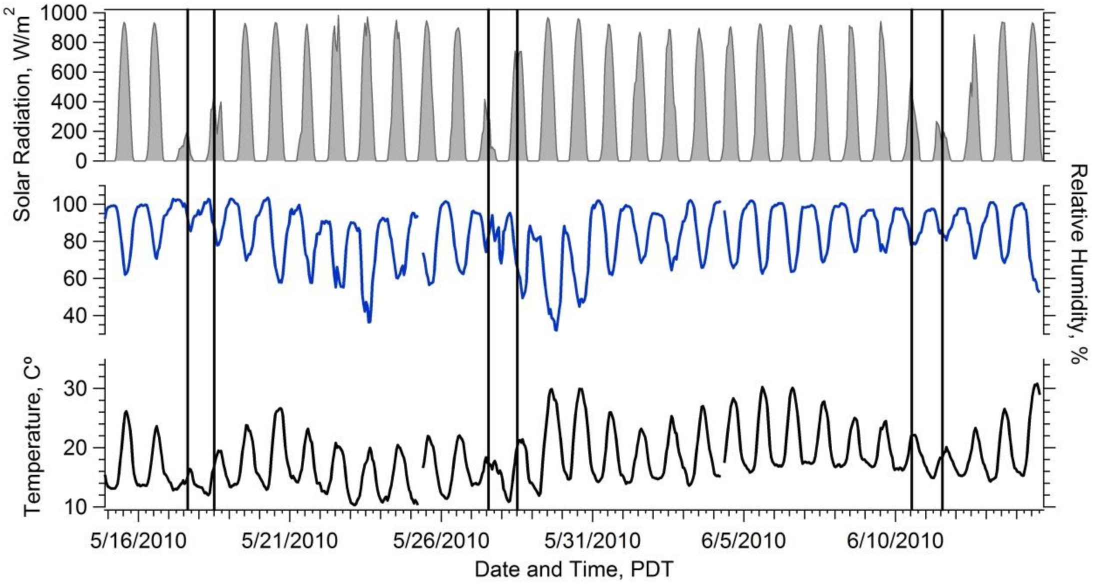

Figure 2.5 Los Angeles time series of solar radiation, temperature and relative humidity during the CalNex-LA campaign (15 May 2010 to 15 June 2010), with three overcast periods (14:30 May 17 to 9:30 May 18, 22:30 May 27 to 15:30 May 28, and 12:30 June 10 to 12:30 June 11, 2010, PDT) identified by times between vertical lines.

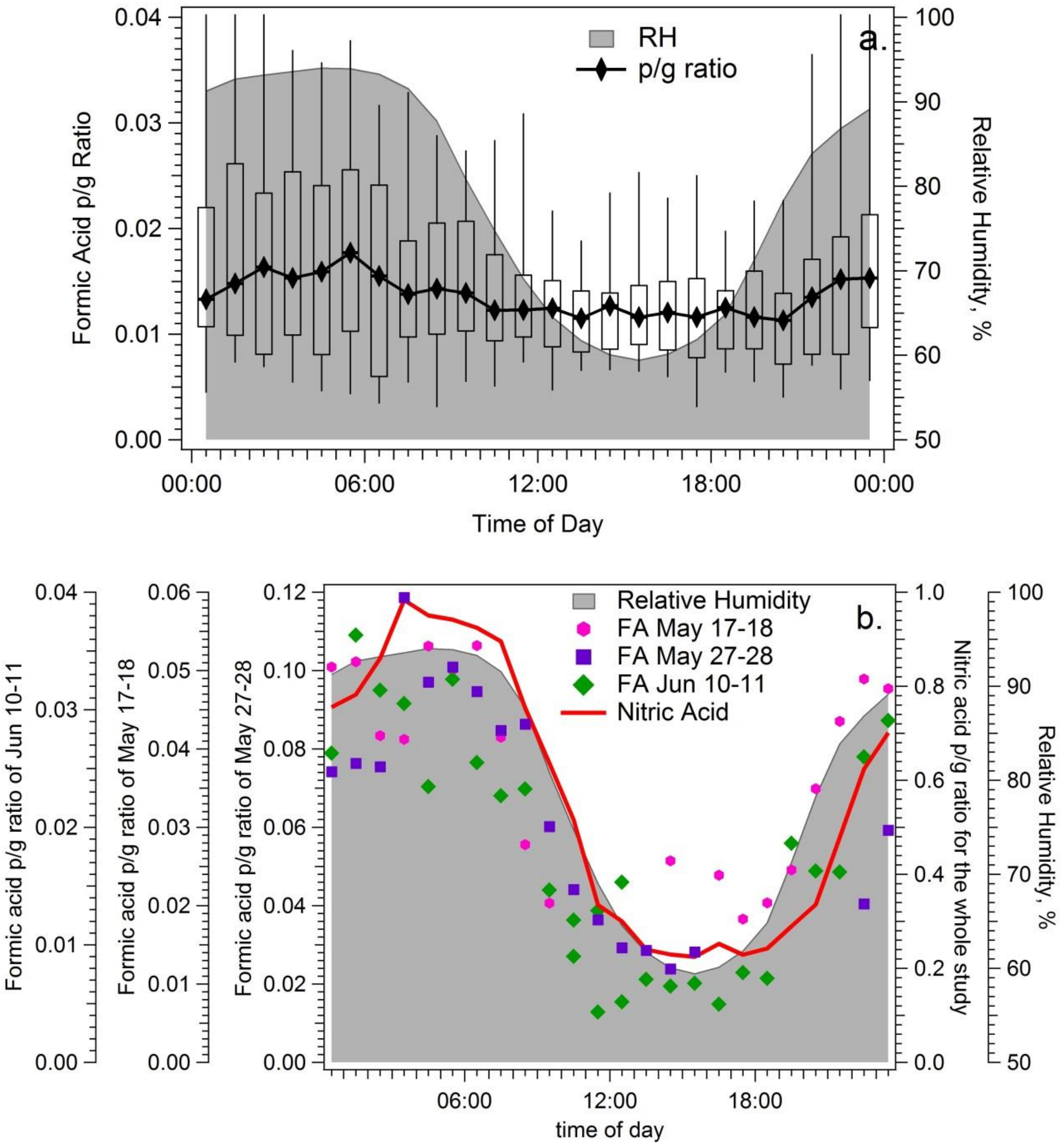

Figure 2.6 Los Angeles (a) Diurnal profile of formic acid p/g ratios and RH, and (b) Hourly averaged data for the three overcast periods as well as the diurnal profiles of nitric acid p/g ratio and RH. In (a), median values (data point within box), 25th and 75th percentiles (lower and upper box bounds), and 10th and 90th percentiles (lower and upper whiskers) of hourly-binned data are plotted. Note the p/g scale differences in graphs (a) and (b).

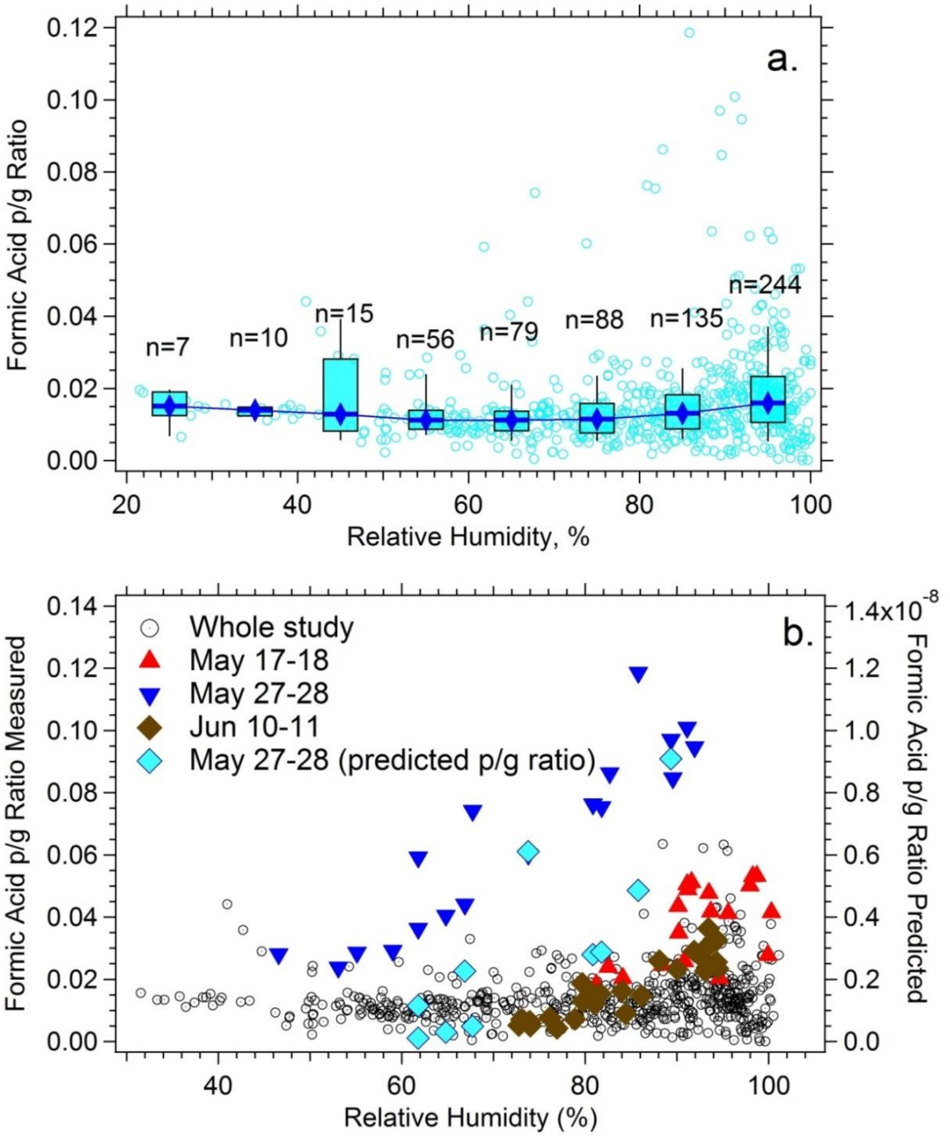

Figure 2.7 CalNex-LA formic acid p/g ratios as a function of RH with (a) p/g statistical results for data binned by 10% RH intervals with number of data points in each bin given, and (b) All data and specific overcast periods identified in Figure 2.5, as well as formic acid p/g ratio predicted by Henry's law during overcast period May 27-28. Box plot description is given in Figure 2.6.

In the following analysis, formic acid partitioning is investigated for the two types of periods that have been discussed; (1) when formic acid appeared to be related to RH (partitioning to liquid water) and (2) when the dependence on liquid water was not as evident.

2.3.2.1 Los Angeles formic acid partitioning to particle water

The overcast periods, when formic acid tracked RH, were associated with much lower daytime concentrations of photo-chemically generated species. For example, during the same time of day (11:30 – 17:30 PDT), HNO_3 concentrations were one-fifth, $WSOC_g$ levels approximately one-half, and gaseous formic acid abundances less than one-third, of the respective study average concentrations. Daytime temperatures were slightly lower than non-overcast conditions (Figure 2.5), which could further favor partitioning to the particle phase. Back-trajectory calculations by HYSPLIT model [*Draxler and Rolph*, 2012; *Rolph*, 2012] do not indicate a common air mass source region during these three overcast periods (Figure 2.8).

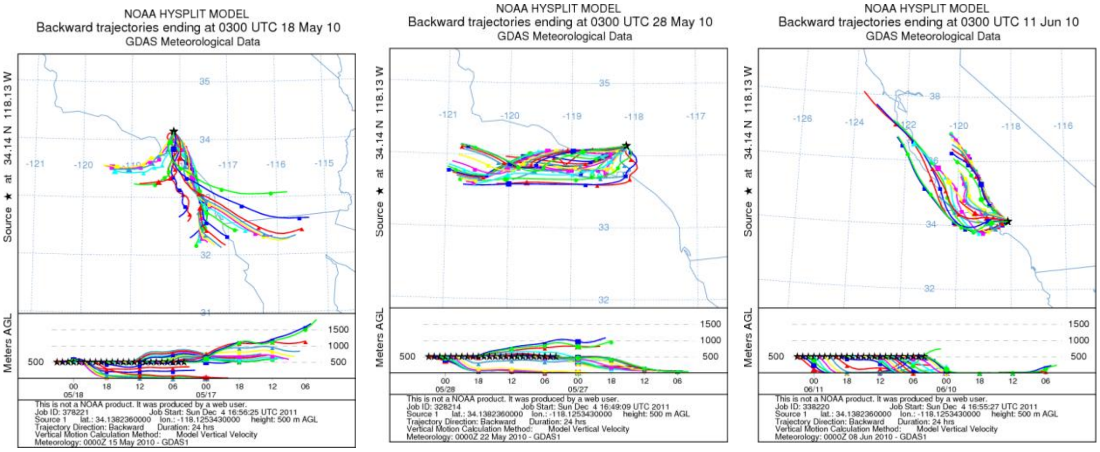
NOAA HYSPLIT MODEL
Backward trajectories ending at 0300 UTC 18 May 10
GDAS Meteorological Data

NOAA HYSPLIT MODEL
Backward trajectories ending at 0300 UTC 28 May 10
GDAS Meteorological Data

NOAA HYSPLIT MODEL
Backward trajectories ending at 0300 UTC 11 Jun 10
GDAS Meteorological Data

Figure 2.8 HYSPLIT back-trajectories for air masses arriving at the Pasadena ground site on an hourly basis during the overcastting periods: May 18, May 28, and Jun 11 of 2010, respectively.

Uptake of gas phase formic acid by aerosol water can be investigated most simply by assuming the gas and particle are in equilibrium and comparing measured p/g ratios to those predicted by Henry's law, assuming ideal solution behavior. Under these assumptions the expected formic acid p/g ratio is:

$$\frac{[HCOO^-]_p}{[HCOOH]_g} = K_H \cdot LWC \cdot \frac{K_a}{[H^+]} \tag{2.1}$$

where LWC is the particle liquid water concentration, K_H the Henry's law constant for formic acid, K_a the formic acid dissociation constant, and $[H^+]$ the hydrogen ion concentration (mol/L). Both K_H and K_a depend on temperature, and were calculated using ambient temperatures by:

$$K_H(T) = K^0{}_H \cdot \exp(d(\ln(k_H))/d(1/T) \cdot \left(\frac{1}{T} - \frac{1}{298.15K}\right)) \tag{2.1a}$$

$$K_a(T) = K^0{}_a \cdot \exp(151 \cdot \left(\frac{1}{T} - \frac{1}{298.15K}\right)) \tag{2.1b}$$

where, $K^0{}_H = 3.7\times10^3$ mol/kg·bar, $d(\ln(k_H))/d(1/T)=5700$ K, $K^0{}_a = 1.8\times10^{-4}$ M [*Chameides,* 1984; *Lelieveld and Crutzen,* 1991]. The application of Henry's law assumes the aerosols have deliquesced.

In the following analysis we apply the pH predicted by *Ellis et al.,* [2012] determined from the Extended-Aerosol Inorganic Model (www.aim.env.uea.ac.uk/aim/aim.php) [*Wexler and Seinfeld,* 1991; *Wexler and Clegg,* 2002] into Eq. (2.1). Although predicting aerosol pH can be highly uncertain [*Yao et al.,* 2006], *Ellis et al.*, [2012] show that pH can be better constrained through measurements of both aerosol ions and gas phase ammonia. Aerosol water content was also predicted by thermodynamic models (either ISORROPIA-II or E-AIM, the results are similar). Measurements and thermodynamic models show that aerosol water concentrations are largely determined by inorganic salt concentrations, with a deviation smaller than ~15% among models [*Fountoukis et al.*, 2009].

2.3.2.1.1 Measured formic acid partitioning compared to Henry's Law

The three periods showing the clearest formic acid p/g dependence on RH were all associated with a clear diurnal trend in RH, weak photochemistry due to low solar radiation, and significant variation in formic p/g ratios. RH was above 70% for the overwhelming majority during the three periods, prompting the assumption that particles were often deliquesced and thus Henry's law is applicable.

The formic acid p/g ratio predicted by Eq. (2.1) has a RH dependence similar to the observed ratio (Figure 2.7b), but is roughly 7 orders of magnitude lower, suggesting no partitioning to the particle phase. For these periods the predicted LWC values ranged from 5-40 $\mu g/m^3$ and particle pH 3.24-4.57 (mean ± std pH = 3.88±0.34). In contrast, based on the predicted LWC and observed formic acid p/g ratio, a pH of 9.31±0.60 is predicted for formic acid to conform to Henry's law, which is not reasonable since most previous studies showed acidified aerosol particles in urban environments impacted by marine aerosols [*Keene et al.*, 2004; *Yao et al.*, 2006].

Under-prediction of $PM_{2.5}$ formate concentrations by Henry's law may be due to several reasons. Formic acid p/g ratios are highly sensitive to pH, and uncertainty in pH of the particle fractions that the gas phase is partitioning to, is potentially a large source of error. Past studies have noted that pH can also vary with aerosol size [*Keene et al.*, 2004]. Other uncertainties associated with using bulk measurements and unknown particle mixing state are possible, including variability in particle water between different particles and other components that may interact with formic acid but are not included in the models (e.g., amines, carbonates). The assumption that formic acid partitions to an ideal solution is also likely not true at all times during the overcast periods, given that many inorganic ions are present. However, even at the highest RHs (e.g., RH>90%) when the particles are expected to be dilute and ideal solution approximation is assumed to be valid, the discrepancy remains. Considering non-ideal solution behavior does not significantly change the large discrepancy; E-AIM estimated formic acid activity coefficients could increase the predicted formic acid p/g ratio by at most roughly a factor of 10 under the lowest RH of the overcast periods.

Similar formic acid discrepancies from an aqueous equilibrium state have also been reported [*Keene et al.*, 2004; *Healy et al.*, 2008]. *Keene et al*. [2004] found that although formic acid was expected to partition almost exclusively to the gas phase, significant particle concentrations were detected. They argued that this discrepancy might have been due to positive artifacts related to filter sampling. Our online measurements, which may be less susceptible to artifacts brought by filters, are consistent with these filter-based studies. A similar result has been observed for other soluble atmospheric components, including hydrogen peroxide [*Arellanes et al.*, 2006], dicarbonyls [*Healy et al.*, 2008; *Volkamer et al.*, 2009], and bulk water-soluble organic carbon (WSOC) [*Hennigan et al.*, 2008], indicating the existence of other possible partitioning pathways and/or absorbing phases.

2.3.2.2 Los Angeles Formic acid partitioning during periods of no observed RH dependence

Highest formic acid concentrations for both gas and particulate phases occurred during daytime hours, peaking in the early afternoon when other photochemically derived compounds (including nitric acid, several organic acids and $WSOC_g$) were also at their highest concentrations [*Veres et al.*, 2011], indicating that photochemistry contributed to the formation of both gas and particle phases. Further evidence for photochemical sources for formic acid in both phases is indicated by a significant weekend enhancement in both, relative to weekdays. Gas phase formic acid mixing ratios were 1.2 times higher on the 5 weekends (10 days) during the study relative to weekdays, and similarly $PM_{2.5}$ formate levels were 1.3 times higher. The difference is thought to be due to higher weekend oxidant concentrations (e.g., O_3 was 1.4 times higher on weekends) resulting from a significant reduction in NO_x emissions on weekends relative to weekdays [*Bahreini et al.*, 2012; *Pollack et al.*, 2012].

Although concentrations of gas and particle formic acid were highest during the early afternoon peak in photochemical production, p/g ratios were lower and less variable than during nighttime periods and overcast episodes with daytime values ranging from 1.1 to 1.3% (Table 2.2). During these afternoon photochemical periods, RH was typically at the daytime minimum of 60%-70% (mean ± stdev = 62 ± 3%), and particle liquid water concentrations are generally expected to be the lowest (8.3 ± 2.8 μg/m^3), in contrast to the high LWC values of greater than 40 μg/m^3 when RH exceeded 95% (e.g., see Figure 2.9).

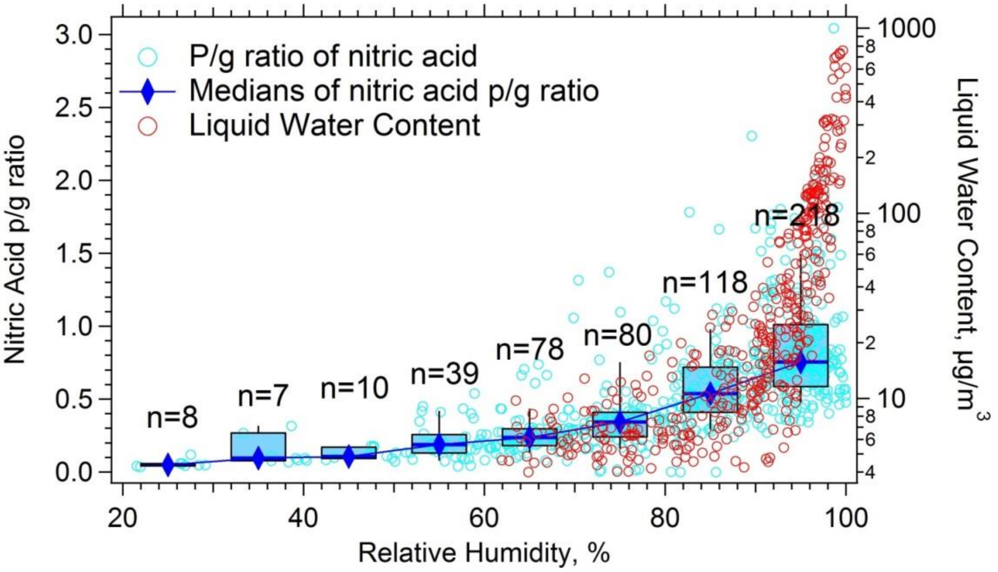

Figure 2.9 Los Angeles p/g ratios of nitric acid as a function of ambient RH. AMS non-refractory PM_1 nitrate is used to determine the ratio. Box plot description is given in Figure 2.6. Also included is the ISORROPIA-II predicted liquid water content (LWC) using PM_1 ammonium, sulfate and nitrate data by AMS. LWC is plotted on a log scale since at RH greater than roughly 95% it is predicted to increase dramatically.

If formic acid has multiple routes for partitioning (i.e. water or OA), it is likely that during overcast periods when OA is low (average OA concentration = 3.68 μg/m3, 54.0% of study average) the particle water route may be relatively more important; in contrast, during the photo-chemically active afternoon periods the opposite conditions occur: OA concentrations are at a maximum and RH (LWC) at a minimum, conditions most conducive for partitioning to OA. However, the specific component of the aerosol the formic acid partitioned to is not completely clear; no correlation was found between formic acid p/g ratio and any other aerosol component, including OA, or AMS PMF factors OOA (sum of the SV-OOA and LV-OOA factors) or HOA (Figure 2.10).

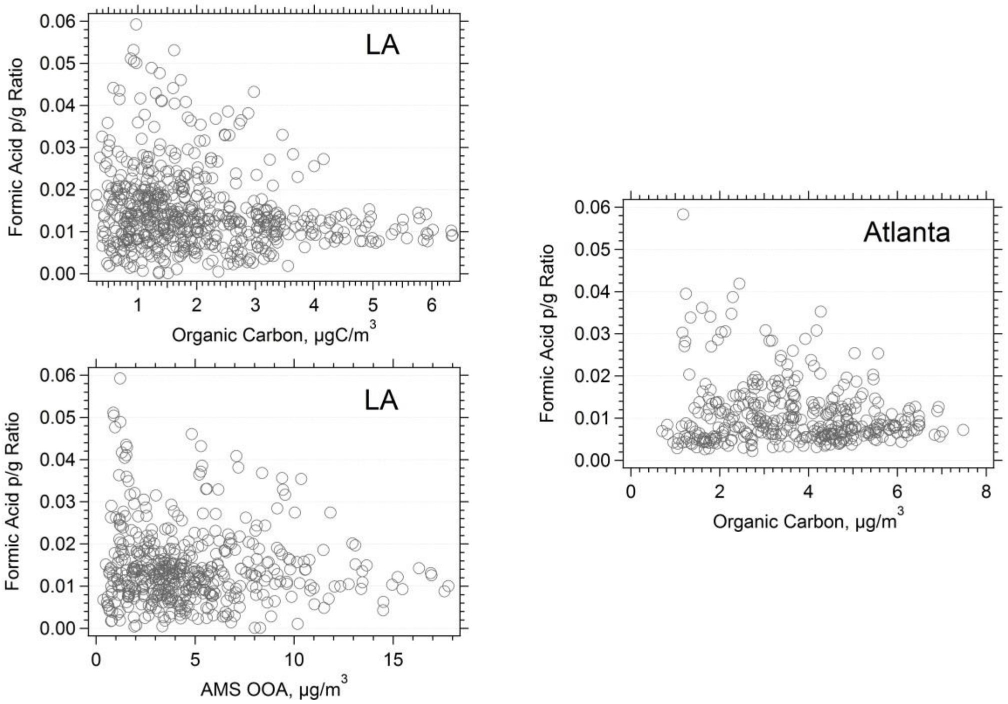

Figure 2.10 Scatter plots of formic acid p/g ratios versus organic aerosol components in LA and ATL; no clear trend was observed.

2.3.2.3 LA Nitric Acid Partitioning and RH as a Contrast to Formic Acid

Like formate, aerosol nitrate is also semi-volatile (excluding nonvolatile forms, such as $NaNO_3$). As noted above, both gas phase formic and nitric acids had similar diurnal profiles, peaking at mid-day along with other photo-chemically generated gaseous species (Figures 2.2 versus 2.11). However, while particle phase formate tended to peak in the afternoon, both AMS and PILS nitrate were usually highest in early morning (Figure 2.11). Note that AMS PM_1 non-refractory nitrate (e.g., dominated by semi-volatile ammonium nitrate) concentrations dropped off relative to $PM_{2.5}$ soluble nitrate (e.g., NH_4NO_3 + $NaNO_3$) as the morning progressed, consistent with the more volatile NH_4NO_3 responding to increasing daytime temperatures.

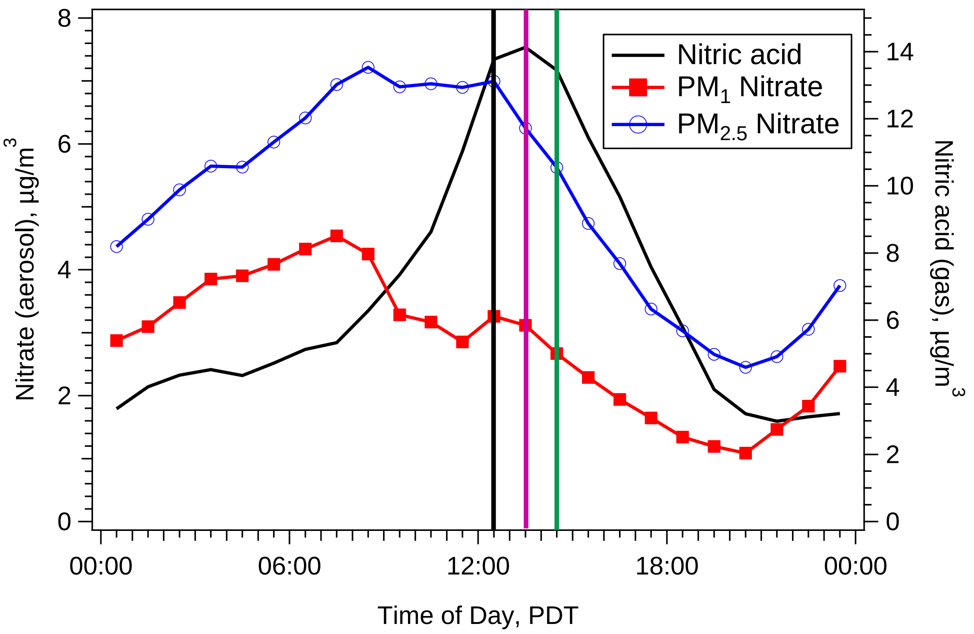

Figure 2.11 Los Angeles diurnal profiles of gas phase nitric acid, AMS non-refractory PM_1 nitrate, and PILS water soluble $PM_{2.5}$ nitrate. Means of hourly-binned data are plotted. The three bars represent the peak concentration timing of primary emission, secondary gases and SOA indicated in Figure 2.2.

The contrasts in the particle phase formate and nitrate diurnal profiles are consistent with differences in formic and nitric p/g ratios relative to RH (particle water). Whereas the formic acid p/g ratio generally did not track RH, nitric acid p/g ratios did follow RH (Figures 2.6b and 2.9). This contrast between the relationship of formic acid and nitric acid p/g ratio with RH further supports the idea that formic acid is able to partition to both aerosol water and other aerosol components, such as the organic aerosol fraction.

2.3.3 Atlanta Formic Acid Concentrations and Partitioning

Observed gas and particle phase formic acid concentrations in Atlanta were shown in Table 2.2. Gas phase formic acid mixing ratios were higher in Atlanta (LA median of 1.61 ppbv, Atlanta median of 2.29 ppbv) and particle phase formate levels were slightly lower in Atlanta (LA median of 49 ng/m^3 versus Atlanta median of 39 ng/m^3). The time series of both gas and particle phase formic acid were not nearly as regular in Atlanta as LA (Figure 2.12), which is expected due to the significantly different meteorological and topographical differences between these two sites: LA is bordered by the Pacific Ocean to the West and San Gabriel Mountains to the East, whereas Atlanta is a continental setting lacking nearby major geological features. In general average diurnal profiles show peak gas and particle formic acid concentrations later in the afternoon (15:30 Eastern Daylight Time (EDT)), suggesting a link to photochemical sources, but roughly three hours later than the peak in solar insolation (12:30 EDT) (Figure 2.13). Curiously, this is the same time that oxalate concentrations reached a maximum (although a small peak relative to a large background) and both may be at least partially due to transport from aloft [*Zhang et al.*, 2012a]. These organic acid peaks are not well synchronized with the overall WSOC$_g$ or WSOC$_p$, except that the gaseous phase formic acid and WSOC$_g$ began to increase together in the early morning (07:30 EDT), while formate and WSOC$_p$ increased together later in the morning (09:30 EDT). Like $WSOC_g$, gas phase formic acid maintained fairly high concentrations until midnight and then dropped off rapidly in the morning, whereas formate concentrations dropped off in the afternoon and maintained fairly consistent levels until the morning increase. The result is that the formic acid p/g ratio tended to be higher in the early morning hours (02:00-08:00), a period of high RH. The same was observed for WSOC, but the extent of WSOC partitioning to the particle phase in the early morning was even stronger [*Zhang et al.*, 2012a].

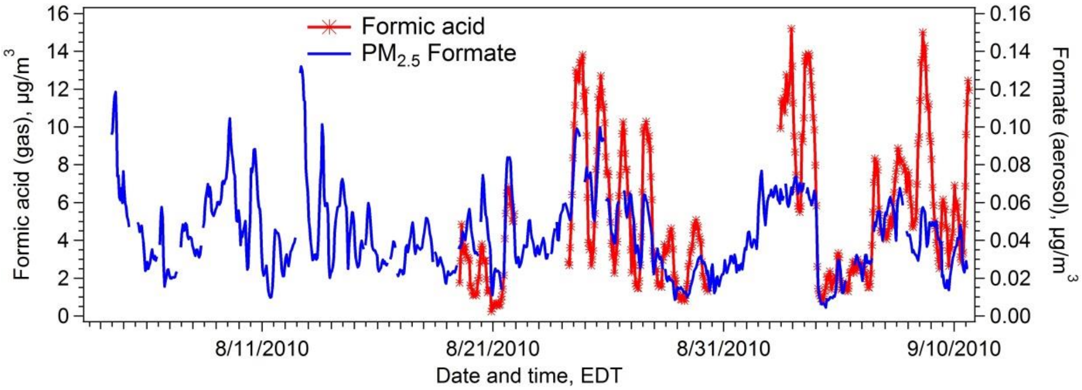

Figure 2.12 Atlanta time series of gaseous and particulate formic acid measured on the campus of the Georgia Institute of Technology from 3 August 2010 to10 September 2010.

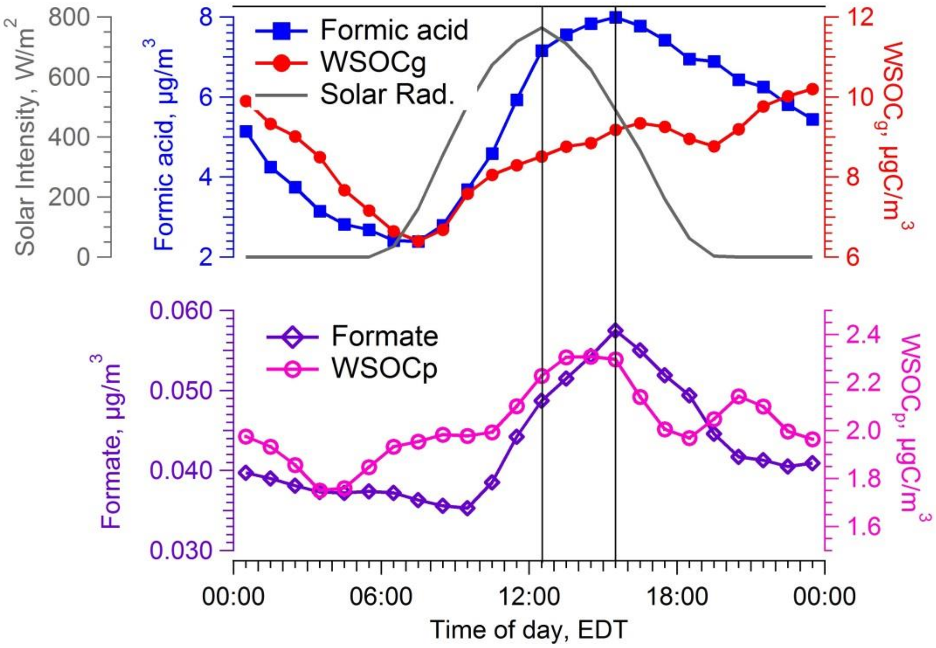

Figure 2.13 Atlanta diurnal profiles of WSOC$_g$ and gas phase formic acid, and PM$_{2.5}$ WSOC$_p$ and formate, as well as solar radiation. Means of hourly-binned data are plotted.

The study average formic acid p/g ratio in Atlanta was on the order of 1% (Table 2.2), slightly lower than LA, but with a more pronounced diurnal variation and more of the extremes biased to higher p/g ratios (Figure 2.14). Gas phase formic acid concentrations were on average higher in Atlanta (Atlanta mean ± stdev = 2.79 ±1.01 ppbv, LA = 1.89 ±0.59 ppbv) while particle phase concentrations were slightly lower (Table 2.2). In contrast to LA, Atlanta formic acid partitioning had a more consistent relationship to RH, and hence apparently to particle water. This can be seen in both the average diurnal profile (Figure 2.14) and the binned p/g ratio versus ambient RH (Figure 2.15), although less data at high RH in Atlanta makes this comparison less robust.

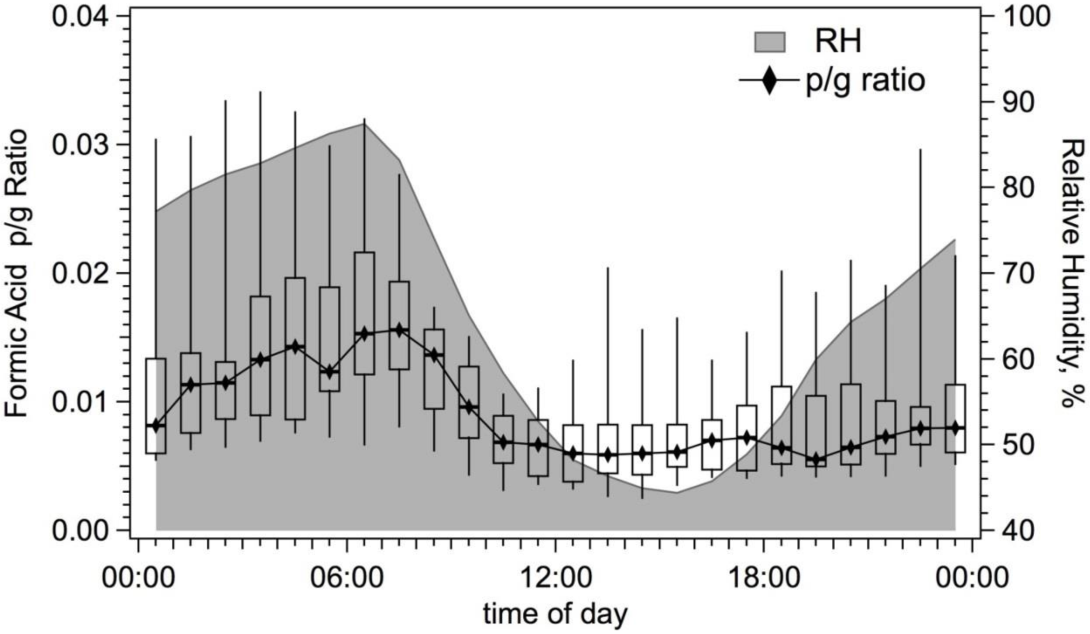

Figure 2.14 Atlanta diurnal profile of formic acid p/g ratios and RH based on averages of hourly binned data. Box plot description is given in Figure 2.6.

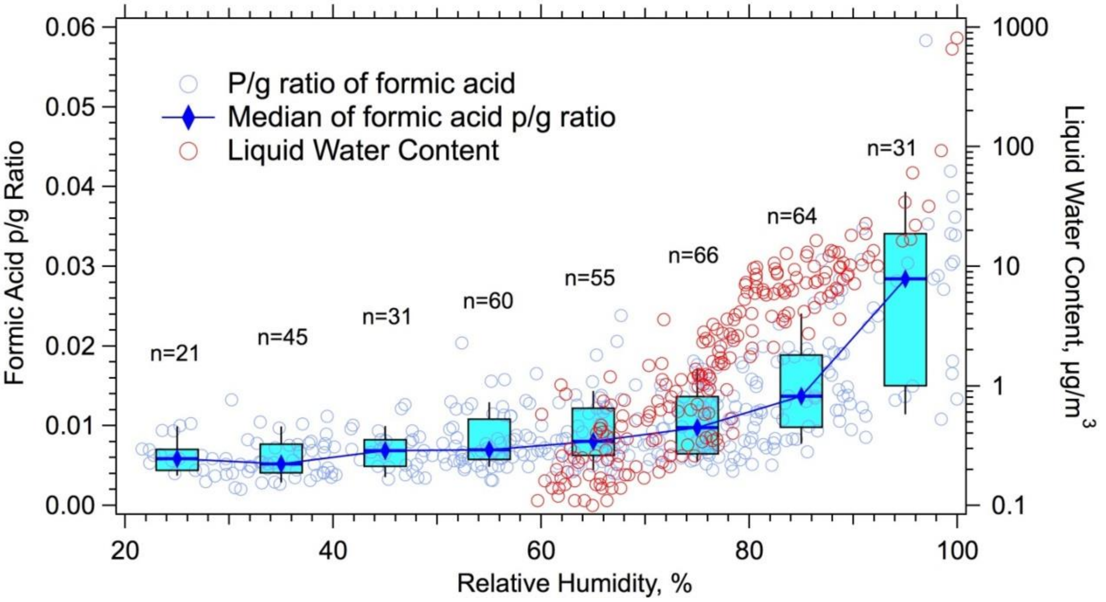

Figure 2.15 Atlanta p/g ratios of formic acid as a function of ambient RH. Box plot description is given in Figure 2.6. ISORROPIA-II predicted liquid water contents (LWC) were based on $PM_{2.5}$ sulfate and nitrate measurements and ammonium assumed to be in ion balance with the anions. LWC is plotted on a log scale since at RH greater than roughly 95% it is predicted to increase dramatically.

2.3.4 Formic Acid Partitioning Absorbing Phases: LA versus Atlanta

A difference in RH-partitioning dependence between LA and Atlanta was also observed for the bulk WSOC measured during these studies [*Zhang et al.*, 2012a]. In LA, WSOC partitioning appeared to be linked to an absorbing phase correlated with OC as opposed to RH, whereas in Atlanta, WSOC partitioning was linked to RH, but not OC, when RH was greater than ~70% (i.e., when LWC is sensitive to RH). When the particles were drier (i.e., RH less than ~70%), there was evidence that WSOC partitioning correlated with OC in Atlanta. Thus, in a general sense, WSOC and formic acid may partition to similar absorbing phases in both locations: more likely the organic components in LA (or some fraction within), and in contrast to particle water in Atlanta.

Causes for the differences in formic acid absorbing phases between these two cities may be due to a number of possibilities.

1) Differences in Aerosol Liquid Water Content: The extent of absorption to particle water or organic mass is sensitive to the mass of the absorbing phase available. The LA experiment was in May/June, whereas the Atlanta experiment was in August/September with generally higher temperatures and lower RH's compared with LA (Figure 2.16). *Zhang et al.* [2012a] used the inorganic species concentrations and found that ISORROPIA-II predicted similar LWC levels at two sites for RH<70%, but higher LWC in LA at RH>70%. By this calculation, there was typically more liquid water available in LA, while observation suggests a greater preference of Atlanta WSOC and formic acid to partitioning to particle water, relative to LA. Differences in organic aerosol composition may also be important in determining LWC available to serve as an absorbing phase, which is not considered by the model employed by *Zhang et al.* [2012a].

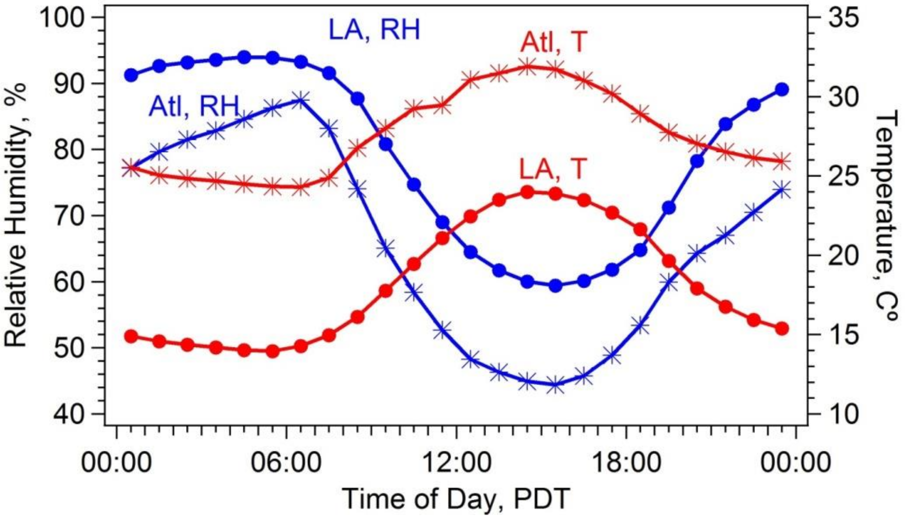

Figure 2.16 Meteorological conditions in Los Angeles and Atlanta during study periods. Means of hourly-binned data are plotted.

2) Differences in OA Concentrations: The theory of equilibrium absorptive partitioning to the organic phase predicts that the particle-to-gas ratio will depend on the concentration of the absorbing phase, in this case possibly OA [*Pankow*, 1994], or some component of the OA (e.g., polar organic compounds). In LA during overcast periods when formic acid partitioned to water, OA was significantly lower than other periods of the study (3.68 μg/m^3 versus study average of 6.81 μg/m^3) making the aqueous phase a more favorable route for partitioning. However, the OA differences between LA and Atlanta are not significant; during these two studies LA AMS OA was on average 6.81 μg/m^3, while ATL OA was at ~5.09 μg/m^3 (estimated by OC × 1.6 for urban aerosols [*Turpin and Lim*, 2001]). Differences in polar organic concentrations, which may be a more likely absorbing phase for formic acid, or the relative polarity of organic aerosols between these two cities, may be a more likely explanation for partitioning preferences of formic acid.

3) Differences in liquid water pH: As a weak acid, formic acid partitioning is greatly influenced by the solution pH (Eq. 2.1). One characteristic of LA ambient air is the high levels of nitric acid that could serve as a strong acid reservoir readily available to partition to water as particle LWC responds to changing RH. During the overcast periods of low photochemistry in LA, nitric acid levels were one-fifth the study average and so a droplet pH closer to neutral is expected and would favor formic acid absorption to liquid water at that time. However, the calculated pH for the overcast periods was not significantly closer to neutral compared to other times, but predicted pHs are uncertain so the possible role of nitric acid is not clear. High concentrations of nitric acid in LA could generally suppress formic acid dissolution and account for little variability in diurnal trends in formic acid p/g ratio. Significantly lower levels of nitric acid in Atlanta may account for a greater partitioning preference to water. Based on measured values, average nitric acid was ~2.5 ppbv during CalNex and ~1.5 ppbv in Atlanta during the 1999 supersite. Whether this is a viable explanation for differences in formic acid partition is not clear, but the effect of pH would only influence a fraction of the WSOC. Given that roughly half the $WSOC_p$ is acidic [*Sullivan and Weber*, 2006], it is doubtful that pH explains differences in partitioning preferences of WSOC in these two cities.

4) Differences in Organic Aerosol Composition: Aerosol composition can influence partitioning by influencing the physical properties of the absorbing organic phase, and to a lesser extent the particle LWC. Aerosol composition is linked to differences in emissions, dispersion and transport, and atmospheric ageing processes. Differences in all these categories exist between LA and Atlanta. In terms of organic components, LA emissions are largely anthropogenic, whereas Atlanta is a mix of biogenic and anthropogenic. LA has a clean upwind sector (Pacific Ocean), a regular land-sea breeze and limited dispersion due to local topology. Atlanta is situated in a mid-continental region with significant biogenic emissions and prevailing winds. Thus, LA has a substantial buildup of fresh anthropogenic SOA (ΔWSOC=1.23 μgC/m^3), whereas in Atlanta greater dispersion and a large regional background results in only a minor increase in fresh SOA (ΔWSOC=0.56 μgC/m^3) that rides on the large regional signal [*Zhang et al.*, 2012b] of aged organics mainly from biogenic emissions [*Weber et al.*, 2007]. Thus it is expected that the Atlanta accumulation mode aerosol would be more oxygenated [*Simon et al.*, 2011], and possibly hygroscopic [*Zhang et al.*, 2012b]. Differences in concentrations of inorganic components may also have some influence. LA is dominated by NH_4^+, NO_3^- and SO_4^{2-}, whereas Atlanta is dominated by NH_4^+ and SO_4^{2-}. Complex interactions between inorganic/organic (polar/non-polar) particle components as a function of O/C ratios have been shown to impact particle interactions with water, resulting in phase separations and transitions between various phases as a function of RH [*Bertram et al.*, 2011]. These processes could play some role in explaining the differences in formic acid partitioning between LA and Atlanta.

2.4 Conclusions

Gas and particle concentrations of formic acid, and factors affecting formic acid particle/gas ratios, are presented based on summer measurements made during separate one-month studies in Los Angeles, CA, and Atlanta, GA, USA. In both studies gas phase formic acid was measured via NI-PT-CIMS and particle formate with a PILS-IC setup to provide continuous data at a 20-minute duty cycle or faster.

Gas phase formic acid concentrations were moderately higher in Atlanta (LA median 1.61 ppbv; Atlanta median 2.29 ppbv), whereas particle phase concentrations were higher in LA (LA median 49 ng/m^3, Atlanta median 39 ng/m^3). Similar diurnal patterns of higher daytime and lower nighttime gas and particle concentrations were observed in both cities, but in LA the gaseous and particle phase formic acid daily trends closely followed most other secondary gas species, whereas in Atlanta they were not as synchronized with other secondary compounds. In LA, photochemistry is clearly a major contributor to formic acid formation; in Atlanta transport (e.g., variation in air mass origin) may play a larger role in the diurnal trends, along with photochemistry.

Formic acid p/g ratios were on the order of a few percent (1%-2%) in both cities. In LA, for the most part, no specific component of the aerosol was correlated with p/g ratios, so the exact nature of the absorbing phase remains unclear; although partitioning to OA, or some component of the OA, may be the most likely route. Formic acid p/g ratios in LA depended little on RH, except on three brief occasions that were all characterized by overcast conditions with little daytime photochemical production. Henry's Law predicts very little partitioning to water, based on particle LWC and pH inferred from thermodynamic models. Including non-ideal solution behavior still significantly under-predicts the particle phase concentrations. In contrast to formic acid, nitric acid partitioning is linked to ambient RH throughout the CalNex-LA study.

In contrast to practically no RH-dependence in LA, formic acid had a clearer trend of partitioning to liquid water in Atlanta based on correlations with ambient RH, despite lower RHs and lower calculated liquid water in Atlanta. This contrast is similar to differences in bulk WSOC partitioning also measured in these two cities during these studies [*Zhang et al.*, 2012a]; WSOC preferentially partitioned to OA in LA, whereas in

Atlanta when particles were expected to have deliquesced (RH>70%), WSOC partitioning was related to RH. Causes for the observed differences in partitioning preferences for formic acid and WSOC between LA and Atlanta are not known, but one of the biggest differences between these two cities is likely the composition of the secondary organic aerosol resulting from differences in VOC emissions.

CHAPTER 3

SIZE-RESOLVED MEASUREMENTS OF BROWN CARBON AND ESTIMATES OF THEIR CONTRIBUTION TO AMBIENT FINE PARTICLE LIGHT ABSORPTION

3.1 Background

Light absorbing components of atmospheric aerosols influence the planetary radiation budget and climate by direct absorption of radiation and through secondary routes that include influences on cloud optics and dynamics, and snow or ice albedo [*Bond et al.*, 2013]. Uncertainties associated with light absorbing aerosol forcing contribute to uncertainty in climate change estimates [*IPCC*, 2007]. Black carbon (BC), largely comprised of elemental carbon (EC), is the strongest of the light-absorbing aerosol components ([*Bond*, 2001; *Moosmuller et al.*, 2009], and references therein). Other absorbing components include mineral dust (e.g., hematite) [*Sokolik and Toon*, 1999] and certain, mostly unidentified [*Zhang et al.*, 2013], constituents of organic matter. Both, preferentially absorb radiation in the lower visible to near-UV wavelength range due to a wavelength-dependent imaginary component of the refractive index. As a group, light-absorbing organic aerosols have been referred to as Brown Carbon [*Andreae and Gelencser*, 2006].

Brown carbon is emitted both from primary sources [*Duarte et al.*, 2005; *Hoffer et* *al.*, 2006; *Lukacs et al.*, 2007] and generated through secondary processes [*Gyawali et al*., 2013]. Particles from incomplete and smoldering combustion of hydrocarbons, especially those associated with biomass or biofuel burning, can contain substantial amounts of brown carbon [*Chakrabarty et al.*, 2010; *Hoffer et al.*, 2006; *Kirchstetter et al.*, 2004; *Kirchstetter and Thatcher*, 2012; *Lack et al.*, 2012; *Lukacs et al.*, 2007; *Qin and Mitchell*, 2009; *Hecobian et al.*, 2010]. Brown carbon also has secondary sources (e.g. *Andreae and Gelencser*, 2006; *Chakrabarty et al.*, 2010; *Chen and Bond*, 2010; *Nakayama et al.*, 2010; *Sareen et al.*, 2010; *Shapiro et al.*, 2009; *Bones et al.*, 2010; *Bateman et al.*, 2011; *Nguyen et al.*, 2012; *de Haan et al.*, 2009a; *Zhang et al.*, 2011; *Zhang et al.*, 2013). Laboratory studies show the production of brown carbon through a variety of formation processes, such as low-temperature oxidation of biogenic materials (e.g., lignin) and their polymerization products, reactions of organic compounds in acidic solutions [*Sareen et al.*, 2010], heterogeneous reactions from dienes like isoprene in the presence of sulfuric acid [*Limbeck et al.*, 2003], and a variety of additional aqueous phase reactions [*Updyke et al.*, 2012; *Chang and Thompson*, 2010].

The mass absorption efficiency of brown carbon increases rapidly from long to shorter wavelengths [*Alexander et al.*, 2008], beginning to absorb near the middle of the visible spectrum (550nm). Attenuation of ultraviolet radiation by brown carbon may, in certain situations, suppress photochemistry [*Jacobson*, 1999; Bahadur et al, 2012] and some studies have suggested brown carbon could affect the planetary radiation balance and climate by direct absorption [*Bahadur et al.*, 2012; *Chung et al.*, 2012; *Feng et al.*, 2013; *Park et al.*, 2010], or through dissolution into cloud droplets resulting in homogeneous absorbing droplets [*Fuzzi et al.*, 2006].

Measuring spectrophotometric properties of aerosol water or filter extracts is a highly sensitive approach to quantify the presence of brown carbon [*Hecobian et al.*, 2010; *Kieber et al.* 2006; *Lukacs et al.*, 2007; *Zhang et al.*, 2011]. Two-years of filter extract measurements in Europe showed brown carbon mainly associated with biomass burning tracers [*Lukacs et al.*, 2007]. *Kieber et al.* [2006] found chromphores ubiquitous in rainwater collected in the southeastern US and concluded they were associated with continental sources. Brown carbon was also found in $PM_{2.5}$ particles throughout the Southeastern US, where the light-absorbing fraction of water-soluble organic carbon (WSOC) was mainly related to biomass burning in winter and apparently secondary sources during summer [*Hecobian et al.*, 2010; *Zhang et al.*, 2011]. Secondary sources of brown carbon are especially prevalent in urban environments with high anthropogenic emissions. Water-extract mass absorption efficiencies (absorption of water soluble carbon at 365nm per WSOC mass concentration) were 6 to 7 times higher in Los Angeles compared to Atlanta [*Zhang et al.*, 2011], the former an urban environment dominated by anthropogenic SOA. These studies of brown carbon in aerosol extracts (solutions) have identified the ubiquitous extent of fine particle brown carbon and explored their sources and chemistry, but do not address the possible optical importance.

Optical instruments that measure particle light absorption coefficients (b_{ap}) typically operate at a limited number of wavelengths and quantify the "total" absorption, which depending on emissions includes varying proportions of black carbon (BC), brown carbon and mineral dust [*Sandradewi et al.*, 2008]. Quantifying brown carbon by difference can be difficult due to the typically large contribution of BC. Particle morphology can also complicate the measurement of brown carbon, such as possible amplifying of BC absorption by lensing effects involving scattering shells over absorbing cores [*Bond et al.*, 2006; *Cappa et al.*, 2012; *Lack et al, 2010*]. In contrast, light absorption measured from liquid extracts does not suffer from the interference by BC or other absorbers, since they can be isolated by dissolution, thereby permitting a direct measurement of brown carbon. Spectrophotometers that measure soluble brown carbon can also provide highly spectrally resolved data (1 nm wavelength resolution) over wide wavelength ranges (e.g., 200 to 900nm), an advantage over several fixed wavelengths associated with optical instruments [*Hecobian et al.*, 2010]. Furthermore, when combined with a long-path absorption cell, spectrophotometry of aerosol extract solutions is a highly sensitive measurement. By performing size-resolved measurements of brown carbon and using the bulk solution light absorption measurements to estimate the absorbing refractive index, we investigate the optical importance of water and methanol-soluble brown carbon absorption predicted from Mie theory and compared it to measurements of BC made with standard optical instruments.

3.2 Methods

3.2.1 Sampling Sites

Sampling was carried out at several sites in and around Atlanta, GA. This included two SEARCH (Southeastern Research and Characterization Experiment) sites (*Hansen et al.,* 2006); Jefferson Street (JST), an urban site not significantly influenced by any strong local sources, and Yorkville (YRK), the SEARCH rural pair to JST located approximately 80 km west (generally up-wind) of Atlanta. A third Road-Side site (RS), was situated within 2m of a major roadway in central Atlanta (interstates 75 and 85, 8 lanes each direction) that has restricted heavy-duty diesel truck access. (Georgia Department of Transportation estimates approximately 320,000 vehicles per day, with 16,000 trucks; also see *Yan et al.*, 2011, and references therein). At all three sites, measurements were made with a suite of online and offline instruments that were moved from site-to-site during the summer and fall of 2012.

3.2.2 Offline Measurements

A 10 stage Micro-Orifice Uniform Deposit Impactor (MOUDI, MSP Corp., Shoreview, MN, USA), operated in non-rotating mode was used to collect size-resolved aerosols for subsequent analysis. Theoretical MOUDI 50% aerodynamic diameter cut-sizes of the stages are: 10.00, 6.20, 3.10, 1.80, 1.00, 0.62, 0.31, 0.18, 0.10, and 0.056 μm. The impactors are followed by an after-filter. All MOUDI samplers were located outside so that particle size selection occurred at ambient temperature and RH. The samples were collected onto impaction plates of prebaked 47mm quartz filters (Pall Life Sciences, Ann Arbor, MI) at a flow rate of nominally 30 L/min for roughly 48 hrs. A punch from each filter was taken for the analysis of OC and EC, and the remaining portion was divided into two halves, one extracted in high purity water the other methanol. Since the MOUDI was not operated in rotation mode during sampling, the non-uniformity of deposits on the quartz impaction filters was accounted for when dividing the filters for subsequent analysis by counting deposits from each jet, for stages of cut-size 0.31 μm and up. For stages below, the deposits were considered uniform and the fraction of the filter analyzed was determined from fractional area. In all, six complete MOUDI samples were collected under sunny, precipitation free periods, summarized in Table 3.1. For every sample run, two quartz filter field blanks were included and data were blank corrected.

Table 3.1 Mean and standard deviation of parameters measured with online instruments (except for EC) during MOUDI sampling periods at various sites.

Start time	**Stop time**	**Location**	**Temperature, ^{0}C**	**RH, %**	**PM$_{2.5}$, µg/m^3**	**OC, µgC/m^3**	**EC*, µgC/m^3**	**OC/EC* ratio**	**BC (Avg of all Aeth. λ), µgC/m^3**	**WSOC, µgC/m^3**
5/17/12 16:45	5/20/12 15:00	JST	22.5±3.5	55.2±13.3	14.63	4.39	0.81	5.4	0.77	2.38
5/25/12 12:00	5/27/12 20:00	JST	28.6±3.4	46.8±11.4	18.96	4.61	0.82	5.6	0.93	2.89
6/15/12 11:35	6/18/12 13:30	YRK	23.8±3.4	55.7±12.6	10.70	4.43	0.38	11.7	0.45	2.44
6/21/12 11:10	6/23/12 11:50	YRK	27.2±3.1	57.8±11.7	16.09	5.24	0.44	11.9	0.44	2.72
6/27/12 12:00	6/29/12 13:55	YRK	28.9±4.5	44.2±15.1	17.73	7.26	0.54	13.4	0.55	4.36
9/26/12 12:00	9/29/12 8:40	RS	24.0±3.7	58.3±16.8	13.36	6.66	1.42	4.7	NAN	2.99

JST: Jefferson Street, a central urban site in Atlanta. YRK: the rural pair to JST. Both JST and YRK are part of the SEARCH network. RS: Road-side site.

NAN: no data

* EC data from MOUDI filter measurements since online thermal EC data were not available due to instrument issues

Organic carbon (OC) and elemental carbon (EC) were quantified with a Sunset OCEC Analyzer (Sunset Laboratory Inc., Tigard, OR) following the NIOSH protocol [*NIOSH*, 1996]. In this analysis, non-uniform MOUDI deposits hinders the optical determination of OC/EC split based on laser attenuation, so a specified split of 500 seconds (corresponding temperature of 700^{0}C) was used based on the temperature split determined by the standard thermal-optical transmittance method (i.e., laser signal reaches its initial value) from regular quartz filter samples collected during the study period. OC and EC blanks ranged from 0.03 to 0.1 μgC/m^3, and below LOD to 0.003 μgC/m^3, respectively, with uncertainties estimated as 13% for OC and 16% for EC based on blank variability (1σ) and uncertainties in flow rates. (Various measurement uncertainties are summarized in Table 3.2).

Table 3.2 Summary of estimated uncertainties for various species reported. In all cases where variability was used to estimate an uncertainty, 1 standard deviation is used.

Instruments/Analysis	**Species Measured/Reported**	**Uncertainty, %**
Sunset OC EC	OC (offline/online)[1]	13/28
Sunset OC EC	EC (offline/online)[2]	16/28
TOC	WSOC (offline/online)[3]	9/7
LWCC-Spectrophotometer	H_2O_Abs(365) (offline/online) [4]	21/20
LWCC-Spectrophotometer	MeOH_Abs(365) [5]	27
TEOM (1 hr)	$PM_{2.5}$ mass	30
MAAP	BC or b_{ap_MAAP}[6]	12
Aethalometer	BC[6]	4
Scattering correction	Aeth BC b_{ap} [7]	35
Mie calculation	b_{ap} of EC and BrC[8]	30
Combined uncertainties in calculated parameters		
b_{ap_Aeth}[9]		36
b_{ap_EC}[10]		34
$b_{ap,H2O}$ (at 365nm)[11]		38
$b_{ap,MeOH}$ (at 365nm)[12]		42
H_2O_brC ratio[13]	relative to b_{ap_Aeth}/ b_{ap_EC}	52/51
MeOH_brC ratio[14]	relative to b_{ap_Aeth}/ b_{ap_EC}	56/54

[1,2] Uncertainty calculated as quadrature sum of relative errors in: filter sampling air volume (flow rate × sampling time), blank filters, field blanks, and standard deviation from duplicate measurements on same filter.

[3] Uncertainty includes relative errors in: filter sampling air volume (flow rate × sampling time), liquid volume of solvents, solvent blanks, field blanks, the variability in calibration standards, and standard deviation from duplicate standards

[4, 5] Uncertainty includes relative errors in: filter sampling air volume (flow rate × sampling time), liquid volume of solvents, solvent blanks, field blanks, and standard deviation from duplicate samples.

[6] Uncertainty includes uncertainty of instrument reported by manufacture and variation in flow rates.

[7] Uncertainty estimated by combining uncertainties of all factors in scattering correction.

[8] Relative uncertainty associated with variables used in the Mie calculation, including that aerosols in each stage were assumed to have the same size, the selection of organic mass vs.

particle mass, real part of the refractive index, and sensitivity to density (ρ), both in Mie calculation and conversion from MOUDI aerodynamic sizes to physical sizes.

[9] Combined uncertainty of 6, and 7.

[10] Combined uncertainty of 2 and 8.

[11] Combined uncertainty of 3, 4, and 8.

[12] Combined uncertainty of 1, 5, and 8.

[13] Combined uncertainty of 10 and 11.

[14] Combined uncertainty of 10 and 12.

Halved quartz impaction plates and backup filters were extracted in high purity water (>18 Mohm) and methanol (VWR International, A.C.S. Grade), by 30 minutes of sonication. All extracts were then filtered through a 25mm diameter 0.45 μm pore syringe filter (Fisher Scientific, Fisherbrand* Syringe Filters) to remove insoluble components and filter remnants generated during the extraction process. Water extracts were transferred into a coupled LWCC-TOC (Liquid Waveguide Capillary Cell-Total Organic Carbon) system to determine the water-soluble light absorption spectra and water-soluble organic carbon (WSOC) mass following the method by *Hecobian et al.* [2010]. LOD of water-soluble brown carbon at 365nm was 0.031 Mm^{-1} and for WSOC 0.084 $\mu gC/m^3$, with estimated uncertainties of 21% and 9%, respectively, mainly due to blank variability (1σ).

For the methanol extracts, only light absorption spectra were analyzed (i.e., methanol soluble brown carbon) since the use of an organic solvent prohibits determining carbon mass (TOC) in these solutions. The estimated LOD for methanol-soluble brown carbon at 365nm is 0.11 Mm^{-1} with an uncertainty of 27% due to blank variability (1σ).

3.2.3 Online Measurements: MAAP, Aethalometer, OC, EC, WSOC, Water-Soluble Brown carbon and TEOM ($PM_{2.5}$)

A suite of online measurements were made at the same time and location as the MOUDIs as part of another study (EPA-SCAPE), which included $PM_{2.5}$ mass by TEOM, Sunset Labs OC and EC, PILS-WSOC and water-soluble absorption, and BC measured by a Multi-Angle Absorption Photometer (MAAP) and 7-wavelength Aethalometer. The OCEC, WSOC and solution light absorption were measured via identical methods to the offline analysis of the MOUDI samples (except, a 1-m path length LWCC was used for the online system versus a 2.5-m path length LWCC for the offline analysis (World Precision Instruments)).

The TEOM (Thermo Scientific, model 1400a) was operated at a temperature of 30 ℃ with a nafion dryer (Perma Pure, Toms River, NJ) upstream of the sensor, which reduced the RH to below 40%. The detection limit and measurement uncertainty is estimated as 0.5 μg/m^3 and 30% (for an hourly average), respectively.

$PM_{2.5}$ OC and EC were determined with a Sunset Labs OC/EC analyzer (Model 3F, Forest Grove, OR), which operated at a 45-min sampling period followed by 15-min of analysis. A parallel plate carbon denuder [*Eatough et al.*, 1993] upstream of the instrument was installed to reduce positive sampling artifacts from volatile gases. Systematic blank measurements were made throughout the study period by installing a Teflon filter (47 mm diameter, 2.0 μm pore size, Pall Life Sciences) on the cyclone inlet on a daily basis. A linear interpolation was applied between consecutive blanks and was subtracted from the ambient data. OC blanks ranged from 0.44 to 1.05 μgC/m^3 and optical EC blanks varied from 0.02 to 0.03 μgC/m^3. Uncertainty due to random measurement errors is estimated to be 28%.

The measurement of online WSOC and light absorption was provided by a PILS-LWCC-TOC system. A Particle-Into-Liquid Sampler (PILS) that continuously transfers ambient PM$_{2.5}$ aerosol to an aqueous flow of purified water was coupled in series with a long-path UV/VIS spectrophotometer (DT-Mini-2 light source and USB4000 spectrometer, both from Ocean Optics, Dunedin, FL) for measurement of soluble aerosol light absorption spectra (200–800 nm), followed by a TOC analyzer to obtain the WSOC concentration, similar to the method of *Hecobian et al.* [2010]. PILS-generated liquid sample was filtered with a Whatman 25mm filter (Puradisc Disposable Syringe Filters, 0.2 μm core size) to remove any insoluble aerosol components larger than 0.2 μm. Complete absorption spectra (200-800nm) were recorded every 15 minutes. Every three days, the LWCC was cleaned using 0.6N solution of HCl and Milli-Q (>18 MΩ) DI water. Following cleaning, the baseline was zeroed using the

Spectra-Suite software so that zero absorption was recorded at all wavelengths for milli-Q (>18 MΩ) DI water. For the offline system, this cleaning and zeroing was done prior to every sample. Similar to online OCEC measurement, an automated valve that directed sample air-flow through a Teflon filter performed dynamic blanks three times every day and a linear interpolation between successive blanks was assumed to blank correct the online measurements. Instrument LOD and measurement uncertainty are estimated at 0.20 µgC/m^3 and 7% for WSOC, 0.1 Mm^{-1} and 20% for water-soluble absorption at 365nm, respectively.

Online black carbon (BC) was measured with an Aethalometer (Magee Scientific, Berkeley, CA) and MAAP (Thermo-Scientific model 5012), both based on measurements of light attenuation through a particle-laden filter. The aethalometer operates at seven wavelengths covering the ultra-violet to the near-infrared wavelength range (370, 450, 571, 590, 660, 880, and 950 nm). Data interpretation requires scattering corrections, which are discussed further below. The MAAP operates at a single wavelength of 670nm and is designed to account for scattering error when measuring BC; no corrections are applied in this case. MAAP b_{ap} uncertainty is estimated at 12% [*Petzold and Schönlinner*, 2004]. (Aethalometer measurement uncertainties are discussed below). The MAAP was operated only at the JST site and the Aethalometer was operational only at the JST and YRK sites.

3.2.4 Data Interpretation: Aethalometer Scattering Correction and Mie Theory Calculation

3.2.4.1 Aethalometer scattering correction

As noted, the MAAP corrects for scattering and thus the absorption (b_{ap_MAAP}) was determined directly from the instrument's reported BC concentration using the fixed mass absorption coefficient of 6.6 m^2 g^{-1} at 670nm. (See acronyms listed below). The Aethalometer b_{ap} (b_{ap_Aeth}) was corrected for multiple scattering based on the combination of two correction schemes: *Weingartner et al.* [2003] and *Jung et al.* [2010] by,

$$b_{ap} = \frac{Batn}{C \times Ratn} \tag{3.1}$$

$$Ratn = \left(\frac{1}{f} - 1\right) \times \frac{\ln(ATN) - \ln(10\%)}{\ln(50\%) - \ln(10\%)} + 1 \tag{3.2}$$

$$f = a(1 - w0) + 1 \tag{3.3}$$

$$C = 4.05 \times \left(\frac{[BC]}{[EC]}\right) - 1.55 \tag{3.4}$$

where B_{atn} is directly derived from the BC concentration reported by the instrument by $B_{atn} = BC * \frac{14625}{\lambda}$ (unit: BC in ng/m^3, B_{atn} in m^{-1}), R_{atn} (unitless) is a calculated parameter based on equation (3.2), f is an empirical factor that depends on parameter a, which is equal to 0.87 at 660 nm, and estimated single scattering albedo, *w0*. As there was no direct measurement of scattering on-site during the MOUDI sampling periods, scattering was inferred from TEOM $PM_{2.5}$ data. The linear regression slope of scattering (at 530nm) and TEOM $PM_{2.5}$ reported in *Carrico et al.* [2003] was applied to our TEOM data to estimate scattering, then a scattering Ångström exponent of 1.4 [*Yang et al.*, 2009] was used to estimate the scattering at 670nm and the single scattering albedo. The estimated single scattering albedo ranged from 0.85-0.91. The correction factor C depends on the aerosol type and was determined from the hourly measured EC and online BC averaged over the EC sampling time. Aethalometer b_{ap} uncertainty, including scattering correction, is estimated to be 36% due to uncertainty in a range of parameters, including measurements of BC, EC, TEOM $PM_{2.5}$, and related uncertainties associated with the scattering estimation. The magnitude of the scattering correction factor was 3.75 ± 0.83 (mean ± standard deviation).

For comparison, b_{ap_Aeth} at 660nm was converted to the MAAP operational wavelength of 670nm based on an absorption Ångström exponent determined from the aethalometer multiple wavelength measurements (i.e., power law regression fit). For the JST measurements, when both MAAP and Aethalometer data were available, the scattering-corrected b_{ap_Aeth} agreed with b_{ap_MAAP} (Figure 3.1, regression slope of 1.02, $r^2 = 0.95$), indicating the scattering correction at 670 nm is reasonable.

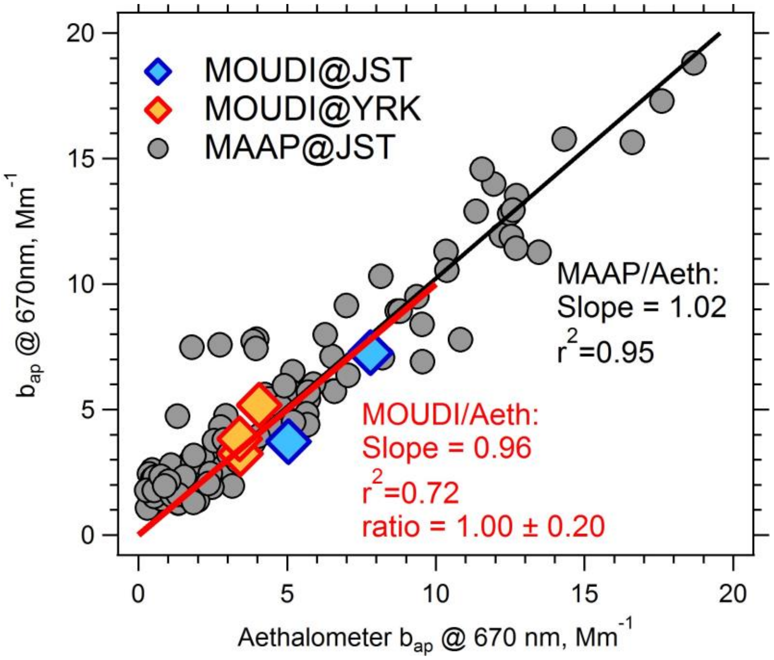

Figure 3.1 Comparison of absorption at 670 nm between scattering-corrected aethalometer and MAAP for 1 hour averaged data (grey filled circles) and aethalometer absorption averaged over MOUDI sampling times to absorption determined from the EC size distribution and Mie theory (diamonds).

3.2.4.2 Mie theory calculations

An absorption measurement of solutions containing aerosol extracts is not directly comparable with absorption by ambient aerosols. However, the complex part of refractive indices can be obtained from the solution light absorption data and used with Mie theory to infer the brown carbon absorption by ambient aerosols, under a range of assumptions.

Spectrophotometric measurements of the solution light absorbance at a given wavelength (A_λ, unitless) can be used to determine the bulk solution mass absorption efficiency (α/ρ) by:

$$\frac{\alpha(\lambda)}{\rho} = \frac{(\mathrm{A}_\lambda - \mathrm{A}_{700})}{\mathrm{M}} \frac{V_l}{\mathrm{V_a} \cdot \mathrm{l}} \cdot \ln(10) = \frac{Abs(\lambda)}{M} \tag{3.5}$$

Measurements at wavelengths below 700nm are referenced to absorption at 700nm (A_λ - A_{700}) to account for any uniform signal drift that may occur over time after LWCC cleaning and zeroing to reference (DI) spectra (only necessary for the online system since offline system was cleaned and zeroed between each measurement). V_l is the liquid volume the filter is extracted into and V_a the volume of air sampled through the filter. The waveguide optical path length is l and $ln(10)$ converts from base 10 (the form provided by the spectrophotometer) to natural logarithms. $Abs(\lambda)$ is then the solution absorption at a given wavelength (units Mm^{-1}). M is the normalizing mass concentration used to determine the bulk solution mass absorption efficiency ($Abs(\lambda)/M$ in units of m^2/g). In this work M is taken to be the ambient WSOC concentration for the water extract and ambient OC concentration for the methanol extract. The complex component (k) of the particle refractive index $m = n + i\,k$ can then be calculated from Eq. (3.5) [*Bohren and Hoffman*, 1998; *Chen and Bond,* 2010; *Sun et al.*, 2007] for the water and methanol extracts by:

$$k = \frac{\rho\lambda\left(\frac{\alpha(\lambda)}{\rho}\right)}{4\,\pi} = \frac{\rho\lambda\, H_2O\_Abs(\lambda)}{4\,\pi\, WSOC} \text{ for water extracts} \tag{3.6}$$

$$k = \frac{\rho\lambda\left(\frac{\alpha(\lambda)}{\rho}\right)}{4\,\pi} = \frac{\rho\lambda\, MeOH\_Abs(\lambda)}{4\,\pi\, OC} \text{ for methanol extracts} \tag{3.7}$$

where $H_2O\_Abs(\lambda)$ and $MeOH\_Abs(\lambda)$ are the solution absorption at a given wavelength for the water and methanol extracts. Note that using a normalizing mass (M)

of WSOC or OC (µgC/m^3) results in reported k values for organic carbon mass, not particle mass, and in subsequent Mie calculations of brown carbon absorption, these same mass concentrations must be used for consistency. Alternatively, one could use the total particle mass (PM) measured on each stage (not measured in this study). Since PM/WSOC and PM/OC mass fractions (µgC/ug) likely range from roughly 2 to 4, k would decrease by similar factors if PM were used instead. Sensitivity tests show that there is at most a 20% difference in Mie-predicted carbon absorption if PM is used instead of carbon mass. In this study, a particle density (ρ) of 1.5 g/cm^3 for both water and methanol extracts for all particle sizes is assumed. Mie calculated b_{ap} is largely insensitive to the value chosen; sensitivity tests with our data show a 10% difference in density results in ~ 6% change in b_{ap} for EC or brown carbon (methanol or water) calculations. Particle density is also used to convert aerodynamic diameters to physical particle diameters needed in the Mie calculation, assuming spherical particles. This added uncertainty is discussed below. For all data collected, the real part of the refractive index (m) was set to 1.55 for all wavelengths, representative of the organic-sulfate mix that comprises fine particles in the study region [*Carrico et al.*, 2003]. An uncertainty analysis shows that the relative change in estimated b_{ap} due to m (ranging from 1.4 to 2.0) is within 18%.

For each MOUDI stage (and backup filter), and for each extract solution, the refractive index was determined and used in a Mie theory calculation to estimate the single particle absorption efficiency (*Q*) for a particle of size D_{pg}, the geometric mean of physical diameter for that stage. The light absorption coefficient for all particles of that size is then estimated by,

$$b_{ap}\left(\lambda, D_{p_g}\right) = \frac{\pi}{4} \cdot {D_{p_g}}^2 \cdot Q \cdot N \qquad (3.8)$$

Where *N* is the particle number concentration. Since *N* is not known, the mass concentration, *M* for the given MOUDI stage, is used to estimate *N*, assuming spherical particles, which gives

$$b_{ap}\left(\lambda, D_{p_g}\right) = \frac{3}{2} \cdot \frac{Q \cdot \mathrm{M}}{\mathrm{D_{p_g}} \cdot \rho} \qquad (3.9)$$

For consistency with the calculated complex refractive index (*k*), *M* is either the WSOC or OC ambient concentration determined from the MOUDI measurement. The calculation is repeated for all stages with cut sizes 3.1 μm and below, including the after-filter, and then summed to obtain the total fine particle light absorption coefficient at a given wavelength. The process is repeated for other wavelengths of interest.

This analysis makes a number of simplifying assumptions, including that the particles are spherical and of uniform composition, but externally mixed with other absorbing aerosol components (e.g., EC). As a test of the method, Mie calculations, under similar assumptions, are also made to estimate the absorption by pure BC at 670 nm based on MOUDI size-resolved EC measurements and are compared to Aethalometer and MAAP measurements of BC b_{ap} for the JST data. Aethalometer-measured absorption at lower wavelengths is then compared to water and methanol brown carbon b_{ap} derived from a similar Mie calculation.

3.3 Results

3.3.1 MOUDI vs Online data: Data Quality Assessment

Off-line MOUDI data were integrated over stages of aerodynamic cut size 3.1 µm and smaller (including the after-filter) and compared to the $PM_{2.5}$ online measurements, averaged over MOUDI sampling times. Comparisons for WSOC, OC, EC, and *H_2O_Abs(365)* (i.e., at a wavelength of 365 nm) are shown in Figure 3.2. (Note, only water extracts were available for the online method, so no comparison of *MeOH_Abs(365)* is available). There is good agreement between the online and offline methods. For all four components the correlations (r^2) were greater than 0.84 and slopes within 10% of one, well within the instrumental measurement uncertainties of roughly 10 to 30% (Table 3.2).

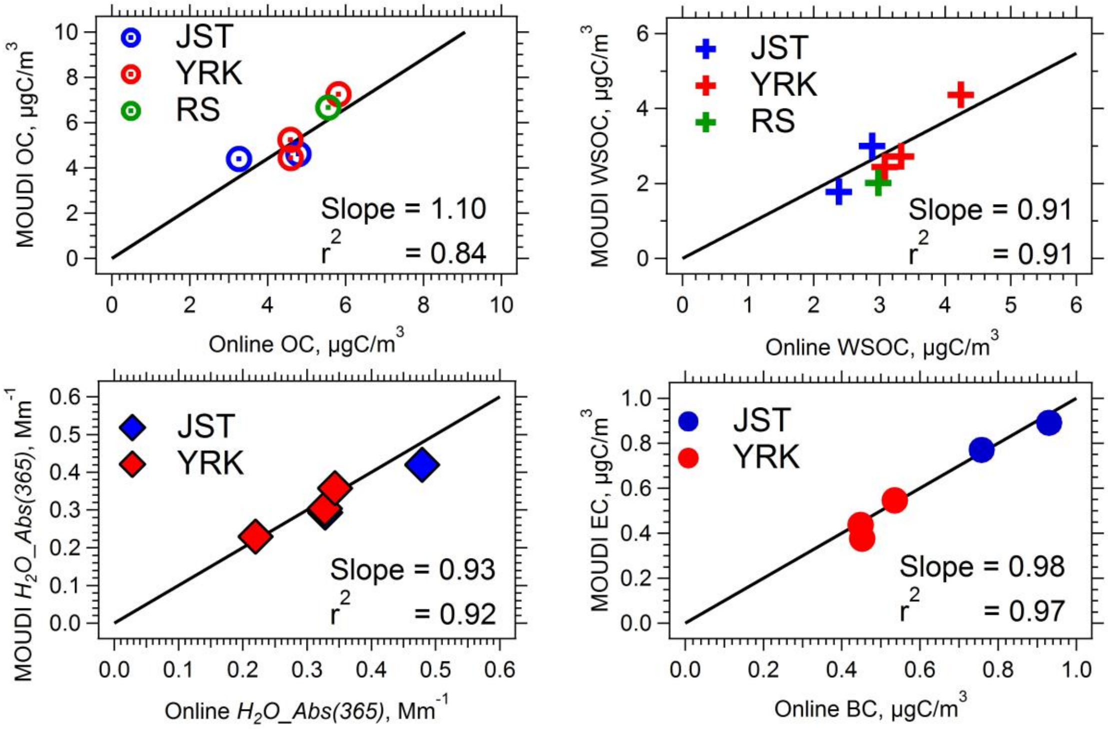

Figure 3.2 Comparison of offline fine particle MOUDI OC, EC, WSOC, water-extracted absorption at 365nm and online OC, BC, WSOC, and water-soluble absorption at 365nm using orthogonal distance regressions with slopes forced through zero. Online data are $PM_{2.5}$ and MOUDI summed over all stages of 3.1 µm cut and below (plus after-filter). The sites are: JST (urban), YRK (rural) and RS (road-side). No online *H_2O_Abs* or BC was available at the RS site during the MOUDI sampling period.

3.3.2 MOUDI Size Distributions

A summary of MOUDI sampling dates and times, and average conditions measured with the various online instruments during these periods is given in Table 3.1. Although measurements were not made simultaneously at the different sites, the comparisons between sites show differences (or lack there of) expected for primary and secondary aerosol components. For example, both EC and OC concentrations were highest at the RS site, compared to JST and YRK, which tended to be closer in magnitude. WSOC concentrations were similar among all three sites. OC/EC ratios were highest at the rural site and lowest at the RS site. These results are consistent with known high spatial variability in primary species, EC and some fraction of OC, and more uniformity in secondary species, (e.g., WSOC), and high OC/EC ratios in regions dominated by secondary organic aerosols.

MOUDI size distributions for the individual species, including extract solutions of water-soluble ($H_2O\_Abs(365)$) and methanol-soluble absorption at 365 nm (*MeOH_Abs(365)*) at the three sites are shown in Figure 3.3. Geometric mean aerodynamic diameters and standard deviations, based on lognormal fits to the data over fine particle ranges (i.e., MOUDI stages with cut sizes 3.1 µm and below), are included in the plots.

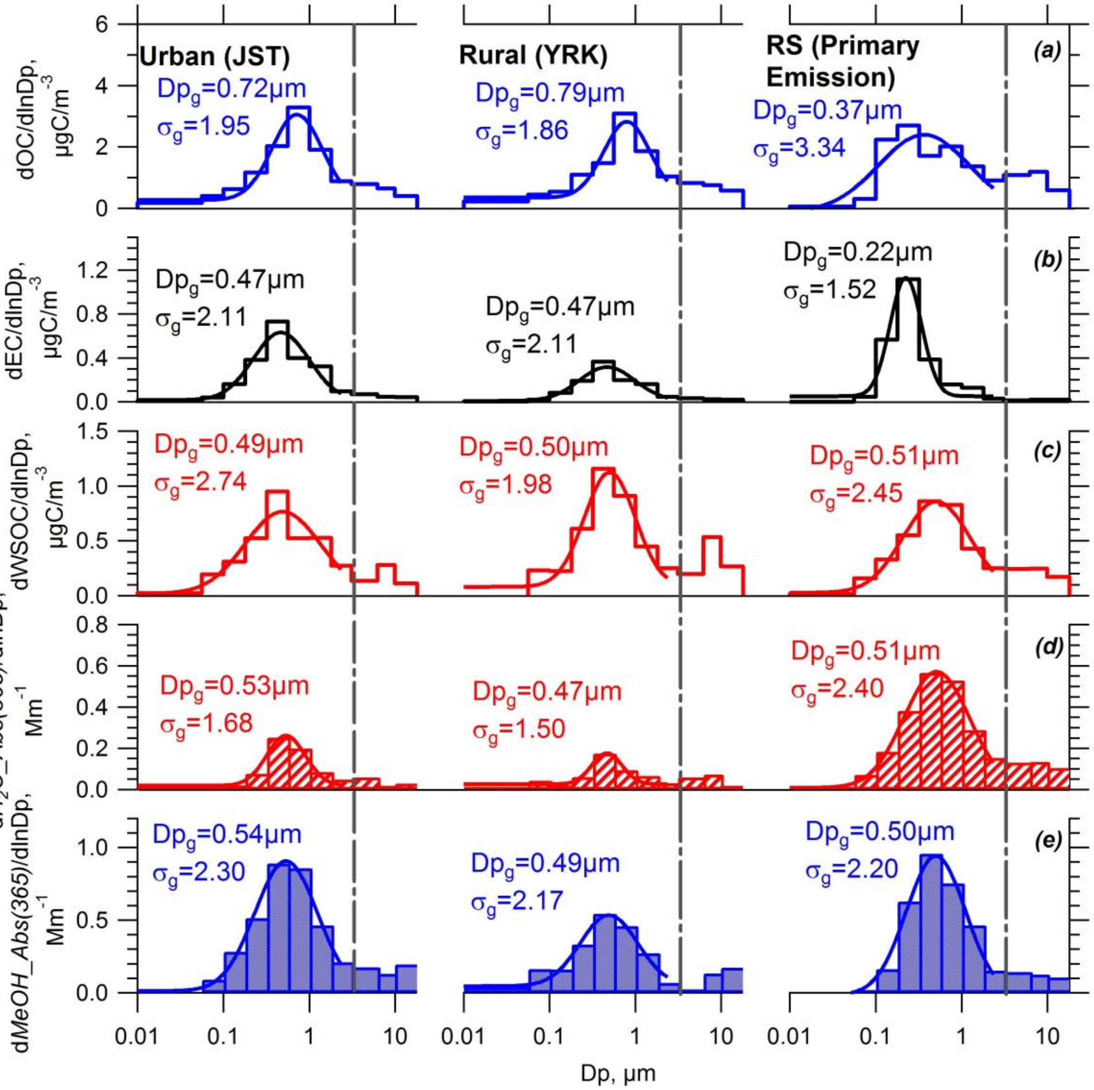

Figure 3.3 Size distributions of (a) OC, (b) EC, (c) WSOC, (d) water-soluble absorption (365nm), and (e) methanol-soluble absorption (365nm) from MOUDI samples collected at JST, YRK and RS sites. The after-filter is included as a size channel from 0.01 to 0.056 μm. The vertical line at 3.1 μm and all measurements below that size are viewed as fine particles. For JST and YRK the multiple measurements have been averaged. Geometric mean diameters and geometric standard deviations from lognormal fits to fine particles are included. Particle sizes are aerodynamic diameters.

Like the online data, the size distributions of EC and OC were generally consistent among the five sets of samples collected at JST and YRK, but differed from the RS sample. RS OC and EC were significantly shifted to lower size ranges, similar to previous observations which show that fresh vehicular emissions are associated with smaller sizes. Aged carbonaceous particles tend to be larger due to accretion of mass, with typical urban carbonaceous aerosols often peaking at size ranges of 0.56–1.0 µm [*Chow et al.*, 2008; *Huang et al.*, 2006; *Lan et al.*, 2011]. In contrast, measurements of WSOC and brown carbon (both water and methanol extracts) had similar distributions among all three sites, including RS, with geometric mean diameters all near 0.5 µm. Light absorption for the water and methanol extracts at other wavelengths ($H_2O\_Abs(\lambda)$ and $MeOH\_Abs(\lambda)$) had similar size distributions as those plotted and all were very similar to those of WSOC.

3.3.2.1 Water and Methanol Extract Spectrophotometric Results

Before calculating the light absorption due to the chromophores, the bulk solution properties for both water and methanol extractions are first discussed. Figure 3.4 shows typical spectra of water and methanol extracts from the same sample (JST MOUDI stage 6, aerodynamic diameter between 0.56 and 1.00 µm). Although the complete light absorption spectra were recorded from 200 to 800 nm, signals below 300nm and larger than 700nm have a substantial amount of noise and therefore were not included in the analysis of optical properties. The absorption spectra are consistent in shape with other studies (e.g., *Duarte et al.*, 2005; *Sun et al.*, 2007; *Hecobian, et al.*, 2010; *Chen and Bond*, 2010; *Zhang et al.*, 2013) of brown carbon and have the common characteristic of increasing absorbance with decreasing wavelength, with little to no absorption above mid-visible. These spectra are in stark contrast to black carbon absorption, with absorption Ångström exponents close to 1 (discussed further below) and confirm that light absorption is due to a different aerosol component (i.e., brown carbon).

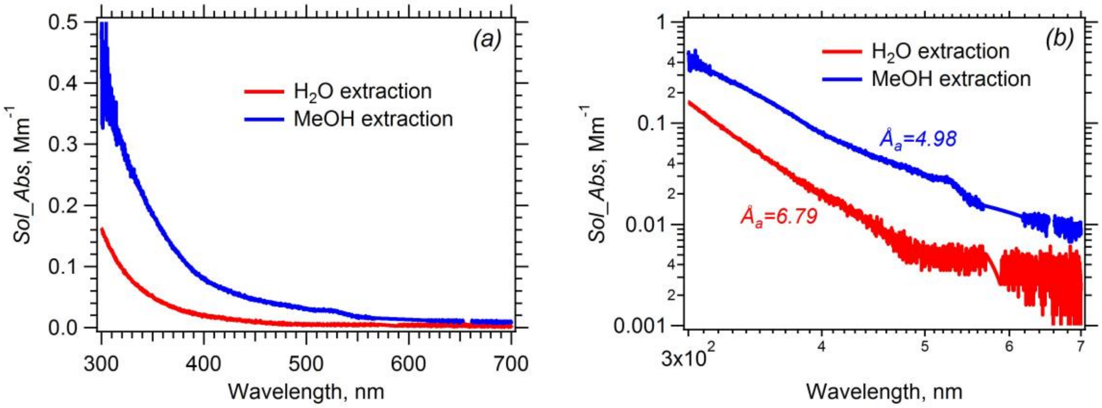

Figure 3.4 Example solution spectra of H_2O and MeOH (methanol) extracts from the same MOUDI stage (JST, May 25 – 27, 2012, stage 6 with particle aerodynamic diameter between 0.56 and 1.0 µm). Figure (a) is in linear scale and (b) in log-log scale. Absorption Ångström exponent is calculated by linear regression fit to logAbs vs. logλ in the wavelength range of 300-500nm.

Table 3.3 compares light absorption in water and methanol extracts over fine particle sizes for all three sites (data averaged at each site) at different wavelengths. Comparisons from the table show a number of interesting features.

1. Light absorption by organic carbon extracted in water is always smaller than methanol extracts, although the value varies with wavelength and site. This is expected since methanol should extract a greater range of compounds than just

the polar compounds dissolved by the water extraction process, as has been seen in other studies [*Chen and Bond*, 2010; *Zhang et al.*, 2013].

2. Although absorption drops off with increasing wavelength, *MeOH_Abs(λ)* decreased more slowly and so absorbs more at higher wavelengths than water extracts (water/methanol ratio is much smaller at 571nm compared to smaller wavelengths). This is similar to the findings of *Zhang et al.*, [2013] and thought to be due to higher molecular weight chromophores exclusive to the methanol extract that absorb at higher wavelengths.
3. Mass absorption efficiencies (α/ρ) are higher at the RS site indicating the role of primary vehicle emissions as a brown carbon source [*Hecobian et al.*, 2010; *Zhang et al.*, 2011]).
4. Surprisingly, fresher emissions at the RS site have a greater fraction of water-soluble chromophores compared with the more aged regional JST and YRK samples. For example, water/methanol absorption ratios were higher than 0.53 at the RS site, but range between about 0.1 and 0.4 at JST and YRK, and (α/ρ water)/(α/ρ methanol) ratios were greater than 1.5 at RS, but less than 0.6 for JST and YRK. This may suggest that the chromophores become less water-soluble with age, possibly due to chemical aging. However, because

measurements at various sites were not made simultaneously, these contrasts are somewhat uncertain.

Table 3.3 Values of absorption, absorption per mass α/ρ (normalized by WSOC for water extracts and OC for methanol extracts) and the ratio between water and methanol extracts for samples collected at JST (urban), YRK (rural) and RS (road-side). Data are averages for all stages 3.1 μm and below, plus the final filter. Unit of absorption (Abs) is Mm^{-1}, and for α/ρ the unit is m^2g^{-1} (see Eq. 3.5).

	Abs (water)				**α/ρ (water)**			
	350nm	365nm	450nm	571nm	350nm	365nm	450nm	571nm
JST	0.40	0.33	0.17	0.019	0.16	0.14	0.071	0.0078
YRK	0.46	0.32	0.18	0.019	0.19	0.13	0.072	0.0078
RS	1.75	1.27	0.24	0.04	0.73	0.53	0.10	0.016
	Abs (methanol)				**α/ρ (methanol)**			
	350nm	365nm	450nm	571nm	350nm	365nm	450nm	571nm
JST	0.99	1.34	0.64	0.20	0.29	0.39	0.19	0.060
YRK	1.33	1.39	0.66	0.18	0.39	0.41	0.19	0.054
RS	2.38	1.80	0.36	0.08	0.36	0.27	0.056	0.011
	Ratio of Absorption (water/methanol)				**Ratio of α/ρ(water/methanol)**			
	350nm	365nm	450nm	571nm	350nm	365nm	450nm	571nm
JST	0.40	0.24	0.27	0.09	0.56	0.34	0.38	0.13
YRK	0.35	0.23	0.26	0.10	0.49	0.32	0.38	0.15
RS	0.74	0.71	0.67	0.53	2.03	1.96	1.79	1.45

3.3.3 Light Absorption from Mie Calculations

3.3.3.1 Comparison of predicted BC absorption based on EC size distributions to measured BC

To roughly test the validity of the MOUDI size-resolved Mie calculation (with its inherent assumptions) at predicting light absorption by aerosols, Mie theory was first used to estimate b_{ap} from MOUDI-EC data (b_{ap_EC}), which is then compared with the co-located, scattering corrected, b_{ap} by Aethalometer (b_{ap_Aeth}). First, Mie calculations were done at the MAAP wavelength of 670nm, a wavelength where b_{ap_Aeth} should not be affected by brown carbon (see Figure 3.4), and where b_{ap_Aeth} and b_{ap_MAAP} are in close agreement. Later, b_{ap_EC} is compared to b_{ap_Aeth} over a range of wavelengths. The Mie calculation is based on: the EC concentrations (NIOSH method, thermal EC) measured on each stage, an assumed refractive index of 1.97-0.79*i*, [*Bond and Bergstrom*, 2006] and an EC density of 1.8 g cm^{-3} [*Bond and Bergstrom*, 2006]. Light absorption (b_{ap}) is calculated for each stage and the sum for the 3.1 μm stage and below (plus after-filter) compared to b_{ap_Aeth}, shown in Figure 3.1. Five direct comparisons are possible from the JST and YRK studies (Aethalometer data is not available at the RS site). b_{ap_EC} is in good agreement with the Aethalometer measurements, with a largest deviation of 27%. The mean ± stdev of the MOUDI/Aeth b_{ap} ratio was 1.00 ± 0.20. The good agreement between b_{ap_EC} and light absorption data by optical instruments is similar to that found by *Carrico et al.* [2003], which reported a model/measured ratio of 1.12±0.36. The results suggest that it is not necessary to apply more complex internal mixtures and/or core/shell assumptions for particles to accurately estimate the light absorption coefficient based on size distributions measurements of EC at longer visible wavelengths.

3.3.3.1.1 Uncertainties in Mie-Predicted Absorption

The sensitivity of predicted b_{ap_EC} (and similarly for $b_{ap,H2O}$ and $b_{ap,MeOH}$ discussed below) to the various measured and assumed parameters used in the calculation were assessed. Variability in particle density (±10%), both directly in the Mie calculation and conversion of aerodynamic to physical diameter, the use of a single particle size for each MOUDI stage, sensitivity to the real part of the refractive index (m range of 1.4 to 2.0), and including variability in using carbon mass for M (discussed above), leads to an overall uncertainty in b_{ap_EC} (and $b_{ap,H2O}$ and $b_{ap,MeOH}$) of 30%, when combined by quadrature sum of squares (see Table 3.2). Including uncertainty associated with the EC measurement, the b_{ap_EC} uncertainty is 34%. Thus, differences between online b_{ap_Aeth} and b_{ap_EC} of less than 27% are well within associated uncertainties (b_{ap_Aeth} ±36% and b_{ap_EC} ±34%).

3.3.3.2 Brown Carbon Refractive Index for Mie Calculations

There is limited data on the complex component (k) of the ambient particle refractive index due to brown carbon. k depends on wavelength, which accounts for the color, and can vary with particle size. Reported values range from 0.002 to 0.27 at wavelengths between roughly 500-550nm [*Dinar et al.*, 2008; *Hoffer et al.*, 2006; *Lukacs et al.*, 2007; *Kirchstetter et al.*, 2004]. *Alexander et al.* [2008] reported a k of 0.27 at 550nm for aerosols in East Asian–Pacific outflow, applying TEM to individual particles. Biomass burning HULIS extracted in water had a solution k of 0.0018 at 532nm [*Hoffer* *et al.* 2006]. *Lack et al.* [2013] reported a *k* value of 0.009 at 404 nm for aerosols originated from biomass burning plumes. Given the variety of locations, expected variability in aerosol sources and analytical methods used to determine *k*, wide variability in *k* may be expected.

Table 3.4 summarizes values of *k* determined from the MOUDI samples at the three sites for three wavelengths, and for each MOUDI stage (particle size). As noted, the *k* values reported here are referenced to organic mass. As expected, wavelength has the largest effect on *k*. Variability in *k* was fairly small over the various MOUDI stages for water-soluble brown carbon. This is because size distributions for both water-soluble brown carbon absorption and WSOC concentration have a similar shape and so α/ρ does not vary significantly among the MOUDI stages. More variability is seen in *k* for methanol-extractable brown carbon due to larger differences between *MeOH_Abs(λ)* and OC distributions. Averaged over all fine particle sizes (average is determined by including a mass concentration weighting), for JST and YRK samples, *k* is 0.0040±0.0011 for water-soluble and 0.0082±0.0036 for methanol soluble extracts at 350 nm. These values decrease to 0.0002±0.0001 and 0.0009±0.0004 at 571 nm, assuming the same particle density for both WSOC and OC of 1.5 g/cm^3 [*Carrico et al.*, 2003]. These values are significantly higher at the RS site, where there is a larger impact from primary vehicle emissions.

Table 3.4 Derived absorbing component of the complex refractive index (*k*) of brown carbon from MOUDI substrates extracted in water or methanol ($H_2O\_Abs(\lambda)$ or $MeOH\_Abs(\lambda)$). Tabulated values are $k\ x\ 10^3$. Note that these refractive indices are assuming externally mixed aerosols composed of only WSOC or OC, i.e., they are calculated by normalizing to WSOC and OC mass, see Eqs (3.6) and (3.7).

	JST						**YRK**						**RS**					
Dp_{50}, µm	350nm		450nm		571nm		350nm		450nm		571nm		350nm		450nm		571nm	
	H_2O	MeOH	H_2O	MeOH	H_2O	MeOH	H_2O	MeOH	H_2O	MeOH	H_2O	MeOH	H_2O	MeOH	H_2O	MeOH	H_2O	MeOH
2.36	3.14	4.64	0.39	2.76	~0	0.78	2.58	3.23	0.90	0.83	0.29	0.21	13.58	3.79	1.96	0.67	0.31	0.12
1.34	2.66	4.91	0.69	2.62	0.38	0.49	2.55	6.71	0.93	1.89	0.16	0.51	14.93	7.58	2.16	1.34	0.34	0.25
0.75	5.16	5.32	1.12	3.20	0.22	1.13	4.67	7.30	1.16	2.18	0.16	0.64	14.03	8.36	2.03	1.48	0.32	0.27
0.42	4.36	10.38	1.74	4.55	0.10	1.46	5.71	14.54	1.26	4.66	0.18	1.47	14.70	12.48	2.12	2.20	0.34	0.41
0.24	3.67	8.91	0.90	4.25	0.26	1.54	3.52	11.95	0.91	3.64	0.12	1.00	15.37	8.05	2.22	1.42	0.35	0.26
0.13	3.23	7.23	0.58	2.88	0. 30	0.99	4.59	10.94	0.87	3.66	0.28	1.09	12.48	1.63	1.80	0.29	0.29	0.05
0.07	3.57	3.41	1.75	2.56	0.31	0.55	5.79	14.12	0.45	4.46	0.33	1.16	10.03	1.33	1.45	0.23	0.23	0.04

3.3.3.3 Water and Methanol Mie Results: Brown Carbon b_{ap}

3.3.3.3.1 Solution vs Mie-predicted Light Absorption

Figure 3.5 shows the comparisons between the absorption measured in the solutions at 365 nm (*Abs(365)*) and Mie-predicted brown carbon light absorption by the particles for both water ($b_{ap,H2O}$) and methanol ($b_{ap,MeOH}$) extracts at 365nm. For both water and methanol-extracts, the correlations are high and very similar among all three sampling sites. They also did not change significantly with aerosol size. Mie predicted $b_{ap,H2O}$ and $b_{ap,MeOH}$ were factors of 2 and 1.8, respectively, times the bulk solution measurement (i.e., $b_{ap,H2O}/H_2O\_Abs$ and $b_{ap,MeOH}/MeOH\_Abs$, at 365 nm). For higher wavelengths, the ratios were similar (e.g., 1.9 and 1.8, respectively, at 450nm). Previous studies generally assume a small particle limit, where the particle size is not comparable to wavelength, when estimating particle light absorption from bulk solutions, in which case the factor is 0.69 to 0.75 [*Nakayama et al.*, 2013; *Sun et al.*, 2007]. In contrast, our results suggest that because the ambient brown carbon aerosols are in the accumulation mode, the actual atmospheric absorption is approximately 2 times higher than what is estimated by bulk absorption in liquids and that this is a fairly robust conversion factor.

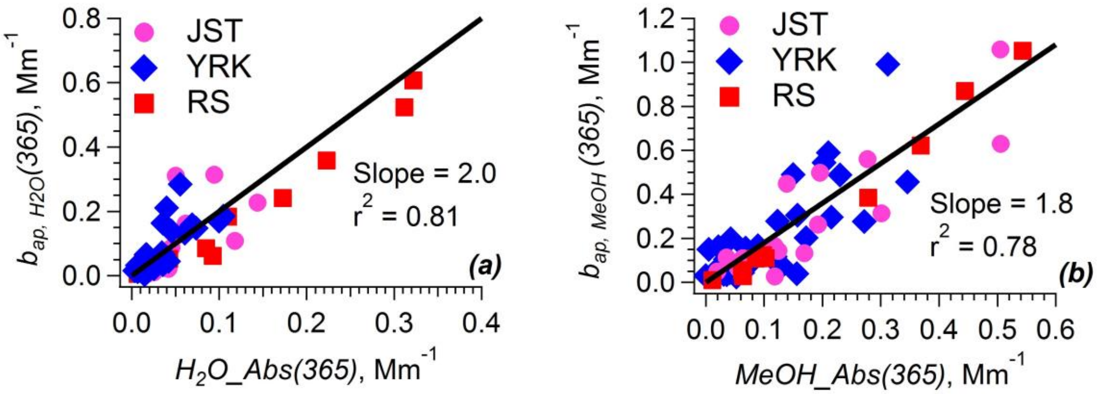

Figure 3.5 Comparison of Mie-predicted absorption to solution absorption for (a) water-extracts and (b) methanol-extracts at 365nm. Data are all fine stages from the 6 MOUDI samples collected. The correlation did not change with either aerosol size or sampling sites suggesting a robust relationship. The slope and r^2 given is for combined data.

3.3.3.3.2 Comparison of brown carbon absorption to black carbon

Comparisons between calculated brown carbon absorption ($b_{ap,H2O}$ and $b_{ap,MeOH}$) to that of EC absorption predicted by the Mie calculation (b_{ap_EC}) and BC absorption measured by the Aethalometer (b_{ap_Aeth}), for all three sites, are shown in Figure 3.6a. The Mie calculations were made at the various Aethalometer measurement wavelengths. In each case, the b_{ap} data are fitted with a power law to provide the absorption Ångström exponents. Representative uncertainties are included in the plot and summarized in Table 3.2. Data for Figure 3.6 are provided in Table 3.5.

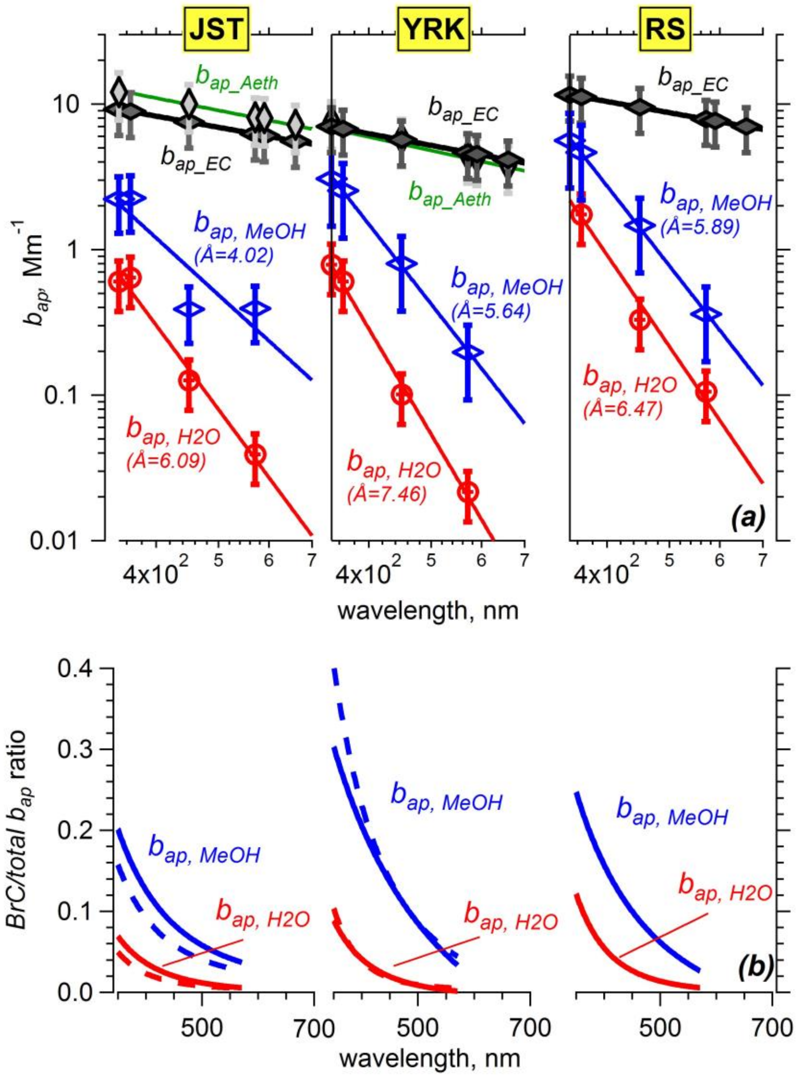

Figure 3.6 (a) Mie-predicted absorption of methaol-soluble brown carbon, water-soluble brown carbon, and BC absorption from EC data, and Aethalometer-measured BC, absorption, all at the 7 wavelengths of the Aethalometer. (b) Contribution of brown carbon (water-soluble and methanol-soluble) to total light absorption at JST, YRK and RS sites, where solid lines show the relative fraction to EC plus BrC (e.g., $b_{ap,MeOH}/(b_{ap,MeOH} + b_{ap\_EC})$, or $b_{ap,H2O}/(b_{ap,H2O} + b_{ap\_EC})$), and dotted lines show the fraction relative to Aethalometer absorption (e.g., $b_{ap,MeOH}/b_{ap\_Aeth}$ or $b_{ap,H2O}/b_{ap\_Aeth}$). No Aethalometer data were available at the RS site. For JST and YRK, where multiple MOUDI measurements were made, averages are plotted. Error bars are based on calculations summarized in Table 3.2, where additional estimates of errors can be found.

Table 3.5 Values of Mie-calculated EC absorption (b_{ap_EC}), water-soluble fine particle brown carbon absorption ($b_{ap,H2O}$), methanol-soluble fine particle brown carbon absorption ($b_{ap,MeOH}$), and scattering corrected Aethalometer absorption (b_{ap_Aeth}) for various wavelengths at all three sites. Units are Mm^{-1}. Data are averages for cases of multiple MOUDI measurements at a given site and are also plotted in Figure 3.6.

	JST				**YRK**				**RS**		
	b_{ap_Aeth}	b_{ap_EC}	$b_{ap,H2O}$	$b_{ap,MeOH}$	b_{ap_Aeth}	b_{ap_EC}	$b_{ap,H2O}$	$b_{ap,MeOH}$	b_{ap_EC}	$b_{ap,H2O}$	$b_{ap,MeOH}$
350	12.11	9.18	0.60	2.22	7.62	6.99	0.79	3.07	11.57	NAN	5.62
365	NAN	8.88	0.64	2.26	NAN	6.76	0.60	2.54	11.20	1.74	4.65
450	9.97	7.53	0.13	0.39	5.78	5.68	0.10	0.80	9.49	0.33	1.47
571	8.08	6.24	0.04	0.39	4.45	4.66	0.02	0.20	7.86	0.11	0.36
590	8.03	6.08	BDL	BDL	4.29	4.53	BDL	BDL	7.66	BDL	BDL
660	7.20	5.56	BDL	BDL	3.79	4.13	BDL	BDL	7.01	BDL	BDL

NAN: no data; BDL: below detection limit

From Figure 3.6a it is noted that differences in b_{ap_EC} between sites for the various λ is similar to what was discussed above for the EC concentrations. As a rural site, YRK b_{ap_EC} is somewhat lower compared to JST, and both were significantly lower than the RS site, which was almost twice the YRK level. Similar differences are seen for Brown carbon ($b_{ap,H2O}$ and $b_{ap,MeOH}$), with highest absorption for the various λ at the RS site, and more similar levels at JST and YRK. Curiously, $b_{ap,H2O}$ and $b_{ap,MeOH}$ at YRK were slightly higher than JST, although b_{ap_EC} was lower, suggesting a source in the rural region.

Comparing Mie-predicted EC absorption to the Aethalometer measurement shows that when multiple measurements at a given site were averaged, b_{ap_EC} was systematically lower than b_{ap_Aeth} by ~30% at JST for all wavelengths, but the two were similar at YRK, over the 300-700 nm wavelength ranges (also see Table 3.5). This can also been seen in the comparison at 670 nm shown in Figure 3.1. The cause of this is unknown. *Bond and Bergstrom* [2006] have suggested that Mie theory leads to an under-prediction of the mass absorption efficiency for EC due to interactions between the spherules that form the aggregate, but no such discrepancy is seen at YRK.

Absorption Ångström exponents for the Aethalometer data were 0.95 ± 0.02 and 0.91 ± 0.03 for JST and YRK (no Aethalometer data available at RS), respectively, (± is 1 σ regression uncertainty), and $b_{ap,\,EC}$ had similar values. These exponents are consistent with that of pure black carbon, where a value of ~1 is typical [*Kirchstetter et al.*, 2004]. In contrast, the brown carbon had significantly higher absorption Ångström exponents, ranging from 4 to 6 for $b_{ap,MeOH}$ and 6 to 8 for $b_{ap,H2O}$ among sampling sites. This is the typical spectral characteristic of brown carbon of increasing absorption with lower wavelength, and with little absorption at wavelengths greater than roughly 550 nm. Note that these absorption Ångström exponents from the Mie-predicted brown carbon absorption by particles (b_{ap}) are similar to those of the bulk solution (Figure 3.4 and see *Zhang, et al.*, [2013] and references therein) suggesting bulk solutions can reasonably be used to estimate particle absorption Ångström exponents.

Figure 3.6b shows the magnitude of $b_{ap,MeOH}$ and $b_{ap,H2O}$ at different wavelengths relative to total absorption, with total absorption estimated in two ways; 1) from the sum of b_{ap_EC} plus water or methanol brown carbon (solid line), and 2) relative to just the Aethalometer data (b_{ap_Aeth}, dotted line). The two estimates differed by typically less than 10%. These results suggest the contribution of brown carbon is approximately 5-10% relative to total absorption for water-soluble, and 20-40% for methanol-soluble components at 350 nm. At larger wavelengths the fraction drops rapidly, reaching approximately zero near 550nm.

Comparing these fractional contributions of brown carbon among the three sites it is seen that although levels of brown carbon at the RS were largest, due to primary emissions (EC and BC was also elevated), the fraction of brown to total light absorption was not correspondingly higher relative to the other sites. The highest fraction of brown carbon was at YRK, due to relatively high WSOC and OC concentrations with significantly lower EC concentrations (e.g., highest OC/EC ratios, see Table 3.1). The results suggest that, from a relative point of view, (but not in in terms of absolute absorption), the role of brown carbon may be most important in regions not associated with strong EC sources, such as remote locations. Possible contributions from natural (biogenic) sources, or generation of secondary brown carbon due to chemical aging, may account for the higher proportion of brown to black carbon. It is noted that this study was not significantly impacted by biomass burning emissions, which are a known strong source for brown carbon.

3.3.3.3.3 Comparisons to Other Studies

The results of this direct measurement of brown carbon combined with a simple Mie calculation shows significant absorption at UV wavelengths relative to BC. Similar results have been reported from both observations and model simulations using a variety of methods to infer brown carbon b_{ap}. Comparisons are summarized in Table 3.6, where the fraction of brown carbon to total light absorption is listed along with typical b_{ap} values from the various studies to provide some measure of the aerosol loading for each location. Most of the studies are substantially more polluted compared to conditions during our observations, but generally the fraction of brown carbon light absorption is similar. *Hoffer et al.* [2006] estimated that the contribution of HULIS to light absorption was only a few percent in Amazonia biomass burning aerosols at 532nm and 35-50% at 300nm. Biomass burning aerosols are known to have high mass absorption efficiencies [*Hecobian et al.*, 2010; *Lack et al.*, 2012] and this may account for the high values. Observations from more highly polluted urban areas, including Xianghe (China) and Mexico City have fractional levels of brown carbon to total absorption of 30 to 40% at 400nm, that decreases to 10% at 550nm [*Barnard et al.*, 2008; *Yang et al.*, 2009]. Using column-integrated satellite data, *Bahadur et al.* [2012] also reported a similar fraction of brown carbon (~40% of the EC at 440nm) from 10 AERONET sites in CA. *Cappa et al.*, [2012] reports lower fractions of brown carbon in

Los Angeles, at 13% at ~400nm, by directly measuring the enhancement in aerosol absorption. Our results are similar, or slightly lower, compared to previous observations, but they are generally in cleaner environments.

Table 3.6 Comparison of estimated brown carbon contribution in the present study with previous reports.

Wavelength (nm)	**BrC fraction**	b_{ap} **(Mm^{-1})**	**Location**	**Instrumentation/ Method**	**Reference**
300	Up to 50%	-	Rondˆonia, Brazil	PAS and Nephelometer+Mie	Hoffer et al., 2006
400	~40%	~200	Mexico City	Multi-Filter Rotating Shadowband Radiometer	Barnard et al., 2008
400	~30%	~80	Xianghe, China	PSAP, Aethalometer and Nephelometer	Yang et al., 2009
550	~10%	~50	Xianghe, China		Yang et al., 2009
440	~40%	-	CA	AERONET dataset	Bahadur et al., 2012
405	13%	-	Los Angeles region, CA	Photoacoustic-spectroscopy	Cappa et al., 2012
532	6%	-	Los Angeles region, CA		Cappa et al., 2012
400	**10 to 30%**	**10-15**	**YRK, JST, RS**	**Spectrophotometer measurements of liquid extracts+Mie calculations**	**This study, Methanol**
500	**5 to 10%**	**8-12**	**YRK, JST, RS**		**This study, Methanol**

3.4 Summary

Spectrophotometric measurements of fine particle extracts [*Hecobian et al.*, 2010] have shown that light absorbing compounds with a strong wavelength dependence, and correlation with organic aerosol concentrations [*Hecobian et al.*, 2010], are ubiquitous in the southeastern US. These chromophores are assumed to be components of the so-called brown carbon aerosol. In this study, a cascade impactor (MOUDI) was used to collect size resolved aerosols on quartz filter substrates that were subsequently extracted in water and methanol and the light absorption properties of the extracts analyzed. A total of six MOUDI samples were collected at locations that included a rural, central urban and roadside site. From these data, particle light absorption due solely from brown carbon was estimated using Mie calculations and the results were compared to optical absorption measurements made with Aethalometer and MAAP. Chromophores in MOUDI extracts at all sites were lognormally distributed and associated with the accumulation mode (~0.5 μm geometric mean of aerodynamic diameter), an optically effective size. Mie-predicted light absorption by these particles was roughly two times greater than the bulk solution light absorption, over a range of wavelengths (350 to 571nm) at all sites. This is significantly higher than the small particle limit used in other studies when estimating particle light absorption from bulk solutions (factor of ~0.7).

Brown carbon was optically important at wavelengths less than roughly 600nm with a fractional absorption relative to total absorption between 5 and 10% for water extracts and 20 and 40% for methanol extracts at 350nm. Highest relative absorption was measured at the rural site where OC/EC ratios were highest, possibly indicating a secondary source for brown carbon that may be optically important.

Use of solvent extracts to estimate brown carbon b_{ap} has the advantage that it can be isolated and the light absorption measured directly with high spectral resolution, in contrast to direct measurements of wavelength dependent absorption that must infer a black carbon wavelength dependent absorption. However, assumptions associated with Mie calculations presented in this study may lead to substantial uncertainty, such as assuming the brown carbon is externally mixed with other light absorbers, like EC. This means the method does not consider possible light absorption enhancements due to particle morphology, such as shell-core configurations [*Bond et al.*, 2006; *Cappa et al.*, 2012; *Lack et al, 2010*]. However, the extent of shell-core optical effects is unclear. Recent measurements in Los Angeles suggest that despite coatings on soot, there was little light enhancement (6% at 532nm, [*Cappa et al.*, 2012]).

A multi-wavelength Aethalometer did not show evidence for enhanced light absorption at lower wavelengths. Although the levels of brown carbon absorption are within the Aethalometer measurement uncertainty (35%), the discrepancy is worth exploring further to determine the cause, whether associated with the assumptions inherent in the solution absorption-Mie method applied here (i.e., the method possibly over-predicts brown carbon absorption) or related to Aethalometer operation/data interpretation limitations. Many studies (e.g., *Rizzo et al.*, 2011) have shown that aethalometers detect brown carbon when the levels are high, such as in biomass burning plumes, but the instrument may have difficulty resolving brown from black carbon when relative levels are not greatly enhanced, a condition likely to be found frequently in the ambient troposphere. Repeating this study in an environment more heavily influenced by brown carbon would be useful.

CHAPTER 4

BROWN CARBON AEROSOLS IN THE CONTINENTAL FREE TROPOSPHERE: SOURCES, EXTENT AND CLOSURE ANALYSES

4.1 Background

Carbonaceous components of particles are known to affect climate through directly scattering and absorbing solar radiation. Traditionally, the much larger fine particle organic mass fraction (referred to as organic carbon, OC, or organic matter OM) was assumed to be non-absorbing and through only scattering light acted to cool the climate [*Koch et al.*, 2007; *Myhre et al.*, 2008]. Black carbon (BC), or soot, strongly absorbs light, and although a small mass fraction, substantially warms the climate [*Bond et al.,* 2013]. Globally, BC forcing is ranked as the second most important individual climate-warming agent after carbon dioxide [*Bond et al.,* 2013], considering both direct and indirect effects. Recent studies have shown, however, that components of OM also contribute to light absorption [*Yang, et al.*, 2009; *Zhang et al.*, 2011, 2013], especially those from biomass burning emissions, and that their influence on climate may be substantial [*Bahadur et al.*, 2012; *Chung et al.*, 2012; *Feng et al.*, 2013; *Park et al.*, 2010]. These compounds are referred to as Brown Carbon (BrC hereafter).

A variety of studies have investigated the sources for BrC. Primary BrC is known to be emitted directly from incomplete combustion of fossil or biomass fuels [*Hoffer et* *al.*, 2006; *Lukacs et al.*, 2007; *Andreae and Gelencser,* 2006], while secondary organic aerosol (SOA) formed from these emissions may also be brown [*Saleh et al.*, 2013]. Laboratory studies show that light-absorbing secondary compounds (chromophores) can be formed through a variety of mechanisms, including aromatic-SOA production under high NO_x, and a variety of aqueous phase reactions, such as lignin [*Hoffer et al.*, 2006] and isoprene oxidation [*Limbeck et al.*, 2003], and reactions of carbonyls (e.g., glyoxal, methyglyoxal) in acidic solutions [*Sareen et al.*, 2010], with amino acids [*de Haan et al.*, 2009a], methyl amines [*de Haan et al.*, 2009b], or ammonium salts [*Sareen et al.*, 2010]. Atmospheric aging of chromophores may also lead to a loss of light absorption due to photo-bleaching [*Zhong et al.*, 2013].

BrC can be difficult to identify with standard aerosol optical instruments. *Lack and Langridge* [2013] suggested that use of Absorption Ångström Exponents (AAE) to predict BrC absorption can lead to substantial uncertainties. Difficulties arise because optical instruments cannot directly measure BrC independently of BC. The method is based on differences between absorption at low wavelengths, where BrC absorption is effective, to what is expected from BC alone. Uncertainty arises in both factors used to determine the difference. Often light absorption at low wavelengths is determined from extrapolations based on Absorption Ångström Exponents from a limited number of wavelengths. Uncertainties in what BC absorption should be, further limits identifying a BrC influence to situations where it plays a dominate role. Much higher sensitivity for identifying BrC is possible by directly measuring chromophores in aerosol solution extracts since the method isolates BrC from other absorbers (BC and mineral dust) and long path absorption cells provide high sensitivity. These direct measurements of BrC show that it is ubiquitous. Throughout Europe BrC has been linked with biomass burning and HUmic-Like Substances (HULIS) [*Lukacs et al.*, 2007]. In the southeastern U.S. BrC has been found in rainwater from continental sources [*Kieber et al.*, 2006] and in $PM_{2.5}$ associated with biomass burning in winter and possibly secondary aerosols in summer [*Hecobian et al.,* 2010; *Zhang et al.,* 2012].

The chemical composition of the chromophores in the ambient aerosol is not well characterized. *Zhang et al.* [2013] identified a number of water-soluble nitro-aromatic compounds responsible for brown carbon in Los Angeles SOA, but these compounds only accounted for ~4% of observed BrC absorption at 365nm. 4-nitrocatechol ($C_6H_5NO_4$) was identified as the largest contributor at roughly 1.4%. Curiously, using a similar analytical technique *Desyaterik et al.* [2013] reported identifying roughly half the chromophores in fog samples in a region impacted by biomass burning and 4-Nitrocatechol was a prominent component.

Although these studies of BrC from aerosol extracts have explored the sources, extent and chemistry of fine particle BrC, they have not addressed BrC's possible optical importance. To estimate optical properties, *Liu et al.* [2013] used size resolved measurements of chromophores in solutions from surface sites to estimate light absorption (b_{ap}) by BrC, assuming the brown carbon was externally mixed with other absorbers. In this study, we apply these results to aircraft-based filter measurements and use direct measurements of chromophores in solutions to estimate the extent and sources of BrC throughout the continental troposphere (up to ~12km altitude). A closure analysis is performed comparing the sum of light absorption at 365nm from BC and BrC to measurements extrapolated from a 3-wavelength PSAP (Particle Soot Absorption Photometer) and we assess the fractional contribution of BrC to overall particle light absorption.

4.2 Experimental Methods

4.2.1 NASA DC-8 Research Aircraft Measurements during the DC3 Campaign

Filters analyzed for this study were collected from the NASA DC-8 research aircraft, which was based out of Salina, KS, between May and June of 2012 as part of the Deep Convective Clouds and Chemistry (DC3) campaign. The study area focused on the central USA and the aircraft operated from near-surface to an altitude of roughly 13 km above sea level (pressure altitude). Figure 4.1 shows the locations of filter collection periods during the study, color-coded by altitude, and sampling frequency (number of filters collected/total filters) as a function of altitude.

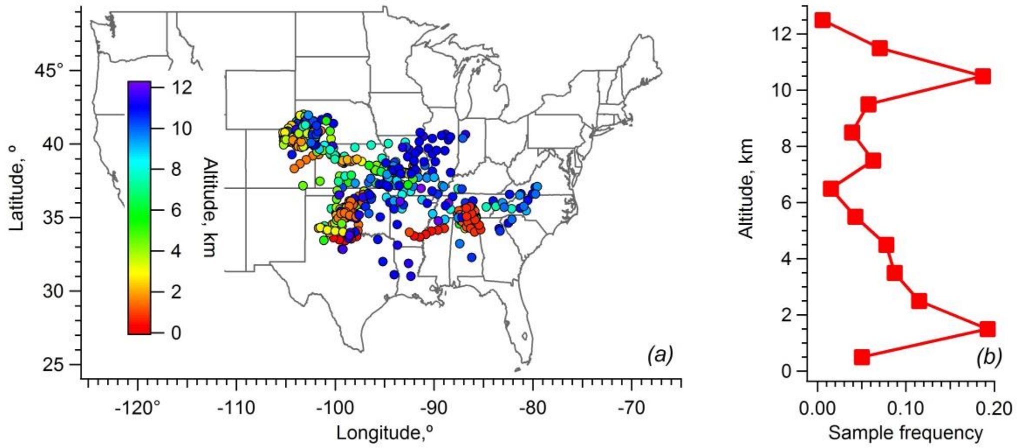

Figure 4.1 (a) Filter collection sampling locations and (b) sampling frequency versus altitude for the complete DC3 mission based out of Salina, KS, US, May-June 2012.

4.2.2 Filter Sampling, Extraction and Analysis

The filter sampling system collected particles nominally smaller than 4.1 µm aerodynamic diameter [*McNaughton et al.*, 2007] onto 1 µm pore, 90mm diameter, Teflon (EMD Millipore) filters. Sampling was generally done during level flight legs with typically 5 min integration times. In total, 609 filter samples were collected from 22 flights, along with 2 field blanks per flight. Data were corrected by subtraction of average of the blank on each flight. Over the course of the study they were not uniformly collected over the measurement column. Figure 4.1b shows the filter sampling frequency as a function of altitude.

Filters were extracted first in 15 mL of high purity water (18.3 Mohm) by 30 minutes of sonication. The extracts were then filtered via a 25mm-diameter 0.45 µm pore syringe filter (Fisher Scientific, Fisherbrand* Syringe Filters) to remove insoluble components and any filter remnants generated during the extraction process. Water extracts were transferred into a Liquid Waveguide Capillary Cell coupled to a Total Organic Carbon (LWCC-TOC) analyzer. The combined system quantifies the water-soluble UV-Vis (nominally 200 to 800nm wavelength range) light absorption spectra ($H_2O\_Abs\ (\lambda)$) and water-soluble organic carbon (WSOC) mass following the method by *Hecobian et al.* [2010]. The limit of detection (LOD) was determined as 3 times the standard deviation of field blanks. At 365 nm the LOD of the solution light absorption measurement ($H_2O\_Abs\ (365)$) was 0.031 Mm^{-1}, whereas the WSOC LOD is estimated at 0.084 $\mu gC/m^3$. Measurement uncertainties are estimated at 20% for $H_2O\_Abs\ (365)$ and 9% for WSOC, based on relative errors in water blanks, field blanks, and standard deviation of standards (or duplicate measurements on same filter for absorption measurements).

Following water extraction, the extraction vial and filter were drained and dried by inverting and the filter re-extracted in 15 mL of methanol (VWR International, A.C.S. Grade) following the same procedure. For the methanol extract, only the UV-Vis absorption spectra were measured. The estimated LOD for Methanol-soluble light absorption measured at a wavelength of 365nm (*MeOH_Abs (365))* is 0.11 Mm^{-1} with an uncertainty of 27%. Here, total solution absorption (*Total_Abs (λ)*) is taken as the sum of water-soluble and methanol-extracted brown carbon absorption from the sequential extraction process, although it is recognized that this process may not extract all chromophores [*Chen and Bond*, 2010].

4.2.3 Online Measurements

4.2.3.1 Gases

Acetonitrile (CH_3CN), used as a biomass-burning tracer in the following analysis, was measured via PTRMS with an uncertainty of ±20%. CO, also used in determining biomass burning events, was provided by a Diode laser spectrometer from NASA Langley Research Center. The uncertainty in CO data is 2%.

4.2.3.2 Aerosols

Particle light absorption coefficients (b_{ap}) were measured with a Particle Soot Absorption Photometer (PSAP, Radiance Research) at wavelengths of 470, 532, and 660 nm. The inlet had an intrinsic 50% cut size of 4.1 μm, consistent with the filter collection. As a filter-based optical instrument, where particle absorption is determined from light attenuation through a filter being loaded with particles, the PSAP suffers from various artifacts associated with the method [*Bond et al.*, 1999; *Petzold et al.*, 2005]. This includes multiple scattering by the filter fibers and by aerosols embedded on or within the filter; the latter increases with filter loading. Reported PSAP b_{ap} data were adjusted using *Virkkula et al.* [2010], with an estimated uncertainty of 20%.

Black carbon (BC) mass concentrations were measured with an SP2 (Humidified Dual Single Particle Soot Photometer) and corrected to account for size truncation errors to provide total accumulation mode BC concentrations [*Schwarz et al.*, 2008]. Estimated uncertainty is 30% from flow and mass calibration and aspiration efficiency. OM was measured with a high resolution time-of-flight Aerodyne Aerosol Mass Spectrometer

(AMS) [*DeCarlo et al.*, 2006] with an estimated uncertainty of 38%. In the following analysis, online data were averaged to filter sampling times. If data were unavailable for greater than 25% of the integration time, the merged data were flagged as NAN. All aircraft data are blank corrected and reported at standard temperature and pressure (273 K & 1013 mb).

4.3 Results

4.3.1 Identifying Biomass-Burning Plumes

During the DC3 campaign, some aircraft flights were targeted specifically to investigate biomass-burning emissions, while many others focused on cloud out flow. For this work, the flights are simply delineated between clearly evident biomass-burning sampling periods and all else, the latter being referred to as background free tropospheric conditions. To identify biomass-burning plumes, CO and CH_3CN were used as tracers following the method of *de Gouw* et al. [2004]. First, enhancements in CO in time-series plots were identified. For these episodes, if r^2 values for CO and CH_3CN were higher than 0.5, the plume was designated as biomass burning. Identified biomass-burning sampling periods are listed in Table 4.1. A filter sample was deemed impacted by biomass burning if greater than 75% of the sampling integration time was identified as a biomass-burning plume. By this criterion roughly 12% of collected filters were identified as biomass burning. Filters not identified are referred to as background measurements, but may still have been influenced by biomass burning due to small-duration identified or unidentified plumes intercepted during the integration time. Residual impacts from dispersed biomass burning emissions may also account for a significant fraction of the ambient aerosol throughout the free troposphere during this study.

Table 4.1 Flight periods identified to be largely impacted by biomass burning contributions.

Time (UTC)
2012/5/25, 22:00-22:26
2012/5/26, 21:20-21:40, 2012/5/27, 00:09-00:21
2012/6/6, 21:27-21:37, 2012/6/7, 00:19-00:36
2012/6/11 16:24-16:57, 17:56-18:11, 21:56-22:06
2012/6/15, 19:51-20:10
2012/6/16, 21:18-21:26, 2012/6/17 01:36-02:13
2012/6/17, whole flight
2012/6/22, whole flight

4.3.2 Study Statistical Summary

A summary of the DC-3 BrC solution measurements is given in Table 4.2. BrC in filter extracts was observed throughout the study region, with over 85% of the data above LOD. A large variation is observed in solution absorption, with *H_2O_Abs(365)* at a level of 0.20±0.53 (average ± stdev) Mm^{-1}, and *Total_Abs(365)* at 0.64±1.38 Mm^{-1} for background conditions. *Total_Abs(365)* was approximately 3-4 times higher than *H_2O_Abs(365)*, similar to previous studies [*Chen and Bond*, 2010; *Zhang et al.*, 2013; *Liu et al.*, 2013]. The BrC variations in biomass burning events were even larger (1.03±4.66

Mm^{-1} for *H_2O_Abs (365)*, and 2.37±8.67 Mm^{-1} for *Total_Abs(365)*). Some of the overall variation is due to the vertical distribution of BrC, discussed later.

Table 4.2 Statistical summary of observed species throughout all flights during DC3 separated into three categories: All samples, samples during identified biomass burning events and samples for background conditions (periods when data could not be clearly identified as biomass burning). For statistical purposes, ½ the LOD value is substituted when observation was below LOD. All data have been merged to the 5-min filter sampling time.

	LOD	**% above LOD**	**Mean**	**Median**	**Std Dev**	**Min**	**Max**
All samples							
WSOC^{a}	0.084	95	1.24	0.81	1.83	0.042	31.37
OM ^{b}	0.3	89	3.48	2.82	10.85	0.15	208.53
BC ^{b}	0.01	84	0.069	0.036	0.189	0.005	3.75
H_2O_Abs(365)^{c}	0.031	87	0.33	0.11	1.93	0.016	39.50
Total_Abs(365)^{c}	0.11	86	0.94	0.44	3.89	0.055	67.19
Biomass Burning events							
WSOC	0.084	94	1.52	0.77	3.93	0.042	31.37
OM	0.3	88	2.69	2.01	2.69	0.15	12.79
BC	0.01	83	0.056	0.035	0.060	0.005	0.399
H_2O_Abs(365)	0.031	92	1.03	0.32	4.66	0.016	39.50
Total_Abs(365)	0.11	93	2.37	0.86	8.67	0.055	67.19
Background conditions							
WSOC	0.084	95	1.19	0.82	1.28	0.042	10.68
OM	0.3	93	7.55	3.73	25.95	0.15	208.53
BC	0.01	88	0.144	0.052	0.470	0.005	3.75
H_2O_Abs(365)	0.031	86	0.20	0.10	0.53	0.016	7.52
Total_Abs(365)	0.11	85	0.64	0.36	1.38	0.055	15.44

^{a} unit: $\mu gC/m^3$; ^{b} unit: $\mu g/m^3$; ^{c} unit: Mm^{-1}

Comparing with background conditions, biomass-burning events were notable by significantly higher BrC levels relative to background conditions. Average *H_2O_Abs(365)* in the identified biomass burning plumes were 5 times higher than background conditions, while *Total_Abs(365)* was approximately 4 time higher. In contrast, the enhancement in other species were smaller; *WSOC* was only ~ 1.3, *OM* 2.8 and *BC* 2.6 times higher than background conditions. *H_2O_Abs(365)* comprised ~ 44% of the *Total_Abs(365)* for biomass burning events, while the ratio decreases to 31% for background conditions. These results confirm that biomass burning is a strong source for both water- and methanol-soluble BrC and are consistent with optical measurements of BrC in biomass burning plumes [*Lack et al.*, 2013]. The observation that the water-soluble BrC fraction (*H_2O_Abs(365)* / *Total_Abs(365)*) is lower in background air masses demonstrates that over time some of the water-soluble BrC may become less-soluble, being transformed to methanol soluble, or that other chemical processes or sources that contribute to BrC formation tend to produce less water-soluble compounds in the atmosphere.

4.3.3 Correlations

Possible associations between various species in both the biomass burning plumes and under background conditions are investigated based on correlations. Results are summarized in Table 4.3. Correlations are shown for *H_2O_Abs(365)* and *Total_Abs(365)*, where *Total_Abs(365)* is the sum of water and methanol extracts. Since a significant fraction of the BrC absorption is associated with the methanol extract, *Total_Abs(365*) correlations with various other species are driven primarily by the methanol-soluble BrC

(For brevity we do not show correlations for just the methanol-soluble BrC). Note that for airborne measurements, temporal correlations actually imply spatial correlations between species.

Table 4.3 Correlations (R values) for biomass and background conditions between selected variables. Bolded values above the matrix diagonal are from biomass burning plumes (69 data points), while italic numbers below the matrix diagonal are from background conditions (334 data points). All data were averaged to filter sampling times.

	WSOC	$H_2O\_Abs(365)$	*Total_Abs(365)*	OM	CO	BC	Acetonitrile	$b_{ap,PSAP}(470)$	$b_{ap,PSAP}(532)$	$b_{ap,PSAP}(660)$
WSOC	1	**0.99**	**0.97**	**0.96**	**0.93**	**0.70**	**0.97**	**0.75**	**0.75**	**0.75**
$H_2O\_Abs(365)$	*0.34*	1	**0.98**	**0.98**	**0.94**	**0.72**	**0.98**	**0.7**	**0.78**	**0.78**
Total_Abs(365)	*0.13*	*0.32*	1	**1.00**	**0.97**	**0.83**	**0.99**	**0.87**	**0.87**	**0.87**
OM	*0.28*	*0.57*	*0.20*	1	**0.97**	**0.85**	**0.99**	**0.89**	**0.89**	**0.89**
CO	*0.15*	*0.48*	*0.17*	*0.76*	1	**0.85**	**0.97**	**0.87**	**0.87**	**0.87**
BC	*0.20*	*0.64*	*0.30*	*0.86*	*0.75*	1	**0.82**	**0.99**	**0.99**	**0.99**
Acetonitrile	*0.11*	*0.57*	*0.23*	*0.48*	*0.52*	*0.57*	1	**0.86**	**0.86**	**0.86**
$b_{ap,PSAP}(470)$	*0.27*	*0.66*	*0.31*	*0.80*	*0.72*	*0.95*	*0.58*	1	**1.00**	**0.9997**
$b_{ap,PSAP}(532)$	*0.27*	*0.63*	*0.31*	*0.80*	*0.72*	*0.95*	*0.55*	*0.99*	1	**0.9999**
$b_{ap,PSAP}(660)$	*0.28*	*0.59*	*0.29*	*0.80*	*0.70*	*0.93*	*0.51*	*0.98*	*0.99*	1

For biomass burning samples, species expected from the smoke plumes (e.g., CO, acetonitrile, OM, WSOC BC and PSAP b_{ap} at all three wavelengths) are highly correlated with each other, and all are highly correlated with both the *H_2O_Abs(365)* and *Total_Abs(365),* consistent with a common source for all these components. The least correlated was WSOC and BC (r=0.70), and *H_2O_Abs(365)* and BC (r=0.72), possibly because some fraction of the water-soluble compounds may be secondary and not as likely to be correlated with a primary component.

In contrast, for background conditions there was a poor correlation between *H_2O_Abs(365)* and *Total_Abs(365)* (r = 0.32) and they were correlated with a different set of species. *H_2O_Abs(365)* is correlated mostly with the PSAP measurements of absorption (r = 0.66 at 470 nm) or with BC (r = 0.64), but is not well correlated with WSOC (r = 0.34). *H_2O_Abs(365)* is somewhat correlated with OM (r = 0.57) and acetonitrile (r = 0.57), suggesting that the water soluble faction in the background free troposphere could mainly be related to primary emissions and possibly linked to aged biomass burning.

Total_Abs(365) is not well correlated with any of the other parameters. Because a significant fraction of the BrC is not water soluble (i.e., *Total_Abs(365)* is roughly 3 to 4 times *H_2O_Abs(365)*), the lack of correlation suggests much of the background free troposphere BrC has undergone some form of chemical processing and may be secondary. A similar situation is observed for WSOC, where it is also not generally correlated with any of the other variables in Table 4.3. In a ground based study, *Liu et al.*

[2013] observed that as aerosols aged, BrC evolved to become less water soluble, also consistent to a chemically aging process that produces more water-insoluble BrC.

In both biomass burning and background conditions, PSAP b_{ap} is mainly correlated to BC. For all three PSAP wavelengths, there is a good correlation with BC. However, there are slight differences in the correlation between PSAP and BrC absorption for differing PSAP wavelengths, which may hint at evidence for brown carbon detected by the PSAP; a slightly higher correlation coefficient is seen between BrC, for both H_2O*_Abs(365)* and *Total_Abs(365)*, for the shorter PSAP wavelengths. This is only observed in the background air masses.

4.3.4 Altitude Profiles of Light Absorbing Aerosols

Our data show that BrC is prevalent throughout the continental free troposphere. Vertical profiles of H_2O*_Abs(365)* and *Total_Abs(365)* are given in Figures 4.2a and 4.2b for both biomass burning plumes and background conditions. The profiles were constructed by binning data into 1-km bins and plotting the bin median. Error bars represent the inner quartile ranges for each bin and demonstrate the large variability in the data, especially for the biomass burning plumes.

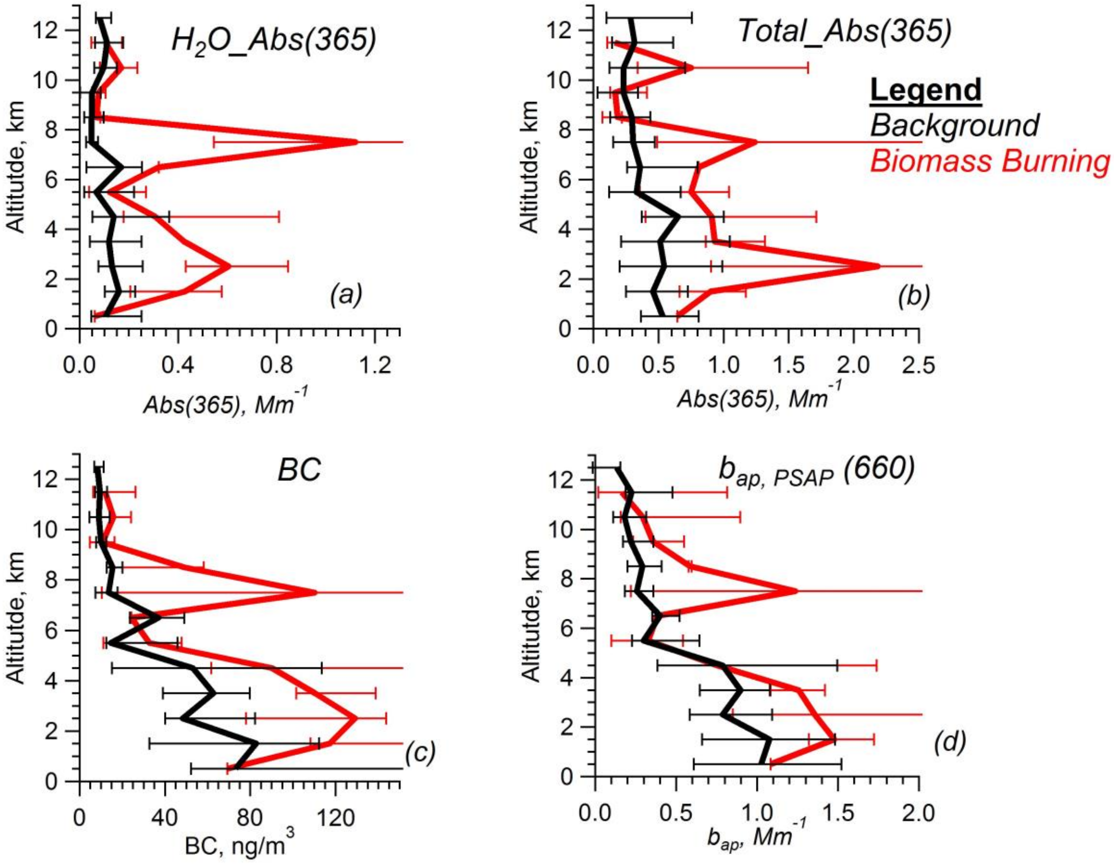

Figure 4.2 Vertical profiles of absorption measured in filter water extracts and the sum of water and methanol extract (total), both at 365nm, and estimates of BC concentration, and PSAP absorption at 660 nm. Data are binned into 1km ranges and the median values are shown. Error bars indicate inter-quartile ranges. The column in the middle shows the number of data points in each altitude bin, with black for background conditions (upper) and red for biomass burning (bottom row).

Estimated BC concentration and PSAP b_{ap} at 660nm are also plotted. BrC, BC and PSAP absorption show large differences between biomass burning events and background conditions, with the biomass burning plumes dominated at a few altitudes where the aircraft encountered and pursued specific plumes. The biomass burning altitude profiles for BrC, BC and PSAP absorption are all somewhat similar, indicating that biomass burning contributes to all carbonaceous aerosol components that absorb light, as previously shown by the high correlations amongst these species. This is less true for background conditions where differences between the light absorbing components can be seen, for example, BC levels generally seem more elevated closer to the surface.

To compare vertical profiles of aerosol light absorbing components in background air masses, the cumulative column fraction of light absorption or BC concentration is plotted in Figure 4.3. At a given altitude, the cumulative fraction is the light absorption or concentration integrated over all altitudes above, relative to the total column. Half the column BC concentration occurs at approximately 3.5 km above sea level (asl), while for brown carbon, water or total (water plus methanol extract), this occurs between 5 and 6 km, indicating a more uniform vertical distribution. PSAP-determined aerosol absorption at 660 nm and light absorption extrapolated to 365 nm is also shown (the method for extrapolating is discussed below, see Eq. 4.5). For PSAP absorption, the 50% point at 365nm is 4.5 km asl, which is between BC and BrC, suggesting a mixture of BC and BrC at 365nm, while the 50% altitude for PSAP absorption at 660 nm is ~4 km asl, much closer to BC and as expected since at 660nm BC should dominate (i.e., BrC does not effectively absorb at high wavelengths, see next section). These relative differences in vertical distributions may be due to contributions from in-situ BrC production from source(s) dispersed throughout the troposphere. Examples include primary and secondary BrC from biomass burning, or possibly some other SOA formation process. Higher BC at the surface may reflect greater contributions from fossil fuel combustion sources. Due to the limited number of data points in some altitude bins, resulting from selective sampling in biomass burning plumes at specific altitudes, similar graphs were not constructed for the biomass burning plumes.

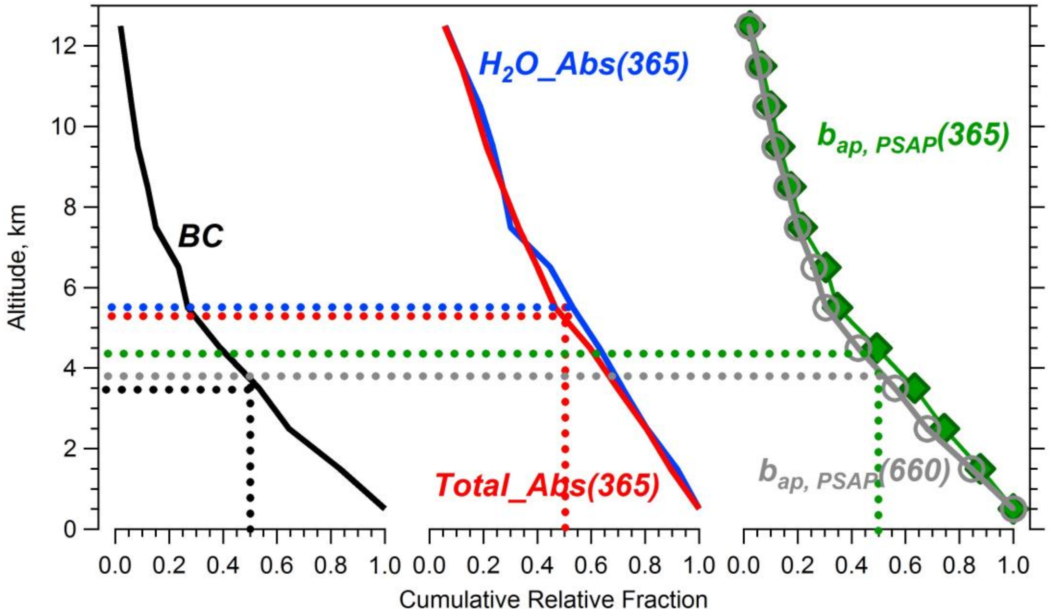

Figure 4.3 Vertical profile of the relative cumulative fraction (summed over all altitudes above vs. the total column), for BC, solution absorptions of brown carbon at 365 nm, PSAP absorption at 660 nm, and estimated PSAP total aerosol absorption at 365 nm, during background conditions.

4.3.5 Absorption Ångström Exponents for BrC and Light Absorbing Aerosols

The wavelength (λ) dependence of absorption of light is often fit with a power law of the form:

$$Abs(\lambda) = K \cdot \lambda^{-AAE} \tag{4.1}$$

Where *Abs(λ)* is the light absorption at a given wavelength (λ) for light passing through a liquid or aerosol layer and *AAE* the Absorption Ångström Exponent, (the factor K is not important in this analysis). For the high spectral resolution data available with spectrophotometric measurements of light absorption in the water or methanol aerosol extracts, the AAE (in this case AAE for BrC, AAE_{BrC}) is determined from a linear regression fit of $ln(Abs(\lambda))$ vs $ln(\lambda)$ between 300 and 500 nm. Although most of our analysis on BrC is based on absorption at 365 nm (a rather arbitrarily chosen wavelength), the spectrophotometric measurements provide highly resolved spectral data; examples for a biomass burning sample and typical background sample are shown in Figure 4.4, along with the regression fit to determine an AAE_{BrC}.

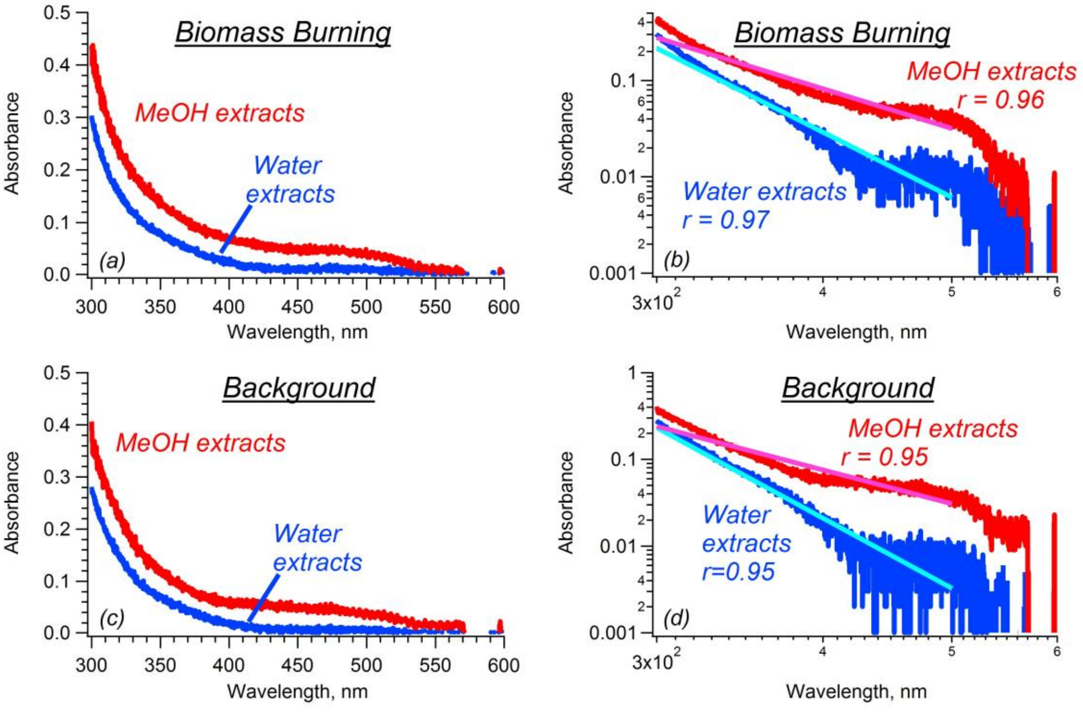

Figure 4.4 Example solution spectra of H_2O and MeOH (methanol) extracts for biomass burning as well as background conditions. Absorption Ångström exponent is calculated by linear regression fit to logAbs vs logλ in the wavelength range of 300-500nm, with an average r value of 0.87 for water extracts, and 0.84 for methanol extracts.

AAE_{BrC} differ only slightly between biomass burning samples and background conditions, however, the largest differences were between water and methanol extracts. For background conditions the mean ± stdev of the AAE_{BrC} was 6.71 ± 2.75 for water extracts and 4.43 ± 3.19 for methanol extracts. For biomass burning samples the AAE_{BrC}, were 7.98 ± 2.56 for water and 4.94 ± 2.51 for methanol extracts. The more significant difference of AAE_{BrC} between water extracts and methanol extracts may be related to the solubility of the compounds [*Zhang et al.*, 2013; *Chen and Bond*, 2010]. *Zhang et al.* (2013) BrC speciation work found that larger molecular weight PAHs absorbed more toward the visible range (i.e., have a lower AAE) and have a lower water-solubility. Following the water extraction, the lower AAE_{BrC} from methanol extract would indicate chromophores are associated with higher molecular weight, more non-polar compounds.

For comparison to AAE_{BrC}, the AAE for the ambient aerosol can also be calculated from the more limited spectral data (three wavelengths) associated with the PSAP. Here, AAE_{PSAP} is calculated using absorption measured at the wavelength pair, 470 and 660 nm by,

$$AAE_{PSAP} = -\frac{\ln\left(b_{ap,PSAP}(660)\right) - \ln\left(b_{ap,PSAP}(470)\right)}{\ln\left(660\right) - \ln(470)} \tag{4.2}$$

AAE altitude profiles are plotted in Figure 4.5. On average, there is not a great deal of variability in the vertical profiles of background air-mass mean AAE_{BrC}, for either water or methanol extracts. There is however, much more variability within each altitude layer. The cause of this variability is likely due to aerosol chemistry, but investigating it is beyond the scope of this analysis.

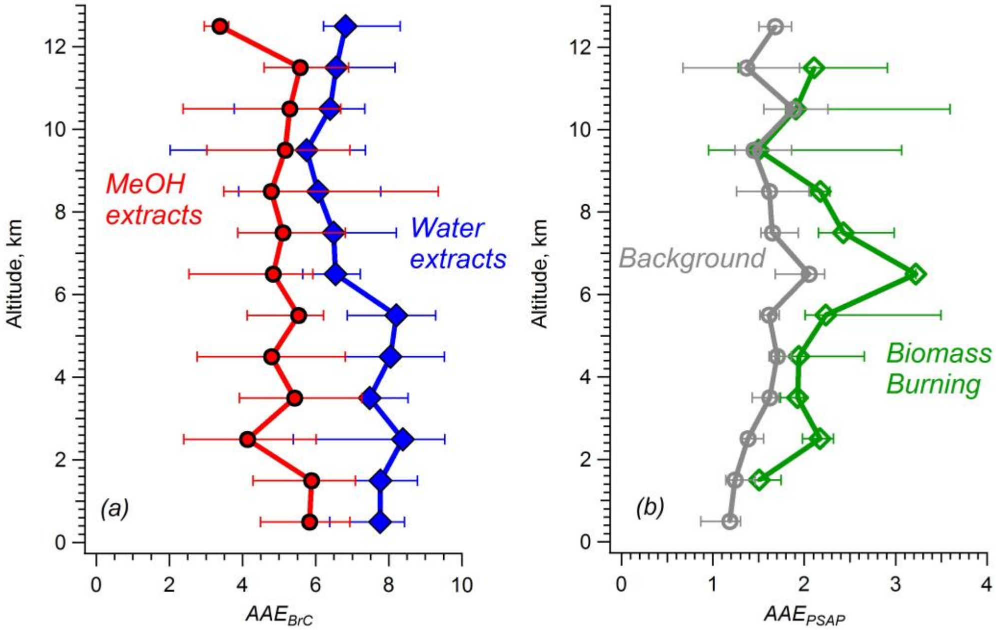

Figure 4.5 Vertical profiles of Absorption Ångström Exponent (AAE) of (a) brown carbon from solution spectra of both water extracts (blue line) and methanol extracts (red line), and (b) PSAP absorption measurements based on the wavelength combination (470 nm, 660 nm). Data were binned on a 1-km basis. Error bars indicated the inter-quartile range.

Average AAE_{PSAP} for the biomass burning periods was 2.15 ± 0.88 (mean ± stdev) and 1.60 ± 0.61 for background conditions. Differences can also be seen in the vertical profiles (Figure 4.5b), where for the most part the AAE_{PSAP} was higher in the biomass burning plumes compared to background conditions. A clear trend in AAE_{PSAP} was also observed in the vertical profile for background conditions, where AAE_{PSAP} increased with altitude. Past studies have interpreted deviation of AAEs from what are expected from BC (e.g., AAEs typically near 1) as an indication of BrC, however, this is fraught with significant uncertainty if BrC levels are not significant [*Lack and Langridge*, 2013]. Qualitatively the higher AAE_{PSAP} for the biomass burning air masses is consistent with the BrC contribution, and an AAE_{PSAP} closer to 1 near the surface is consistent with the observation that BC was more prevalent than BrC in these regions.

4.3.6 Light Absorption Calculations for Comparing BrC to BC and PSAP Data

In the following analysis, BrC solution data is converted to optical absorption and BC absorption is estimated to quantify contributions of BrC and BC as a function of altitude. The sum of BC and BrC absorption are then compared to the PSAP data to test for closure. The analysis could be done at any wavelength, however, 365 nm is chosen since it is in a wavelength range where a reliable BrC measurement is possible (e.g., at lower wavelengths, other non-BrC species begin to impact the data, such as nitrate), but sufficiently low that BrC, if present, should have a significant optical effect (i.e., BrC absorption drops off rapidly with increasing wavelength, as seen above, Figure 4.4).

4.3.6.1 BrC Light Absorption

To convert the solution absorbance to that of the ambient aerosol, knowledge of both particle morphology and how the chromophores are distributed amongst particle size is needed. In the past, most studies have assumed a small particle limit when making this conversion, where light absorption by BrC aerosol is taken as 0.69-0.75 times the light absorption of the solution [e.g., *Sun et al.* 2007]. This likely gives a lower limit for BrC absorption since BrC is not associated with sub nm size particles. *Liu et al.* [2013] measured the size distribution of BrC and showed that the chromophores were consistently found in the accumulation mode in both fresh vehicle emissions and more aged background environments (geometric mean diameter of ~0.5 µm). It is likely that this is more representative of the BrC size distribution measured in this study, given that the aerosols are aged, than assuming the small particle limit, and so it is assumed that those results apply here. From Mie theory calculations, under the assumption that the BrC was externally mixed with other absorbers, *Liu et al.* found that aerosol absorption is approximately 2 times higher than the bulk absorption measured in the extracts. Thus the aerosol BrC absorption at 365 nm is estimated for the two solvent extracts simply as,

$$b_{ap,H_2O\_BrC}(365) = 2 \cdot H_2O\_Abs(365) \tag{4.3}$$

$$b_{ap,Total\_BrC}(365) = 2 \cdot \left[H_2O\_Abs(365) + MeOH\_Abs(365)\right] = 2 \cdot Total\_Abs(365) \tag{4.4}$$

4.3.6.2 BC and PSAP Light Absorption

To estimate light absorption by the ambient aerosol at 365nm, PSAP measurements at higher wavelengths are extrapolated to 365 nm using the observed AAE_{PSAP}. Particle absorption at 365nm, $b_{ap,PSAP}(365)$, is calculated from the AAE_{PSAP} from Equation (4.2) and the light absorption measured at 660nm,

$$b_{ap,PSAP}(365) = b_{ap,PSAP}(660) * \left(\frac{365}{660}\right)^{-AAE_{PSAP}} \tag{4.5}$$

It is noted that AAE_{PSAP}, given in Eq. 4.2, could have been determined from different wavelength combinations (i.e., 470-532 nm, 532-660 nm). For this data set, the other wavelength pairs led to a predicted $b_{ap,PSAP}(365)$ within roughly ±20% of that predicted by equations (4.2) and (4.5).

No direct measurements are possible of light absorption solely by BC and so it must be estimated. A number of possible methods are available. In the first case, BC absorption at 365 nm ($b_{ap,\ BC}(365)$) is calculated from light absorption coefficients recorded at high wavelengths, where contributions from BrC should be minimal, which are then extrapolated to lower wavelengths using an assumed BC AAE (AAE_{BC}) by,

$$b_{ap,BC1}(365) = b_{ap,PSAP}(660) \cdot (\frac{365}{660})^{-AAE_{BC}} \tag{4.6}$$

Note, this equation is identical to Eq. 4.5, except with a different AAE. Typically, an AAE_{BC} of 1 is used [*Bergstrom et al.*, 2002; *Schnaiter et al.*, 2005; *Kirchstetter et al.*, 2004].

An alternative approach to calculate BC absorption is to assume a characteristic BC mass absorption cross-section (MAC) at a given wavelength. When multiplied by the measured BC concentration, BC absorption at that wavelength can be determined, and then the AAE_{BC} applied to estimate BC absorption at other wavelengths (i.e., 365nm). *Bond and Bergstrom* [2006] have suggested for pure uncoated BC, $MAC_{BC} = 7.5 \pm 1.2$ m^2/g at 550 nm, which has often been applied in other studies [e.g., *Yang et al.*, 2009, *Zhang et al.*, 2013]. Here, we refer to this method of calculating the BC absorption with a subscript 2, and calculate it by,

$$b_{ap,BC2}(365) = MAC_{BC} \cdot BC \cdot (\frac{365}{550})^{-AAE_{BC}} \tag{4.7}$$

For consistency, this prediction of BC absorption is compared to the ambient aerosol absorption at 365 nm (*b*ap2) estimated by applying AAE determined by PSAP, as

$$b_{ap2}(365) = b_{ap,BC2}(365) \times \left(\frac{660}{365}\right)^{-AAE_{BC}} \times \left(\frac{365}{660}\right)^{-AAE_{PSAP}} \quad (8)$$

A schematic showing the various optical calculations is given in Figure 4.6.

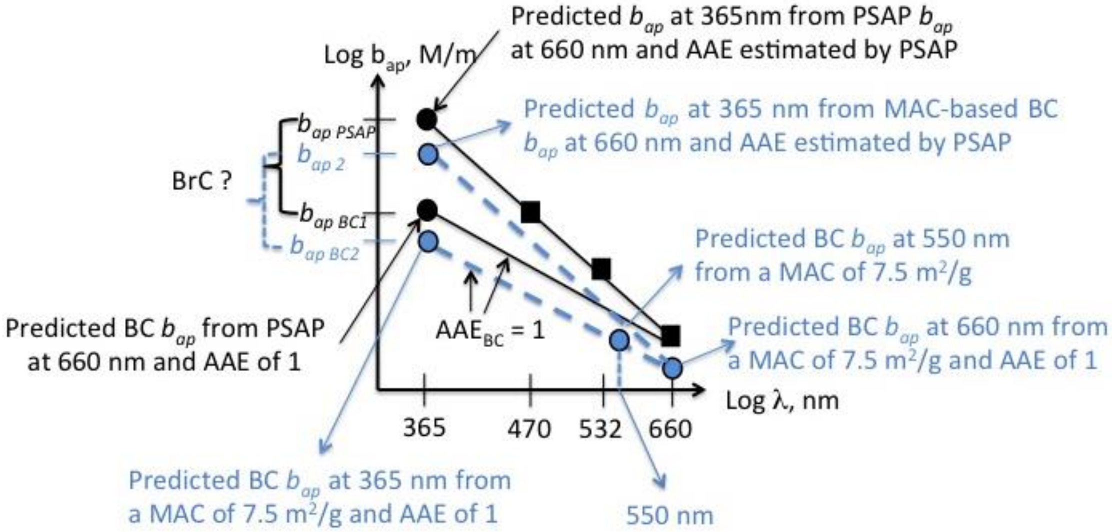

Figure 4.6 Schematic ambient aerosol and BC absorption extrapolated to lower wavelengths. Square data points represent PSAP measurement, which are used to estimate the ambient aerosol *AAE* (AAE_{PSAP}, not shown but slope of upper lines), and used to predict ambient aerosol absorption at 365 nm ($b_{ap\ PSAP}$). Light absorption by black carbon ($b_{ap\ BC}$) is estimated assuming an AAE_{BC} of 1 and extrapolating from the PSAP measurement at 660nm, a size where BrC absorption is minimal, or alternatively assuming a BC MAC of 7.5 m^2/g at 550 nm and extrapolating to 365 nm with an AAE_{BC} of 1.

In this data set, the second approach leads to a lower prediction of BC absorption compared to the first method (i.e., $b_{ap\ BC2} < b_{ap\ BC1}$, see Figure 4.6) due to differences between the assumed MAC_{BC} and the actual MAC. Figure 4.7 shows that the observed non-biomass burning study-average MAC at 660nm to be 10.9 m^2/g. This is higher than the assumed MAC_{BC}, where MAC_{BC} at 550 nm converted to a MAC_{BC} at 660 nm by assuming an AAE_{BC} of 1 gives MAC_{BC} at 660nm = 6.3 m^2/g. Observed MACs are often found to vary substantially due to particle sources, atmospheric processing and air mass origin [*Chan et al.*, 2011], but at 660nm this should not be due to the influence of BrC. Differences in particles sizes associated with these measurements could also play some role; both PSAP and filter-collected BrC included particles up to 4.1 μm, whereas the BC sampled only the accumulation mode. Although the magnitude of $b_{ap,BC2}$ and $b_{ap,BC1}$ differ, they are highly correlated, since $b_{ap,BC2}$ depends on the BC concentration (Eq. 4.7) and $b_{ap,BC1}$ on $b_{ap,PSAP}(660)$ (Eq. 4.6), and the correlation between BC and $b_{ap,PSAP}(660)$ is high, r = 0.93 (see Table 4.3 for background conditions).

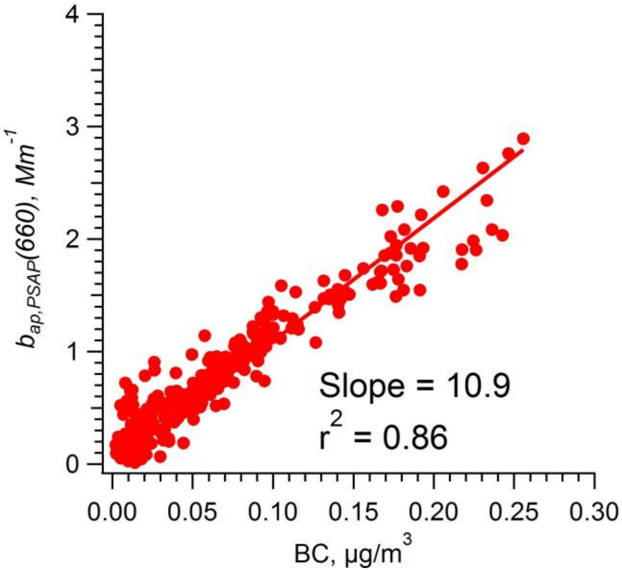

Figure 4.7 Correlation between PSAP absorption at 660 nm and BC concentration. The red line shows the orthogonal distance regression (ODR) fit result, with the slope

representing the mass absorption coefficient (MAC) of BC (intercept forced through zero).

The schematic in Figure 4.6 suggests that light absorption by the ambient aerosol at 365nm (e.g., $b_{ap,\,PSAP}(365)$) is higher than that predicted at the same wavelength for BC (e.g., $b_{ap,\,BC1}(365)$). This is often interpreted to be due to additional absorption by BrC [*Kirchstetter et al.*, 2004; *Sandradewi et al.*, 2008; *Chen and Bond*, 2010; *Sun et al.*, 2007; *Clarke et al.*, 2007] and is due to the inferred ambient AAE (AAE_{PSAP}) being greater than AAE_{BC} (i.e., 1). However, as noted above, due to the uncertainty with these various calculations, definitively assuming that there is a real difference and that it is due to BrC, can be uncertain. With these various data, optical closure can be assessed by summing BrC absorption estimated from the aerosol extracts with that of BC and compared to the PSAP-predicted ambient absorption, as shown in Figure 4.6.

4.3.7 Optical Importance of BrC Relative to BC and Closure Assessment by Comparison to PSAP

In the following analysis we focus on BC absorption based on the PSAP measurements and an assumed AAE_{BC} of 1 (i.e., $b_{ap\ BC1}$). Results using the other measure of BC absorption ($b_{ap\ BC2}$) are included but not plotted.

4.3.7.1 Background Conditions

Vertical profiles are shown of altitude-binned median data of the light absorption coefficients at 365nm for BC ($b_{ap\ BC1}$), BrC from water extraction ($b_{ap,\,H2O\_BrC}$) (Figure

4.8a), or for the total of water followed by methanol extraction ($b_{ap,\ Total\_BrC}$) (Figure 4.8b), along with the PSAP data extrapolated to 365nm ($b_{ap,\ PSAP}$) representing the actual ambient light absorption coefficient.   In these plots, BC and BrC absorption coefficients are summed for comparison to the ambient coefficient.

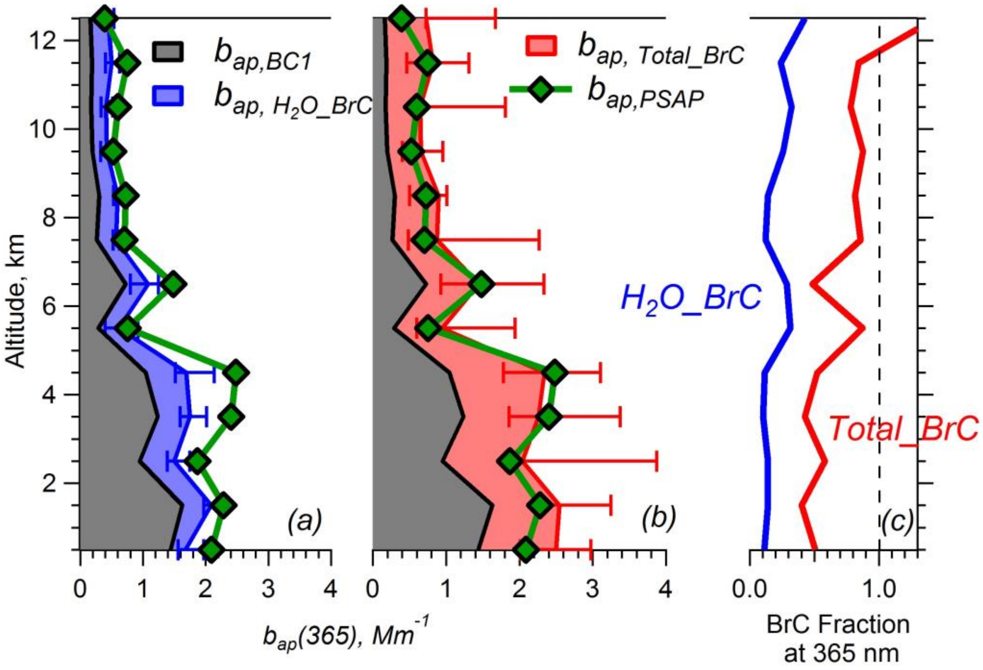

Figure 4.8 For background conditions, vertical profiles of estimated aerosol optical absorption at 365nm by brown carbon, BC, determined by an extrapolation from PSAP absorption at 660 nm ($b_{ap,BC1}$ shown in the schematic), and the sum of BrC and BC compared to total light-absorbing determined from the PSAP data. Figure (a) shows water-soluble BrC (blue shaded), (b) shows the total BrC (red shaded) and (c) shows the range of relative contribution of BrC to total aerosol absorption, with lower limit estimated from water-soluble BrC and upper limit from total BrC. In all plots, median values are shown, with error bars indicating the inter-quartile range of estimated BrC absorption at each 1-km altitude bin.

The vertical profiles show that absorption drops off with increasing altitude and that the general shape of the profiles for BC and BrC are similar to the PSAP data.

From Figure 4.8a, it is seen that water-soluble brown carbon absorption, $b_{ap,\ H2O\_BrC}(365)$, is small relative to BC and the sum of the two is always lower than the estimated ambient aerosol absorption by the PSAP, which is reasonable as the water-soluble fraction is only a portion of the light-absorbing organics. Total BrC absorption, $b_{ap,Total\_BrC}$(365), on the other hand, is more comparable to BC absorption over most of the altitude ranges.

A more quantitative assessment of closure for background conditions can be seen in a scatter plot with orthogonal distance regression of the sum of the estimated BC and BrC versus PSAP absorption (Figure 4.9). For assessing the influence of the BrC, scatter plots of just BC versus observed absorption is plotted, then BC plus water soluble BrC and then BC plus total BrC. The sum of $b_{ap,BC1}(365)$ and $b_{ap,\ H2O\_BrC}(365)$ is highly correlated (r = 0.96) to $b_{ap,PSAP}(365)$, and the slope of 0.89 as well as the near-zero intercept (Figure 4.9b) indicates that the BC plus water-soluble BrC slightly under-predicts the light absorption coefficient. When the total BrC is used (water + methanol extractions) the sum of BC and BrC are still fairly well correlated with ambient absorption, with a slope of 0.97, but with an positive intercept at 0.56 Mm-1. If force the regression through zero, on average, the BC and BrC over-predicts light absorption coefficients by 16% (slope is 1.16). Note, that if we used the low particle limit in these conversion of solvent extracts absorption to ambient particle absorption, the slope would be 0.76 for BC + water-soluble BrC versus ambient, and 0.85 for BC + total BrC vs. ambient. The small particle limit assumption is less applicable for ambient particles, however, given all the assumptions listed in *Liu et al.* [2013], the conversion factor of 2 is more likely an upper limit. Furthermore, the AAE for ambient BC particles has often been observed to deviate from 1, generally lower for fresh primary emissions and biomass burning and higher for aged aerosols [i.e., *Gyawali et al.*, 2009]. In our study, an AAE_{BC} value of 0.82 would result in perfect closure (regression slope of 1) between sum of BC and BrC absorption and $b_{ap,\ PSAP}$ at 365 nm.

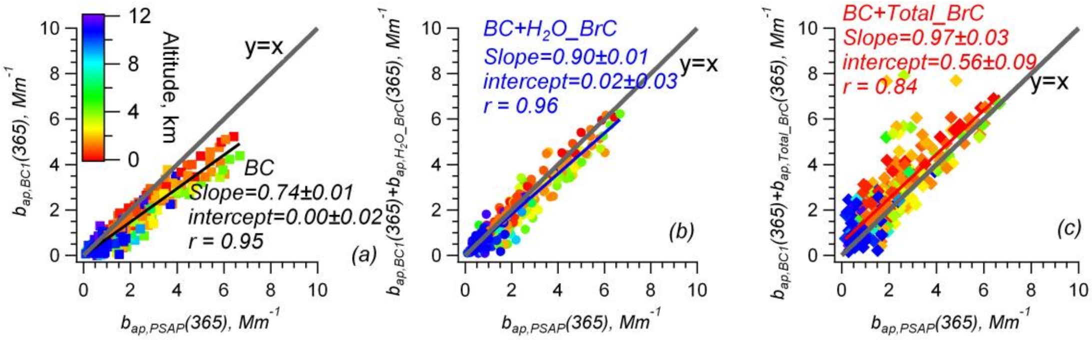

Figure 4.9 Scatter plots of estimated (a) BC absorption, and (b) sum of BC absorption and water-soluble BrC absorption, and (c) sum of BC absorption and Total BrC absorption , all at 365 nm, compared with total aerosol absorption estimated by PSAP also at 365 nm, for background conditions. Markers were color-coded by altitude. Orthogonal distance regression (ODR) fit results, with intercepts forced through zero are shown. The 1:1 line is also included, as the grey line shown in the figure.

The fraction of brown carbon absorption (both water and total BrC) relative to ambient (PSAP) absorption as a function of altitude is shown in Figure 4.8c. These results suggest that the fraction of BrC substantially increases with increasing altitude, reaching approximately 40% of by water-soluble BrC at ~12km, and nearly 100% at the highest altitudes, a region where ambient absorption coefficients are low.

4.3.7.2 Biomass burning events

Applying a vertical distribution analysis is not possible for biomass burning plumes, since there were limited data points for some of the altitudes, but closure analysis based on the combined data is shown in Figure 4.10. Note that there are several data points showing inconsistency, with very low BC levels and relatively high PSAP b_{ap} at 660 nm, and those data points have not been included in the scatter plot. Similar with the analysis for the background data, good correlations are found among biomass burning samples for filters collected at all altitudes. For BC plus water-soluble BrC the slope is 77% of PSAP absorption at 365 nm, for BC plus total BrC the slope is 122%, similar to that of background conditions. The relatively low slope for BC vs. PSAP b_{ap} comparing to background conditions indicate a higher relative abundance of brown carbon during biomass burning events.

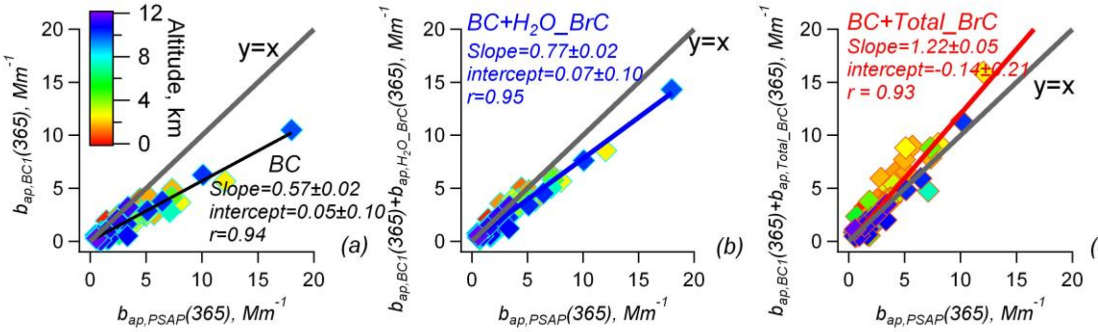

Figure 4.10 Biomass burning period scatter plots of estimated (a) BC absorption, and (b) sum of BC absorption and water-soluble BrC absorption, and (c) sum of BC absorption and Total BrC absorption compared with total aerosol absorption based on PSAP data, all at 365 nm. Markers were color-coded by altitude. Orthogonal distance regression (ODR) fit results, with intercepts forced through zero are shown. The 1:1 line is also included, as the grey line shown in the figure.

Just considering the fraction of BrC to total absorption, the contribution from BrC relative to PSAP is 20% ± 4.6% for water-soluble, and 58.9% ± 21.8% for total_BrC, similar to background conditions. Overall, these closure results are good given all the uncertainties associated with these light absorption coefficients.

4.3.7.3 Use of the MAC in closure calculations

A similar analysis, but where BC and ambient light absorption are based on an assumed BC MAC (ie, see Figure 4.6, $b_{ap,BC2}$ and b_{ap2})), can also be performed. For these components, the closure analysis for BC and water-soluble BrC versus ambient light absorption (b_{ap2}) result in a slope of 0.97 and for total BrC the slope is 1.40. When the fraction of BrC light absorption relative to total is calculated by this method the total BrC often exceeds the predicted ambient absorption, suggesting that use of the MAC_{BC} in this case does not produce as reasonable result as absorption coefficients based on just the PSAP data.

4.3.8 Limitations and Uncertainties

The fact that the sum of BC and BrC absorption was consistently higher than PSAP absorption by ~20% is worth exploring. Under our assumption of external mixing, a better closure could be achieved by 1) using a different method estimating $b_{ap,BC}$ *(365)*, and 2) changing the conversion factor from solution absorption of BrC to absorption by BrC aerosols.

The impact of using different methods for estimating BC absorption is large since it is not clear if the MAC of pure BC should be used or the observed PSAP data. In this case the PSAP data may be more reasonable compared to the MAC from BC since the particle size sampling ranges for the PSAP and BrC filters was consistent (upper limit of 4.1 μm aerodynamic diameter), whereas the BC was determined only for the accumulation mode. Shown in section 4.3.7, a much better closure is observed using the PSAP data. On the other hand, considering the uncertainties associated with the extrapolation from 660 nm to 365 nm, we used an AAE_{BC} value of 1, whereas other studies have used different values, such as 0.86 for biomass burning [*Kirchstetter and Thatcher*, 2012] or 0.9 from *Feng et al.* [2013]. A ±15% change in AAE_{BC} results in ±10% difference in the derived BC absorption at 365 nm. In our estimation, an AAE_{BC} value of 0.82 could provide a perfect closure for background conditions (regression slope equals to 1), but still a 9% over-estimation in biomass burning plumes.

Due to the significant contribution from BrC, the conversion factor is a key component controlling the light absorption closure. Our analysis has shown that the factor of 0.7 based on small particle limit assumption tended to under-estimate BrC absorption, while the factor of 2 showed an over-estimation, for both biomass burning and background conditions. Numerically speaking, a factor between 1.2 and 1.4 could reasonably estimate BrC b_{ap}, resulting in a closure slope within 3% of 1. The physical reason is not clear yet, possible causes include mixing state of light absorbers, aerosol morphology and the differences in suspended state of aerosols in solution versus in the atmosphere.

Significant uncertainties exist in all of these calculations, including $b_{ap,PSAP}(365)$, $b_{ap,BC1}$ *(365)* and the absorption of brown carbon, $b_{ap,H2O\_BrC}$ *(365)* and $b_{ap,\ total\_BrC}$ *(365)*). For $b_{ap,PSAP}(365)$, as discussed, we chose the wavelength pair of 470 nm and 660 nm to estimate the AAE of total aerosols. Other combinations result in a difference of ±20% on the estimated aerosol absorption coefficient at 365 nm. The PSAP absorption itself has an uncertainty of 20% due to measurement and artifact correction, which results in a combined uncertainty (assuming all are independent) of 29%.

For BrC absorption in the extracts, the uncertainties were estimated at 21% for H_2O*_Abs (365)*, 27% for *MeOH_Abs (365)* and for the sum (*Total_Abs(365)* the combined uncertainty is ±34%. It is difficult to estimate the uncertainty in the conversion of solution absorption to aerosol absorption since the assumption of the factor of 2 multiplier is based on assuming BrC size distributions from a limited number of surface measurements, none of which involved significant biomass burning emissions. Furthermore, the uncertainties in the assumptions associated with the Mie calculations are not negligible and estimated at 30% [*Liu et al.*, 2013]. Overall, we estimate that for each measure of light absorption (BC, BrC, and ambient), there is roughly a 30-45% uncertainty.

4.4 Summary

Direct measurements of BrC were made on solvent extracts from filters collected at altitudes ranging from approximately 1 to ~13 km over the central US during summer.

The data were segregated into periods of sampling in biomass burning plumes and more typical background free troposphere conditions. The filter extraction procedure involved sequential extraction, first in water, then in methanol (the sum of the water plus methanol extract BrC is referred to as the total BrC). During biomass burning periods, both water and methanol-soluble BrC was highly correlated with other known emissions from biomass burning plumes, including CO, acetonitrile and BC. Under background conditions the water-soluble fraction of BrC was somewhat correlated with smoke tracers, whereas the methanol soluble BrC was not well correlated with any specific tracers, but most correlated with WSOC, suggesting the BrC evolves to a more water-insoluble state as chemically aged. Under both background and biomass burning conditions total BrC was significantly higher than water-soluble (i.e., total relative to water extracted BrC ratios were 3.2 and 2.3 for background and biomass burning plumes), but BrC levels in biomass burning plumes were much higher (5 and 4 times higher for water-soluble and total BrC, respectively). BrC was found to be abundant throughout the tropospheric column and for background conditions BrC was more evenly distributed throughout the column than BC. Estimates were made of BC and BrC absorption coefficients at 365nm (for BrC, extracts absorption multiplied by 2) and the sum compared to observed absorption based on Ångström exponents inferred from the 3-wavelength PSAP to extrapolate to 365nm. The increasing prevalence of observed BrC with altitude in the background free troposphere was consistent with PSAP AAEs that are larger than one and increase with altitude. The sum of BC and BrC over-predicted observed PSAP absorption by 16%, whereas for biomass-burning the closure was within 3%. Although the uncertainties associated with the various estimates of light absorption coefficients are large, the closure is close and suggests that BrC directly estimated from solution extracts agree reasonably well with optical instruments, and that PSAP AAEs greater than one are mainly due to the presence of BrC.

Chapter 5

CONCLUSIONS AND FUTURE WORK

5.1 Summary of the Major Findings

5.1.1 Comparative Investigation of SOA Formation Pathways in Atlanta and LA

The first part of the dissertation (Chapter 2) is devoted to a detailed analysis of gas/particle partitioning behavior of formic acid, in Atlanta and LA. The objective is to better understand the sources and formation processes of SOA in two urban environments with contrasting emissions, when LA is mainly impacted by anthropogenic pollutions, while Atlanta is characterized by extensive biogenic emissions of SOA precursors mixed with moderate extent of anthropogenic emissions.

First, through concurrent measurements of chemical species in both gas and particles phases, it is found that both phases of formic acid and WSOC had clear diurnal patterns. Daily maximum concentrations of gas phase WSOC occurred together with the peak of solar insolation, while particle phase WSOC reached peak concentration approximately 1 hour later, indicating a gas-to-particle conversion process. On the other hand, both gas phase and particle phase formic acid had similar peak times, which occurred in the early afternoon together with other photochemical products. The partitioning of formic acid, represented by the particle-to-gas (p/g) ratio, typically ranged between 1 to 2% throughout the study, while that of WSOC is approximately 10 to 20%. The relatively high volatility may partially explain why the average diurnal trend of particle formic acid tended to track the gas phases species, instead of other SOA components.

Gas-phase organic components could partition to the particle phase through absorption to the preexisting organic phase, or undergo dissolution into aerosol water, or some combination of both. Due to its high volatility, formic acid partitioning did not show correlation with organic mass in either LA or Atlanta, but a different RH-partitioning dependence between the two cities was observed. There was not a clear trend of formic acid partitioning to LWC in LA except for three overcast periods, which were associated with much lower daytime concentrations of photo-chemically generated species due to depressed photochemical activities. RH was above 70% for the overwhelming majority during the three periods, prompting the assumption that particles were often deliquesced, but the application of Henry's law greatly under-estimated the partitioning ratio of formic acid, based on particle LWC and pH inferred from thermodynamic models. During periods with no observed RH-dependence of formic acid, the early-afternoon peak concentrations of both gas and particle phases suggested the significant contribution of photochemical production, and the diurnal variation in p/g ratios were small, in contrast to the large variation during overcast periods. It is likely that formic acid has multiple routes for partitioning. During overcast periods when organic mass was low, the particle water route appeared to be relatively more important; in contrast, during the photo-chemically active periods when organic mass concentrations were high and liquid water content was relatively low, conditions were most conducive for partitioning to organic mass.

In contrast to practically no RH-dependence in LA, formic acid had a clearer trend of partitioning to liquid water in Atlanta based on correlations with ambient RH. This contrast is similar to differences in bulk WSOC partitioning. *Zhang et al.* [2012] showed that in LA, WSOC partitioning appeared to be linked to an absorbing phase correlated with OC as opposed to RH, whereas in Atlanta, WSOC partitioning showed a linkage with RH, especially when RH was greater than ~70% (i.e., when LWC is sensitive to RH). Possible causes for the observed differences in partitioning preferences for formic acid and WSOC between LA and Atlanta included difference in aerosol pH, and the relative abundance of organic mass concentration and liquid water content, but one of the biggest differences between these two cities is likely the composition of the secondary organic aerosol resulting from differences in VOC emissions.

5.1.2 Prevalence and Optical Importance of Brown Carbon from Surface to Tropopause

The comparative study of formic acid partitioning in LA and Atlanta suggests that SOA formation in summer is governed by multiple pathways, which is driven by different VOC emissions in various environments. Organic aerosols in different environments were also featured with differing optical properties, which is investigated in the second half of the dissertation (Chapter 3 and 4).

In chapter 3, size-resolved aerosols samples were collected at three surface sites featuring different aerosol origins: YRK represents the regional background of biogenic emission, JST is a typical urban site impacted by a mix of anthropogenic emissions and the substantial biogenic emission signal, and RS site is largely impacted by primary vehicle emissions. WSOC and brown carbon (both water and methanol extracts) had similar distributions among all three sites, while OC and EC were significantly shifted to lower size ranges at RS. The results showed that fresh vehicular emissions are associated with smaller sizes, and aged carbonaceous particles tend to be larger due to accretion of mass. Light absorption by organic carbon extracted in water is always smaller than methanol extracts, but the fresher emissions at the RS site have a greater fraction of water-soluble chromophores compared with the more aged regional JST and YRK samples, which may suggest that the chromophores become less water-soluble with age. Later, the complex part of refractive index of brown carbon was retrieved from solution results, and was applied as the Mie calculation input together with aerosol size distribution. The predicted light absorption of brown carbon absorption was a factor of 2 higher than solution absorption for both water and methanol extracts, and the conversion factor was consistent among three sites. The estimated brown carbon absorption at 350 nm contributed a significant fraction (20 to 40%) relative to total light absorption, Although brown carbon absorption was highest at RS due to vehicle emissions, highest contributions were found to be at the rural site where primary elemental carbon level was relatively low.

The MOUDI study established a connection on how to estimate light absorption of ambient brown carbon aerosols from solution extracts. The connection was then applied to aerosol samples collected throughout the free tropospheric column during DC3 campaign, to estimate the vertical profile and optical importance of brown carbon. Data were grouped into biomass burning plume samples and background conditions, and biomass burning samples showed significantly higher brown carbon levels for both water extracts and total (sum of water and methanol extracts). Correlation analyses suggested that water soluble brown carbon in background troposphere could mainly be related to primary emissions and possibly linked to aged biomass burning, while total brown carbon is more likely to be secondary. Background conditions were found to have a lower water-soluble fraction of brown carbon than biomass burning plumes, consistent with our finding during MOUDI study that brown carbon may become less water-soluble with age. The vertical profile of brown carbon is more uniform, compared with the rapid-drop of BC with increasing altitudes, which implied the existence of brown carbon sources in the atmosphere, possibly in-cloud formation. PSAP absorption, a measure of total aerosol light absorption, has a median altitude of 50% cumulative relative fraction between BC and BrC at 365 nm, suggesting contributions from both BC and BrC. A closure analysis provided further evidence, that the estimated light absorption by the sum of BC and BrC aerosols agreed pretty well with total aerosol absorption determined by optical instruments, with a deviation less than 20%, for either biomass burning or background conditions. The contribution of BrC relative to PSAP total aerosol absorption is ~40% on average, and the ratio increases with altitude. Overall, the direct measurement of brown carbon in solutions definitively shows that it is ubiquitous in the free troposphere, and the estimation based on Mie calculation is reasonable as it agreed pretty well with optical instruments.

5.2 Recommendations for Future Work

The scientific findings resulting from this thesis are important for better understanding chemical and optical properties of organic aerosols, including the formation pathway preferences in different environments, refractive indices of brown carbon through direct measurements, and the connection between solution absorption and absorption by brown carbon aerosols. Many subsequent questions come out of this work as well, which are summarized below.

5.2.1 Gas-Particle Partitioning of Single Organic Compounds

Our studies suggested that the gas-particle partitioning of formic acid showed different preferences in LA and Atlanta, which is consistent with the partitioning behavior of bulk WSOC, providing additional contrast between the two environments. However, the partitioning behavior of formic acid is quite different than WSOC due to its high volatility, which hinders a better comparison. Oxalic acid is the most ubiquitous carboxylic acid condensed phase component. Our measurements during the spring and summer of 2010 indicated that oxalic acid comprised 2.0% of the particle phase WSOC in LA and 2.7% in Atlanta on a carbon mass basis. Furthermore, oxalate is a product of mostly aqueous phase chemistry. It is speculated that oxalate aerosol would form in the aerosol water and thus tracking oxalic acid as a tracer is important for aqueous chemistry forming SOA. For these reasons, studying the partitioning of oxalic acid and comparing it with the partitioning of bulk WSOC would help characterize the chemical nature of WSOC and enhance the overall understanding of WSOC partitioning.

5.2.2 Aerosol Morphology and Mixing State

The conversion from solution absorption of brown carbon and the light absorption by brown carbon aerosols are based on a series of simplifying assumptions, including that the particles are spherical and of uniform composition, but externally mixed with other absorbing aerosol components, such as BC. This means the method does not consider possible light absorption enhancements due to particle morphology, such as shell-core configurations [*Bond et al.*, 2006; *Cappa et al.*, 2012; *Lack et al, 2010*]. Though some recent measurements in Los Angeles suggest that the enhancement by coating is small (e.g., 6% at 532nm, [*Cappa et al.*, 2012]), the extent of shell-core optical effect remains uncertain, which leaves our estimates of brown carbon optical importance less accurate. Detailed investigation on the suspended state of ambient brown carbon aerosols, mixing state of single particles, and how it would affect the interaction with solar radiation, is essential to help answer the question.

5.2.3 Chemical Characterization of Brown Carbon

Our results presented in Chapter 3 and 4 are based on bulk measurements of brown carbon in solutions, but the chemical components or functional groups that contribute to brown carbon absorption is not clear yet. *Zhang et al.* [2013] showed that speciated organic compounds only accounted for a few percent of the total absorption. Besides, our results suggested that the light-absorbing properties of brown carbon differs due to aerosol origins, and the relative fraction of water-soluble BrC changes with chemical aging, but the specific chemical reactions corresponding to the evolution have not been well understood. Thus, it would be informative to perform chemical speciation on samples collected from various locations and compare the results. Chamber studies to track the formation and evolution of brown carbon would also be essential.

5.2.4 Radiative Forcing of Brown Carbon

Our work has suggested the relative importance of brown carbon to black carbon in light absorption in UV wavelength. Nevertheless, solar radiation covers a much wider spectrum range (up to 3000 nm), and it is not clear if brown carbon is a significant atmospheric absorber of solar radiation. Furthermore, our analysis did not consider aerosol scattering as well as gaseous absorbers, which are also important components contributing to the radiative balance of the earth. Several recent studies have estimated the direct radiative forcing by light-absorbing organic aerosols (e.g., *Feng et al.*, 2013), while most of them were retrieved from satellite data and the separation of BrC is questionable, as mentioned in Chapter 4. On the other hand, our brown carbon absorption directly determined from aerosol extracts successfully excluded the influence from other light absorbers. Therefore, the more accurate refractive indices determined by our method could be directly introduced into a comprehensive radiative forcing model, thus help to provide a more robust estimation on the global radiative balance and a better understanding of the radiative forcing due to light-absorbing organic aerosols.

REFERENCES

Alexander, D. T. L., P. A. Crozier, and J. R. Anderson (2008), Brown carbon spheres in East Asian outflow and their optical properties, *Science*, *321*(5890), 833-836.

Andreae, M. O., and P. J. Crutzen (1997), Atmospheric Aerosols: Biogeochemical Sources and Role in Atmospheric Chemistry, *Science*, *276* (5315), 1052-1058.

Andreae, M., and A. Gelencser (2006), Black carbon or brown carbon? The nature of light-absorbing carbonaceous aerosols, *Atm. Chem. Phys.*, *6*, 3131-3148.

Arellanes, C., S. E. Paulson, P. M. Fine, and C. Sioutas (2006), Exceeding of Henry’s law by hydrogen peroxide associated with urban aerosols, *Environ. Sci. Technol.*, *40*, 4859–4866.

Asa-Awuku, A., et al. (2008), Investigation of Molar Volume and Surfactant Characteristics of Water-Soluble Organic Compounds in Biomass Burning Aerosol, *Atm. Chem. Phys.*, *8* 4: 799-812.

Baboukas, E. D., M. Kanakidou, and N. Mihalopoulos (2000), Carboxylic acids in gas and particulate phase above the Atlantic Ocean, *J. Geophys. Res.*, *105*, 14459–14472.

Bahadur, R., P. S. Praveen, Y. Y. Xu, and V. Ramanathan (2012), Solar absorption by elemental and brown carbon determined from spectral observations, *Proceedings of the National Academy of Sciences of the United States of America*, *109*(43), 17366-17371.

Bahreini, R., A. M. Middlebrook, J. A. de Gouw, C. Warneke, M. Trainer, C.A. Brock, H. Stark, S. S. Brown, W. P. Dube, J. B. Gilman, K. Hall, J. S. Holloway, W. C. Kuster, A. E. Perring, A. S. H. Prevot, J. P. Schwarz, J. R. Spackman, S. Szidat, N. L. Wagner, R. J. Weber, P. Zotter, D. D. Parrish (2012), Gasoline emissions dominate over diesel in formation of secondary organic aerosol mass, *Geophys. Res. Lett.*, *39*, L06805, doi:10.1029/2011GL050718.

Barnard J. C., R. Volkamer, and E. I. Kassianov (2008), Estimation of the mass absorption cross section of the organic carbon component of aerosols in the Mexico City Metropolitan Area, *Atmos. Chem. Phys., 8*, 6665–6679, 2008, www.atmos-chem-phys.net/8/6665/2008/.

Bateman, A.P., Nizkorodov, S.A., Laskin, J., Laskin, A., 2011. Photolytic processing of secondary organic aerosols dissolved in cloud droplets. *Phys. Chem. Chem. Phys. 13* (26), 12199e12212.

Bergstrom, R. W., Russell, P. B., and Hignett, P. B.: The Wave- length Dependence of Black Carbon Particles: Predictions and Results from the TARFOX experiment and Implications for the Aerosol Single Scattering Albedo, *J. Atmos. Sci., 59*, 567–577, 2002.

Bertram A. K., S. T. Martin, S. J. Hanna, M. L. Smith, A. Bodsworth, Q. Chen, M. Kuwata, A. Liu, Y. You, and S. R. Zorn (2011), Predicting the relative humidities of liquid-liquid phase separation, efflorescence, and deliquescence of mixed particles of ammonium sulfate, organic material, and water using the organic-to-sulfate mass ratio of the particle and the oxygen-to-carbon elemental ratio of the organic component, *Atmos. Chem. Phys., 11*, 10995–11006.

Bohren, C. F., and D. R. Hoffman (Published 1998), Absorption and Scattering of Light by Small Particles, *john Wilely and Sons Inc, New York*.

Bond, T. C. (2001), Spectral dependence of visible light absorption by carbonaceous particles emitted from coal combustion, *Geophysical Research Letters, 28*(21), 4075-4078.

Bond, T. C., and R. W. Bergstrom (2006), Light absorption by carbonaceous particles: An investigative review, *Aerosol Sci. and Tech., 40*, 27-67.

Bond, T. C., et al. (2013), Bounding the role of black carbon in the climate system: A scientific assessment, *J. Geophys. Res. Atmos., 118*, 5380–5552, doi:10.1002/jgrd.50171.

Bond, T. C., G. Habib, and R. W. Bergstrom (2006), Limitations in the enhancement of visible light absorption due to mixing state, *Journal of Geophysical Research: Atmospheres, 111*(D20), D20211，doi:10.1029/2006JD007315.

Bones, D. L., D. K. Henricksen, S. A. Mang, M. Gonsior, A. P. Bateman, T. B. Nguyen, W. J. Cooper, and S. A. Nizkorodov (2010), Appearance of strong absorbers and fluorophores in limonene-O3 secondary organic aerosol due to NH4+-mediated chemical aging over long time scales, *J. Geophys. Res., 115*, D05203, doi:05210.01029/02009JD012864.

Cahill, T. M., V. Y. Seaman, M. J. Charles, R. Holzinger, and A. H. Goldstein (2006), Secondary organic aerosols formed from oxidation of biogenic volatile organic compounds in the Sierra Nevada Mountains of California, *J. Geophys. Res., 111*, D16312, doi:10.1029/2006JD007178.

Canagaratna, M., J. Jayne, J. L. Jimenez, J. D. Allan, M. R. Alfarra, Q. Zhang, T. B. Onasch, F. Drewnick, H. Coe, A. Middlebrook, A. Delia, L. R. Williams, A. M. Trimborn, M. J. Northway, C. E. Kolb, P. Davidovits, and D. R. Worsnop (2007), Chemical and microphysical characterization of aerosols with the aerosol mass spectrometry, *Mass Spectrom. Rev., 26*, 185–222.

Cappa, C. D., et al. (2012), Radiative Absorption Enhancements Due to the Mixing State of Atmospheric Black Carbon, *Science, 337*(6098), 1078-1081.

Carrico, C. M., M. H. Bergin, J. Xu, K. Baumann, and H. Maring (2003), Urban aerosol radiative properties: Measurements during the 1999 Atlanta Supersite Experiment, *Journal of Geophysical Research-Atmospheres, 108*(D7), doi:10.1029/2001JD001222.

Chakrabarty, R. K., H. Moosmuller, L. W. A. Chen, K. Lewis, W. P. Arnott, C. Mazzoleni, M. K. Dubey, C. E. Wold, W. M. Hao, and S. M. Kreidenweis (2010), Brown carbon in tar balls from smoldering biomass combustion, *Atmospheric Chemistry and Physics, 10*(13), 6363-6370.

Chameides, W. L. (1984), The photochemistry of a remote marine stratiform cloud, *J. Geophys. Res., 89*D, 4739-4755.

Chan, T. W., J. R. Brook, G. J. Smallwood, and G. Lu (2011), Time-resolved measurements of black carbon light absorption enhancement in urban and near-urban locations of southern Ontario, Canada, *Atm. Chem. Phys., 11*, 10407-10432.

Chang, J. L., and J. E. Thompson (2010), Characterization of colored products formed during irradiation of aqueous solutions containing H2O2 and phenolic compounds, *Atmospheric Environment, 44*(4), 541-551.

Chang, W. L., R. J. Griffin, D. Dabdub (2010), Partitioning phase preference for secondary organic aerosol in an urban atmosphere, *Proc. Natl. Acad. Sci. U.S.A., 107*, 6705-6710.

Charlson, R. J., et al. (1992), Climate Forcing by Anthropogenic Aerosols, *Science 255* 5043: 423-30.

Chebbi, A., and P. Carlier (1996), Carboxylic acids in the troposphere, occurrence, sources, and sinks: A review, *Atmos. Environ., 30*, 4233–4249.

Chen, Y., and T. C. Bond (2010), Light absorption by organic carbon from wood combustion, *Atmospheric Chemistry and Physics, 10*(4), 1773-1787.

Chow, J. C., J. G. Watson, D. H. Lowenthal, and K. L. Magliano (2008), Size-resolved aerosol chemical concentrations at rural and urban sites in Central California, USA, *Atmospheric Research, 90*(2-4), 243-252.

Christian, T. J., B. Kleiss, R. J. Yokelson, R. Holzinger, P. J. Crutzen, W. M. Hao, B. H. Saharjo, and D. E. Ward (2003), Comprehensive laboratory measurements of biomass-burning emissions: 1. Emissions from Indonesian, African, and other fuels, *J. Geophys. Res., 108*, 4719, doi:10.1029/2003JD003704.

Chung, C. E., V. Ramanathan, and D. Decremer (2012), Observationally constrained estimates of carbonaceous aerosol radiative forcing, *Proceedings of the National Academy of Sciences of the United States of America, 109*(29), 11624-11629.

Chung, S. H. and Seinfeld, J. (2002), Global distribution and climate forcing of carbonaceous aerosols, *Journal of Geophysical Research, 107*(D19), 4407, doi:101029/2001JD001397.

Clarke, A., McNaughton, C., Kapustin, V., Shinozuka, Y., Howell, S., Dibb, J., Zhou, J., Anderson, B., Brekhovskikh, V., Turner, H., and Pinkerton, M.: Biomass Burning and Pollution Aerosol over North America: Organic Components and their influence on Spectral Optical Properties and Humidification Response, *J. Geophys. Res., 112*, D12S18, doi:10.1029/2006JD007777, 2007.

Cofer, W. R. and R. A. Edahl (1986), A new technique for collection, concentration and determination of gaseous tropospheric formaldehyde, *Atmos. Environ., 20*(5), 979–984.

de Haan, D. O., A. L. Corrigan, K. W. Smith, D. R. Stroik, J. J. Turley, F. E. Lee, M. A. Tolbert, J. L. Jimenez, K. E. Cordova, and G. R. Ferrell (2009a), Secondary organic aerosol-forming reactions of glyoxal with amino acids, *Environ. Sci. Tech*., *43*, 2818–2824.

de Haan, D. O., M. A. Tolbert, and J. L. Jimenez (2009b), Atmospheric condensed-phase reactions of glyoxal with methylamine, *Geophys. Res. Lett*., *36*, L11819, doi:11810.11029/12009GL037441.

de Gouw, J. A., et al. (2005), Budget of Organic Carbon in a Polluted Atmosphere: Results from the New England Air Quality Study in 2002, *Journal of Geophysical Research-Atmospheres 110* D16.

de Gouw, J.A., Cooper, O.R., Warneke, C., Hudson, P.K., Fehsenfeld, F.C., Holloway, J.S., Hübler, G., Nicks Jr., D.K., Nowak, J.B., Parrish, D.D., Ryerson, T.B., Atlas, E.L., Donnelly, S.G., Schauffler, S.M., Stroud, V., Johnson, K., Carmichael, G.R. and Streets, D.G. (2004). Chemical composition of air masses transported from

Asia to the U.S. West Coast during ITCT 2K2: Fossil fuel combustion versus biomass burning signatures. *Journal of Geophysical Research 109*: doi: 10.1029/2003JD004202. issn: 0148-0227.

de Gouw, J. A., A. M. Middlebrook, C. Warneke, R. Ahmadov, E. L. Atlas, R. Bahreini, D. R. Blake, C. A. Brock, J. Brioude, D. W. Fahey, F. C. Fehsenfeld, J. S. Holloway, M. Le Henaff, R. A. Lueb, S. A. McKeen, J. F. Meagher, D. M. Murphy, C. Paris, D. D. Parrish, A. E. Perring, I. B. Pollack, A. R. Ravishankara, A. L. Robinson, T. B. Ryerson, J. P. Schwarz, J. R. Spackman, A. Srinivasan, and L. A. Watts (2011), Organic aerosol formation downwind from the Deepwater Horizon oil spill, *Science, 331*, 1295–1299.

DeCarlo, P. F., Kimmel, J. R., Trimborn, A., Northway, M. J., Jayne, J. T., Aiken, A. C., Gonin, M., Fuhrer, K., Horvath, T., Docherty, K. S., Worsnop, D. R., and Jimenez, J. L. (2006), Field-deployable, high-resolution, time-of-flight aerosol mass spectrometer, *Anal. Chem., 78*, 8281–8289.

Decesari, S., M. C. Facchini, E. Matta, F. Lettini, M. Mircea, S. Fuzzi, E. Tagliavini, and J.-P. Putaud (2001), Chemical features and seasonal variation of fine aerosol water-soluble organic compounds in the Po Valley, Italy, *Atmos. Environ., 35*, 3691-3699.

Desyaterik, Y., Y. Sun, X. Shen, T. Lee, X. Wang, T. Wang, and J. L. Collett Jr. (2013), Speciation of “brown” carbon in cloud water impacted by agricultural biomass burning in eastern China, *J. Geophys. Res. Atmos., 118*, 7389–7399, doi:10.1002/jgrd.50561.

Dinar, E., A. A. Riziq, C. Spindler, C. Erlick, G. Kiss, and Y. Rudich (2008), The complex refractive index of atmospheric and model humic-like substances (HULIS) retrieved by a cavity ring down aerosol spectrometer (CRD-AS), *Faraday Discussions, 137*, 279-295.

Dockery, D.W., C.A. Pope, X. Xu, J. D. Spengler, J. H. Ware, M.E. Fay, B. G. Ferris, and F. E. Speizer (1993), An association between air pollution and mortality in six U.S. cities, *N. Engl. J. Med., 329*, 1753-1808.

Draxler, R. R., and G. D. Rolph (2012), HYSPLIT (Hybrid Single - Particle Lagrangian Integrated Tracker) Model, Air Resour. Lab., NOAA, Silver Spring, MD. [Available at http://ready.arl.noaa.gov/HYSPLIT.php]

Duarte, R., C. A. Pio, and A. C. Duarte (2005), Spectroscopic study of the water-soluble organic matter isolated from atmospheric aerosols collected under different atmospheric conditions, *Analytica Chimica Acta, 530*(1), 7-14.

Eatough, D. J., A. Wadsworth, D. A. Eatough, J. W. Crawford, L. D. Hansen, and E. A. Lewis (1993), A multiple-system, multichannel diffusion denuder sampler for the determination of fine-particulate organic material in the atmosphere, *Atmospheric Environment Part a-General Topics, 27*(8), 1213-1219.

Ellis, R., J. G. Murphy, P. L. Hayes, M. J. Cubison, A. M. Ortega, J. L. Jimenez, J. Liu, R. J. Weber, P. Veres, A. K. Cochran, and J. M. Roberts, Gas-particle partitioning of ammonia at the CalNex-LA ground site and the influence of aerosol pH, *J. Geophys. Res.*, submitted, 2012.

Ervens, B. and Kreidenweis, S. M. (2007), SOA formation by biogenic and carbonyl compounds: Data evaluation and application, *Environmental Science & Technology, 41*, 3904–3910.

Ervens, B., Carlton, A. G., Turpin, B. J., Altieri, K. E., Kreidenweis, S. M., and Feingold, G. (2008), Secondary organic aerosol yields from cloud-processing of isoprene oxidation products, *Geophysical Research Letters, 35*, L02816, doi:10.1029/2007GL031828.

Feng, Y., Ramanathan, V., and Kotamarthi, V. R.: Brown carbon: a significant atmospheric absorber of solar radiation?, *Atmos. Chem. Phys., 13*, 8607-8621, doi:10.5194/acp-13-8607-2013, 2013.

Fountoukis, C., A. Nenes, A. Sullivan, R. Weber, T. Van Reken, M. Fischer, E. Matas, M. Moya, D. Farmer, and R. C. Cohen (2009), Thermodynamic characterization of Mexico City aerosol during MILAGRO 2006, *Atmos. Chem. Phys., 9*, 2141–2156.

Fuzzi, S., et al. (2006), Critical assessment of the current state of scientific knowledge, terminology, and research needs concerning the role of organic aerosols in the atmosphere, climate, and global change, *Atmospheric Chemistry and Physics, 6*, 2017-2038.

Gilman, J. B., et al. (2009), Measurements of volatile organic compounds during the 2006 TexAQS/GoMACCS campaign: Industrial influences, regional characteristics, and diurnal dependencies of the OH reactivity, *J. Geophys. Res., 114*, D00F06, doi:10.1029/2008JD011525.

Goldstein, A. H. and Galbally, I. E. (2007), Known and unexplored organic constituents in the earth's atmosphere, *Environmental Science & Technology, 41*, 1514–1521.

Goode, J. G., R. J. Yokelson, D. E. Ward, R. A. Susott, R. E. Babbitt, M. A. Davies, and W. M. Hao (2000), Measurements of excess O3, CO2, CH4, C2H4, C2H2, HCN, NO, NH3, HCOOH, CH3COOH, HCHO, and CH3OH in 1997 Alaskan biomass burning plumes by airborne fourier transform infrared spectroscopy (AFTIR), *J. Geophys. Res., 105*, 22147–22166, doi:10.1029/2000JD900287.

Grosjean, D. (1988), Aldehydes, carboxylic acids and inorganic nitrate, *Atmos. Environ., 22*(8), 1637–1648, doi:10.1016/0004-6981(88)90391-5.

Grover, B. D., N. L. Eatough, W. R. Woolwine, and D. J. Eatough (2009), Modifications to the Sunset Laboratory Carbon Aerosol Monitor for the simultaneous measurements of PM2.5 nonvolatile and semi-volatile material, *J. Air Waste Manag. Assoc., 59*, 1007-1017.

Gyawali, M., Arnott, W. P., Lewis, K., and Moosmǘller, H.: In situ aerosol optics in Reno, NV, USA during and after the summer 2008 California wildfires and the influence of absorbing and non-absorbing organic coatings on spectral light absorption, *Atmos. Chem. Phys., 9*, 8007–8015, doi:10.5194/acp-9-8007-2009, 2009.

Gyawali, M., et al. (2013), Evolution of multispectral aerosol optical properties in a biogenically-influencedClimate urban environment during the CARES campaign, *Atm. Chem. Phys. Disc.*, *13*, 7113-7150, 2013.

Hansen, J., M. Sato, R. Ruedy, A. Lacis, and V. Oinas, Global warming in the twenty-first century: An alternative scenario, *Proc. Natl. Acad. Sci. U. S. A.*, *97*(18), 9875–9880, 2000.

Hayes, P. L., et al. (2013), Organic aerosol composition and sources in Pasadena, California during the 2010 CalNex campaign, *J. Geophys. Res. Atmos.*, *118*, 9233–9257, doi:10.1002/jgrd.50530.

Haywood, J., and O. Boucher. (2000), Estimates of the Direct and Indirect Radiative Forcing Due to Tropospheric Aerosols: A Review, *Reviews of Geophysics 38* 4: 513-43.

Healy, R. M., J. C. Wenger, A. Metzger, J. Duplissy, M. Kalberer, J. Dommen (2008), Gas/particle partitioning of carbonyls in the photooxidation of isoprene and 1,3,5-trimethylbenzene, *Atmos. Chem. Phys.*, *8*, 3215–3220.

Hecobian, A., X. Zhang, M. Zheng, N. Frank, E. S. Edgerton, and R. J. Weber (2010), Water-Soluble Organic Aerosol material and the light-absorption characteristics of aqueous extracts measured over the Southeastern United States, *Atmospheric Chemistry and Physics*, *10*(13), 5965-5977.

Hennigan, C. J., M. H. Bergin, J. E. Dibb, and R. J. Weber (2008), Enhanced secondary organic aerosol formation due to water uptake by fine particles, *Geophys. Res. Lett.*, *35*, L18801, 10.1029/2008GL035046.

Henze, D. K., Seinfeld, J. H., Ng, N. L., Kroll, J. H., Fu, T.-M., Jacob, D. J., and Heald, C. L. (2008), Global modeling of secondary organic aerosol formation from aromatic hydrocarbons: high- vs. low-yield pathways, *Atmospheric Chemistry and Physics*, *8*, 2405-2420.

Hersey, S. P., J. S. Craven, K. A. Schilling, A. R. Metcalf, A. Sorooshian, M. N. Chan, R. C. Flagan, and J. H. Seinfeld (2011), The Pasadena Aerosol Characterization Observatory (PACO): chemical and physical analysis of the Western Los Angeles Basin aerosol, *Atm. Chem. Phys.*, *11*, 7417-7443.

Hoffer, A., A. Gelencser, P. Guyon, G. Kiss, O. Schmid, G. P. Frank, P. Artaxo, and M. O. Andreae (2006), Optical properties of humic-like substances (HULIS) in biomass-burning aerosols, *Atmospheric Chemistry and Physics, 6*, 3563-3570.

Hoffmann, T., Odum, J. R., Bowman, F., Collins, D., Klockow, D., Flagan, R. C., and Seinfeld, J. H. (1997), Formation of organic aerosols from the oxidation of biogenic hydrocarbons, *J. Atmos. Chem., 26*, 189–222.

Huang, X. F., J. Z. Yu, L. Y. He, and M. Hu (2006), Size distribution characteristics of elemental carbon emitted from Chinese vehicles: Results of a tunnel study and atmospheric implications, *Environmental Science & Technology, 40*(17), 5355-5360.

Intergovernmental Panel on Climate Change (IPCC): Climate Change 2007: The Physical Science Basis, *Cambridge University Press, UK*, 2007.

Jacobson, M. Z. (1999), Isolating nitrated and aromatic aerosols and nitrated aromatic gases as sources of ultraviolet light absorption, *Journal of Geophysical Research-Atmospheres*, *104*(D3), 3527-3542.

Jacobson, M. Z. (2001), Strong radiative heating due to the mixing state of black carbon in the atmospheric aerosols, *Nature*, *409*, 695–697.

Johnson, B. J., E. A. Betterton, and D. Craig (1996), Henry's law coefficients of formic and acetic acids, *J. Atmos. Chem.*, *24*, 113–119.

Jung, J., Y. J. Kim, K. Y. Lee, M. G.-Cayetano, T. Batmunkh, J.-H. Koo, and J. Kim (2010), Spectral optical properties of long-range transport Asian Dust and pollution aerosols over Northeast Asia in 2007 and 2008, *Atmos. Chem. Phys., 10*, 5391-5408, 2010.

Kanakidou, M., Seinfeld, J. H., Pandis, S. N., Barnes, I., Dentener, F. J., Facchini, M. C., Van Dingenen, R., Ervens, B., Nenes, A., Nielsen, C. J., Swietlicki, E., Putaud, J. P., Balkanski, Y., Fuzzi, S., Horth, J., Moortgat, G. K., Winterhalter, R., Myhre, C. E. L., Tsigaridis, K., Vignati, E., Stephanou, E. G., and Wilson, J. (2005): Organic aerosol and global climate modelling: a review, *Atmospheric Chemistry* *and Physics, 5*, 1053–1123.

Kawamura K. and I. R. Kaplan (1985), Determination of organic acids (C1-C10) in the atmosphere, motor exhausts, and engine oils, *Envir. Sci. Technol. 19*, 1082-1086.

Keene, W. C., A. A. P. Pszenny, J. R. Maben, E. Stevenson, and A. Wall (2004), Closure evaluation of size-resolved aerosol pH in the New England coastal atmosphere during summer, *J. Geophys. Res., 109*, D23307.

Keene, W. C., B. W. Mosher, D. J. Jacob, J. W. Munger, R. W. Talbot, R. S. Artz, J. R. Maben, B. C. Daube, and J. N. Galloway (1995), Carboxylic acids in clouds at a high-elevation forested site in central Virginia, *J. Geophys. Res., 100*D, 9345–9357.

Kesselmeier, J. (2001), Exchange of short-chain oxygenated volatile organic compounds (VOCs) between plants and the atmosphere: A compilation of field and laboratory studies, *J. Atmos. Chem., 39*, 219–233, doi:10.1023/A:1010632302076.

Kesselmeier, J., K. Bode, C. Gerlach, and E. Jork (1998), Exchange of atmospheric formic and acetic acids with trees and crop plants under controlled chamber and purified air conditions, *Atmos. Environ., 32*, 1765–1775, doi:10.1016/S1352-2310(97)00465-2.

Khare, P., N. Kumar, K. M. Kumari, and S. S. Srivastava (1999), Atmospheric formic and acetic acids: An overview, *Rev. Geophys., 37,* 227–248.

Kieber, R. J., R. F. Whitehead, S. N. Reid, J. D. Willey, and P. J. Seaton (2006), Chromophoric dissolved organic matter (CDOM) in rainwater, southeastern North Carolina, USA, *J. Atmos. Chem., 54*, 21-41.

Kirchstetter, T. W., and T. L. Thatcher (2012), Contribution of organic carbon to wood smoke particulate matter absorption of solar radiation, *Atm. Chem. Phys. Disc., 12,* 5803-5816.

Kirchstetter, T. W., T. Novakov, and P. V. Hobbs (2004), Evidence that the spectral dependence of light absorption by aerosols is affected by organic carbon, *Journal* *of Geophysical Research-Atmospheres*, *109*(D21).

Koch, D., Schulz, M., Kinne, S., McNaughton, C., Spackman, J. R., Balkanski, Y., Bauer, S., Berntsen, T., Bond, T. C., Boucher, O., Chin, M., Clarke, A., De Luca, N., Dentener, F., Diehl, T., Dubovik, O., Easter, R., Fahey, D. W., Feichter, J., Fillmore, D., Freitag, S., Ghan, S., Ginoux, P., Gong, S., Horowitz, L., Iversen, T.,Kirkeva˚g,A.,Klimont,Z.,Kondo,Y.,Krol,M.,Liu,X., Miller, R., Montanaro, V., Moteki, N., Myhre, G., Penner, J. E., Perlwitz, J., Pitari, G., Reddy, S., Sahu, L., Sakamoto, H., Schus- ter, G., Schwarz, J. P., Seland, Ø., Stier, P., Takegawa, N., Take- mura, T., Textor, C., van Aardenne, J. A., and Zhao, Y.: Evalu- ation of black carbon estimations in global aerosol models, *Atmos. Chem. Phys., 9*, 9001–9026, doi:10.5194/acp-9-9001-2009, 2009.

Kroll, J. H., Ng, N. L., Murphy, S. M., Flagan, R. C., and Sein- feld, J. H.: Secondary organic aerosol formation from isoprene photooxidation, *Environ. Sci. Technol., 40*, 1869–1877, 2006.

Lack, D. A., and J. M. Langridge (2013), On the attribution of black and brown carbon light absorption using the Ångström exponent, *Atmos. Chem. Phys. Disc., 13*, 15493-15515.

Lack, D. A., M. S. Richardson, D. Law, J. M. Langridge, C. D. Cappa, R. J. McLaughlin, and D. M. Murphy (2012), Aircraft Instrument for Comprehensive Characterization of Aerosol Optical Properties, Part 2: Black and Brown Carbon Absorption and Absorption Enhancement Measured with Photo Acoustic Spectroscopy, *Aerosol Science and Technology, 46*(5), 555-568.

Lack, D. A., R. Bahreini, J. M. Langridge, J. B. Gilman, and A. M. Middlebrook (2013), Brown carbon absorption linked to organic mass tracers in biomass burning particles, *Atm. Chem. Phys., 13*, 2415-2422.

Lack, D.A., and C.D. Cappa, Impact of brown and clear carbon on light absorption enhancement, single scatter albedo and absorption wavelength dependence of black carbon, *Atmospheric Chemistry and Physics*, *10*(9), 4207-4220, doi:10.5194/acp-10-4207-2010, 2010.

Lan, Z. J., D. L. Chen, X. A. Li, X. F. Huang, L. Y. He, Y. G. Deng, N. Feng, and M. Hu (2011), Modal characteristics of carbonaceous aerosol size distribution in an urban atmosphere of South China, *Atmospheric Research, 100*(1), 51-60.

Lee, A., A. H. Goldstein, M. D. Keywood, S. Gao, V. Varutbangkul, R. Bahreini, N. L. Ng, R. C. Flagan, and J. H. Seinfeld (2006), Gas-phase products and secondary aerosol yields from the ozonolysis of ten different terpenes, *J. Geophys. Res., 111*, D07302, doi:10.1029/2005JD006437.

Lelieveld, J., and P. J. Crutzen (1991), The role of clouds in tropospheric photochemistry, *J. Atmos. Chem., 12*, 229–267.

Lim, H. J., and B. J. Turpin (2002), Origins of primary and secondary aerosol in Atlanta: Results of time-resolved measurements during the Atlanta Supersite Experiment, *Environmental Science & Technology, 36*, 4489-4496.

Limbeck, A., M. Kulmala, and H. Puxbaum (2003), Secondary organic aerosol formation in the atmosphere via heterogeneous reaction of gaseous isoprene on acidic particles, *Geophysical Research Letters, 30*(19).

Liu, J., Bergin, M., Guo, H., King, L., Kotra, N., Edgerton, E., and Weber, R. J.: Size-resolved measurements of brown carbon and estimates of their contribution to ambient fine particle light absorption based on water and methanol extracts, *Atmos. Chem. Phys. Discuss., 13*, 18233-18276, doi:10.5194/acpd-13-18233-2013, 2013.

Loflund, M., A. Kasper-Giebl, W. Tscherwenka, M. Schmid, H. Giebl, R. Hitzenberger, G. Reischl, H. Puxbaum (2001), The performance of a gas and aerosol monitoring system (GAMS) for the determination of acidic water soluble organic and inorganic gases and ammonia as well as related particles from the atmosphere, *Atmospheric Environment, 35*, 2861-2869.

Lukacs, H., et al. (2007), Seasonal trends and possible sources of brown carbon based on 2-year aerosol measurements at six sites in Europe, *Journal of Geophysical Research-Atmospheres, 112*(D23).

Madronich, S., and J. G. Calvert (1990), Permutation reactions of organic peroxy-radicals in the troposphere, *J. Geophys. Res.*, *95*, 5697-5717, 1990.

Mang, S. A., et al. (2008), Contribution of Carbonyl Photochemistry to Aging of Atmospheric Secondary Organic Aerosol, *Journal of Physical Chemistry A 112* 36: 8337-44.

McNaughton, C., et al. (2007), Results from the DC-8 inlet characterization experiment (DICE): Airborne versus surface sampling of mineral dust and sea salt aerosols, *Aerosol Sci. and Tech.*, *41*, 136-159.

Middlebrook, A. M., R. Bahreini, J. L. Jimenez, and M. R. Canagaratna (2012), Evaluation of Composition-Dependent Collection Efficiencies for the Aerodyne Aerosol Mass Spectrometer using Field Data, *Aerosol Science and Technology, 46,* 258–271, 2012.

Moosmuller, H., R. K. Chakrabarty, and W. P. Arnott (2009), Aerosol light absorption and its measurement: A review, *Journal of Quantitative Spectroscopy & Radiative Transfer, 110*(11), 844-878.

Myhre, G., Hoyle, C. R., Berglen, T. F., Johnson, B. T., and Haywood, J. M.: Modeling of the solar radiative impact of biomass burning aerosols during the Dust and Biomass- burning Experiment (DABEX), *J. Geophys. Res.*, *113*, D00C16, doi:10.1029/2008JD009857, 2008.

Myriokefalitakis, S., K. Tsigaridis, N. Mihalopoulos, J. Sciare, A. Nenes, K. Kawamura, A. Segers, and M. Kanakidou (2011), In-cloud oxalate formation in the global troposphere: a 3-D modeling study, *Atmos. Chem. Phys.*, *11*, 5761-5782, doi:10.5194/acp-11-5761-2011.

Nakayama, T., Y. Matsumi, K. Sato, T. Imamura, A. Yamazaki, and A. Uchiyama (2010), Laboratory studies on optical properties of secondary organic aerosols generated during the photooxidation of toluene and the ozonolysis of alpha-pinene, *Journal of Geophysical Research-Atmospheres, 115*.

Nakayama, T., K. Sato , Y. Matsumi, T. Imamura , A. Yamazaki , and A. Uchiyama

(2013), Wavelength and NOx dependent complex refractive index of SOAs generated from the photooxidation of toluene, *Atmos. Chem. Phys.*, *13*, 531-545, doi:10.5194/acp-13-531-2013.

Neeb, P., F. Sauer, O. Horie, and G. K. Moortgat (1997), Formation of hydroxymethyl hydroperoxide and formic acid in alkene ozonolysis in the presence of water vapour, *Atmos. Environ.*, *31*, 1417– 1423, doi:10.1016/S1352-2310(96)00322-6.

Ng, N. L., Kroll, J. H., Chan, A. W. H., Chhabra, P. S., Flagan, R. C., and Seinfeld, J. H.: Secondary organic aerosol formation from m-xylene, toluene, and benzene, *Atmos. Chem. Phys.*, *7*, 3909–3922, 2007, http://www.atmos-chem-phys.net/7/3909/2007/.

Nguyen, T.B., Lee, P.B., Updyke, K.M., Bones, D.L., Laskin, J., Laskin, A., Nizkorodov, S.A., 2012. Formation of nitrogen- and sulfur-containing lightabsorbing compounds accelerated by evaporation of water from secondary organic aerosols. *J. Geophys. Res. D 117*, D01207. http://dx.doi.org/10.1029/2011JD016944.

NIOSH (1996), Elemental carbon (diesel particulate): method 5040, in NIOSH Manual of Analytical Methods, P. M. Eller and M. E. Cassinelli, *National Institute for Occupational Safety and Health, Cincinnati.*

Novakov, T., and C. E. Corrigan. (1996), Cloud Condensation Nucleus Activity of the Organic Component of Biomass Smoke Particles, *Geophysical Research Letters 23* 16: 2141-44.

Odum, J. R., Jungkamp, T. P. W., Griffin, R. J., Flagan, R. C., and Seinfeld, J. H. (1997), The atmospheric aerosol forming potential of whole gasoline vapor, *Science, 276*, 96–99.

Orsini, D. A., Y. L. Ma, A. Sullivan, B. Sierau, K. Baumann, and R. J. Weber (2003), Refinements to the particle-into-liquid sampler (PILS) for ground and airborne measurements of water soluble aerosol composition, *Atmos. Environ.*, *37*, 1243–1259.

Pankow, J. F. (1994), An absorption-model of gas-particle partitioning of organic-compounds in the atmosphere, *Atmos. Envir., 28*, 185-188.

Park, R. J., M. J. Kim, J. I. Jeong, D. Yooun, and S. Kim (2010), A contribution of brown carbon aerosol to the aerosol light absorption and its radiative forcing in East Asia, *Atmos. Environ., 44*, 1414–1421, doi:10.1016/j.atmosenv.2010.01.042.

Paulot, F., D. Wunch, J. D. Crounse, G. C. Toon, D. B. Millet, P. F. DeCarlo, C. Vigouroux, N. M. Deutscher, G. González Abad, J. Notholt, Warneke T., J. W. Hannigan, C. Warneke, J. A. de Gouw, E. J. Dunlea, M. De Mazière, D. W. T. Griffith, P. Bernath, J. L. Jimenez, and P. O. Wennberg (2011), Importance of secondary sources in the atmospheric budgets of formic and acetic acids, *Atmos. Chem. Phys., 11*, 1989–2013.

Petzold, A., and M. Schönlinner (2004), Multi-angle absorption photometry—a new method for the measurement of aerosol light absorption and atmospheric black carbon, *Journal of Aerosol Science, 35*(4), 421-441.

Petzold, A., Schloesser, H., Sheridan, P. J., Arnott, W. P., Ogren, J. A. and Virkkula, A. 2005. Evaluation of Multi-Angle Absorption Photometry for Measuring Aerosol Light Absorption. *Aerosol Sci. Technol., 39*: 40–51.

Pollack, I. B., T. B. Ryerson, M. Trainer, D. D. Parrish, A. E. Andrews, E. L. Atlas, D. R. Blake, S. S. Brown, R. Commane, B. C. Daube, J. A. de Gouw, W. P. Dubé, J. Flynn, G. J. Frost, J. B. Gilman, N. Grossberg, J. S. Holloway, J. Kofler, E. A. Kort, W. C. Kuster, P. M. Lang, B. Lefer, R. A. Lueb, J. A. Neuman, J. B. Nowak, P. C. Novelli, J. Peischl, A. E. Perring, J. M. Roberts, G. Santoni, J. P. Schwarz, J. R. Spackman, N. L. Wagner, C. Warneke, R. A. Washenfelder, S. C. Wofsy, and B. Xiang (2012), Airborne and ground-based observations of a weekend effect in ozone, precursors, and oxidation products in the California South Coast Air Basin, *J. Geophys. Res., 117,* D00V05, doi:10.1029/2011JD016772.

Pope, C. A., et al. (2002), Lung Cancer, Cardiopulmonary Mortality, and Long-Term Exposure to Fine Particulate Air Pollution, *Jama-Journal of the American Medical Association 287* 9: 1132-41.

Qin, Y., and R. M. Mitchell (2009), Characterisation of episodic aerosol types over the Australian continent, *Atmospheric Chemistry and Physics*, *9*(6), 1943-1956.

Rizzo, L. V., Correia, A. L., Artaxo, P., Procópio, A. S., and Andreae, M. O.: Spectral dependence of aerosol light absorption over the Amazon Basin, *Atmos. Chem. Phys., 11*, 8899-8912, doi:10.5194/acp-11-8899-2011, 2011.

Roberts, G. C., M. O. Andreae, J. Zhou, and P. Artaxo (2001), Cloud condensation nuclei in the Amazon Basin: “Marine” conditions over a continent? Geophysical Research Letters, 28, 2807-2810. Schwartz, J., D. Slater, T.V. Larson, W.E. Pierson, and J.Z. Koenig (1993), Particulate air pollution and hospital emergency room visits for asthma in Seattle. *American Review of Respiratory Diseases, 147*, 826-831.

Robinson, A. L., Donahue, N. M., Shrivastava, M. K., Weitkamp, E. A., Sage, A. M., Grieshop, A. P., Lane, T. E., Pierce, J. R., and Pandis, S. N.: Rethinking organic aerosols: Semivolatile emis- sions and photochemical aging, *Science*, *315*, 1259–1262, 2007.

Rolph, G.D. (2012), Real-time Environmental Applications and Display sYstem (READY) Website. NOAA Air Resources Laboratory, Silver Spring, MD. [available at http://ready.arl.noaa.gov]

Saleh, R., C. J. Hennigan, G. R. McMeeking, W. K. Chuang, E. S. Robinson, H. Coe, N. M. Donahue, and A. L. Robinson (2013), Absorptivity of brown carbon in fresh and photo-chemically aged biomass-burning emissions, *Atm. Chem. Phys., 13*, 7683-7693.

Sandradewi, J., Prévôt, A. S. H., Alfarra, M. R., Szidat, S., Wehrli, M. N., Ruff, M., Weimer, S., Lanz, V. A., Weingartner, E., Perron, N., Caseiro, A., Kasper-Giebl, A., Puxbaum, H., Wacker, L., and Baltensperger, U.: Comparison of several wood smoke markers and source apportionment methods for wood burning particulate mass, *Atmos. Chem. Phys. Discuss.*, *8*, 8091-8118, doi:10.5194/acpd-8-8091-2008, 2008.

Sareen, N., A. N. Schwier, E. L. Shapiro, D. Mitroo, and V. F. McNeill (2010), Secondary organic material formed by methylglyoxal in aqueous aerosol mimics, *Atmospheric Chemistry and Physics, 10*(3), 997-1016.

Schnaiter, M., Schmid, O., Petzold, A., Fritzsche, L., Klein, K. F., Andreae, M. O., Helas, G., Thielmann, A., Gimmler, M., Mohler, O. M., Linke, C., and Schurath, U.: Measurement of wavelength resolved light absorption by aerosols utilizing a UV-VIS extinc- tion cell, *Aerosol Sci. Technol., 39*, 249–260, 2005.

Schwarz, J. P., et al. (2008), Coatings and their enhancement of black carbon light absorption in the tropical atmosphere, *J. Geophys. Res., 113,* D03203, doi:03210.01029/02007JD009042.

Seinfeld, J. H., and J. F. Pankow. (2003), Organic Atmospheric Particulate Material, *Annual Review of Physical Chemistry 54*: 121-40.

Shapiro, E. L., J. Szprengiel, N. Sareen, C. N. Jen, M. R. Giordano, and V. F. McNeill (2009), Light-absorbing secondary organic material formed by glyoxal in aqueous aerosol mimics, *Atmospheric Chemistry and Physics, 9*(7), 2289-2300.

Simon, H., P.V. Bhave, J.L. Swall, N.H. Frank, W.C. Malm (2011), Determining the spatial and seasonal variability in OM/OC ratios across the US using multiple regression, *Atmos. Chem. Phys., 11*, 2933-2949.

Sokolik, I. N., and O. B. Toon (1999), Incorporation of mineralogical com- position into models of the radiative properties of mineral aerosol from UV to IR wavelengths, *J. Geophys. Res., 104*(D8), 9423-9444.

Sommariva, R., J. A. de Gouw, M. Trainer, E. Atlas, P. D. Goldan, W. C. Kuster, C. Warneke, and F. C. Fehsenfeld (2011), Emissions and photochemistry of oxygenated VOCs in urban plumes in the Northeastern United States, *Atmos. Chem. Phys., 11*, 7081–7096.

Sorooshian, A., Brechtel, F. J., Ma, Y., Weber, R. J., Corliss, A., Flagan, R. C., and Seinfeld, J. H. (2006), Modeling and Characterization of a Particle-into-Liquid-Sampler (PILS), *Aerosol Sci. Technol., 40*, 396–409.

Sorooshian, A., N. L. Ng, A. W. H. Chan, G. Feingold, R. C. Flagan, and J. H. Seinfeld (2007), Particulate organic acids and overall water-soluble aerosol composition measurements from the 2006 Gulf of Mexico Atmospheric Composition and Climate Study (GoMACCS), *Journal of Geophysical Research-Atmospheres, 112*(D13), doi: 10.1029/2007jd008537.

Spaulding, R. S., R. W. Talbot, and M. J. Charles (2002), Optimization of a mist chamber (cofer scrubber) for sampling water-soluble organics in air, *Environ. Sci. Technol., 36*(8), 1798–1808.

Sullivan, A. P., et al. (2006), Airborne Measurements of Carbonaceous Aerosol Soluble in Water over Northeastern United States: Method Development and an Investigation into Water-Soluble Organic Carbon Sources, *Journal of Geophysical Research-Atmospheres 111*, D23.

Sullivan, A. P., R. J. Weber, A. L. Clements, J. R. Turner, M. S. Bae, and J. J. Schauer (2004), A method for on-line measurement of water-soluble organic carbon in ambient aerosol particles: Results from an urban site, *Geophys. Res. Lett., 31*, L13105, doi:10.1029/12004GL019681.

Sullivan, A., and R. J. Weber (2006), Chemical characterization of the ambient organic aerosol soluble in water: 2. Isolation of acid, neutral, and basic fractions by modified size-exclusion chromatography, *J. Geophys. Res., 111*, D05314, doi:10.1029/2005JD006485.

Sun, H. L., L. Biedermann, and T. C. Bond (2007), Color of brown carbon: A model for ultraviolet and visible light absorption by organic carbon aerosol, *Geophysical Research Letters, 34*(17).

Talbot, R. W., K. M. Beecher, R. C. Harriss, and W. R. Cofer (1988), Atmospheric geochemistry of formic and acetic acids at a mid-latitude temperate site, *J. Geophys Res., 93*, 1638- 1652.

Talbot, R. W., M. O. Andreae, H. Berresheim, D. J. Jacob, and K. M. Beecher (1990), Sources and sinks of formic, acetic, and pyruvic acids over central Amazonia 2.

Wet season, *J. Geophys. Res., 95*, 16,799-16,811.

Turpin, B. J., and H. J. Lim (2001), Species contributions to PM2.5 mass concentrations: Revisiting common assumptions for estimating organic mass, *Aerosol Sci. and Tech., 25*, 602-610.

Updyke, K. M., T. B. Nguyen, and S. A. Nizkorodov (2012), Formation of brown carbon via reactions of ammonia with secondary organic aerosols from biogenic and anthropogenic precursors, *Atmospheric Environment, 63*, 22-31.

Veres, P. R., J. M. Roberts, A. K. Cochran, J. B. Gilman, W. C. Kuster, J. S. Holloway, M. Graus, J. Flynn, B. Lefer, C. Warneke, and J. de Gouw (2011), Evidence of rapid production of organic acids in an urban air mass, *Geophys. Res. Lett., 37*, L17807.

Veres, P., J. M. Roberts, C. Warneke, D. Welsh-Bon, M. Zahniser, S. Herndon, R. Fall, and J. de Gouw (2008), Development of negative-ion proton-transfer chemical-ionization mass spectrometry (NI-PT-CIMS) for the measurement of gas-phase organic acids in the atmosphere, *Int. J. Mass Spectrom., 274*, 48-55.

Verma, V., Rico-Martinez, R., Kotra, N., King, L., Liu, J., Snell, T. W., and Weber, R. J.: Contri- bution of water-soluble and insoluble components and their hydrophobic/hydrophilic subfrac- tions to the reactive oxygen species-generating potential of fine ambient aerosols, *Environ. Sci. Tech., 46*, 11384–11392, 2012. 9109

Virkkula, A. 2010. Correction of the calibration of the 3-wavelength particle soot absorption photometer (3 PSAP). *Aerosol Sci. Technol.44*, 706–712.

Volkamer, R., et al. (2006), Secondary Organic Aerosol Formation from Anthropogenic Air Pollution: Rapid and Higher Than Expected, *Geophysical Research Letters 33* 17.

Volkamer, R., P. J. Ziemann, and M. J. Molina (2009), Secondary organic aerosol formation from acetylene (C2H2): seed effect on SOA yields due to organic photochemistry in the aerosol aqueous phase, *Atmos. Chem. Phys., 9*, 1907–1928.

Weber R. J., A. P. Sullivan, R.E. Peltier, A. Russell, B. Yan, M. Zheng, J. de Gouw, C. Warneke, C. Brock, J. S. Holloway, E. L. Atlas, and E. Edgerton (2007), A study of secondary organic aerosol formation in the anthropogenic-influenced southeastern United States, *Journal of Geophysical Research*, *112*, D13302, doi:10.1029/2007JD008408.

Weingartner, E., H. Saathoff, M. Schnaiter, N. Streit, B. Bitnar, and U. Baltensperger (2003), Absorption of light by soot particles: determination of the absorption coefficient by means of aethalometers, *Journal of Aerosol Science*, *34*(10), 1445-1463.

Wexler, A. S. and J. H. Seinfeld (1991), Second-generation inorganic aerosol model, *Atmos. Environ. 12*, 2731-2748.

Wexler, A. S. and S. L. Clegg (2002), Atmospheric aerosol models for systems including the ions H+, NH4+, Na+, SO42−, NO3−, Cl−, Br− and H2O., *J. Geophys. Res., 107* (D14), ISSN 0148-0227

Yan F, Winijkul E, Jung S, Bond TC, Streets DG (2011), Global emission projections of particulate matter (PM): I. Exhaust emissions from on-road vehicles. *Atmos Environ., 45*: 4830–4844.

Yang, M., S.G.Howell, J. Zhuang, and B.J. Huebert (2009), Attribution of aerosol light absorption to black carbon, brown carbon, and dust in China e interpretations of atmospheric measurements during EAST-AIRE. *Atmos. Chem. Phys. 9*, 2035-2050, 2009, doi:10.5194/acp-9-2035-2009.

Yao, X. H., T. Y. Ling, M. Fang, and C. K. Chan (2006), Comparison of thermodynamic predictions for in‐situ pH in PM2.5, *Atmos. Environ., 40,* 2835–2844.

Yokelson, R. J., J. D. Crounse, P. F. DeCarlo, T. Karl, S. Urbanski, E. Atlas, T. Campos, Y. Shinozuka, V. Kapustin, A. D. Clarke, A. Weinheimer, D. J. Knapp, D. D. Montzka, J. Holloway, P. Weibring, F. Flocke, W. Zheng, D. Toohey, P. O. Wennberg, C. Wiedinmyer, L. Mauldin, A. Fried, D. Richter, J. Walega, J. L. Jimenez, K. Adachi, P. R. Buseck, S. R. Hall, and R. Shetter (2009), Emissions from biomass burning in the Yucatan, *Atmos. Chem. Phys., 9*, 5785–5812, doi:10.5194/acp-9-5785-2009.

Zappoli, S., A. Andracchio, S. Fuzzi, M. C. Facchini, A. Gelencser, G. Kiss, Z. Krivacsy, A. Molnar, E. Meszaros, H.-C. Hansson, K. Rosman, and Y. Zebuhr (1999), Inorganic, organic and macromolecular components of fine aerosol in different areas of Europe in relation to their water solubility, *Atmos. Environ., 33*, 2733-2743.

Zhang, X. L., J. M. Liu, E. T. Parker, P. L. Hayes, J. L. Jimenez, J. A. de Gouw, J. H. Flynn, N. Grossberg, B. L. Lefer, and R. J. Weber (2012a), On the gas-particle partitioning of soluble organic aerosol in two urban atmospheres with contrasting emissions: 1. Bulk water-soluble organic carbon, *Journal of Geophysical Research-Atmospheres, 117*.

Zhang, X., Y.-H. Lin, J. D. Surratt, and R. J. Weber (2013), Sources, Composition and Absorption Angström Exponent of Light-absorbing Organic Components in Aerosol Extracts from the Los Angeles Basin, *Environ. Sci. Technol., 47* (8), 3685-3693.

Zhang, X. L., Y. H. Lin, J. D. Surratt, P. Zotter, A. S. H. Prevot, and R. J. Weber (2011), Light-absorbing soluble organic aerosol in Los Angeles and Atlanta: A contrast in secondary organic aerosol, *Geophysical Research Letters*, 38.

Zhang, X., Z. Liu, A. Hecobian, M. Zheng, N. H. Frank, E. S. Edgerton, and R. J. Weber (2012b), Spatial and seasonal variations of fine particle water-soluble organic carbon (WSOC) over the southeastern United States: Implications for secondary organic aerosol formation, *Atmos. Chem. Phys., 12*, 6593-6607, doi:10.5194/acp-12-6593-2012.

Zhong, M. and Jang, M.: Dynamic light absorption of biomass burning organic carbon photochemically aged under natural sunlight, *Atmos. Chem. Phys. Discuss., 13*, 20783-20807, doi:10.5194/acpd-13-20783-2013, 2013.

VITA

JIUMENG LIU

Jiumeng Liu was born in Harbin, Heilongjiang, China in 1986. She attended Peking University in Beijing, China, where she received bachelor degrees in Environmental Sciences and Economics as a second major in 2008 before coming to Georgia Tech to pursue a doctorate in Atmospheric Sciences. When she is not working on her research, Ms. Liu enjoys reading and playing piano.